University of Alberta

Probing the Lipid-bound Conformation of Apolipophorin III

By

Daisy Sahoo ©

A thesis to be submitted to the Faculty of Graduate Studies and Research in partial fulfillment of the requirements for the degree of Doctor of Philosophy

Department of Biochemistry

Edmonton, Alberta

Spring 2001

National Library of Canada
Acquisitions and Bibliographic Services
395 Wellington Street
Ottawa ON K1A 0N4
Canada

Bibliothèque nationale du Canada
Acquisitions et services bibliographiques
395, rue Wellington
Ottawa ON K1A 0N4
Canada

Your file Votre référence

Our file Notre référence

The author has granted a non-exclusive licence allowing the National Library of Canada to reproduce, loan, distribute or sell copies of this thesis in microform, paper or electronic formats.

L'auteur a accordé une licence non exclusive permettant à la Bibliothèque nationale du Canada de reproduire, prêter, distribuer ou vendre des copies de cette thèse sous la forme de microfiche/film, de reproduction sur papier ou sur format électronique.

The author retains ownership of the copyright in this thesis. Neither the thesis nor substantial extracts from it may be printed or otherwise reproduced without the author's permission.

L'auteur conserve la propriété du droit d'auteur qui protège cette thèse. Ni la thèse ni des extraits substantiels de celle-ci ne doivent être imprimés ou autrement reproduits sans son autorisation.

0-612-60341-5

Canada

University of Alberta

Library Release Form

Name of Author:	Daisy Sahoo
Title of Thesis	Probing the Lipid-bound Conformation of Apolipophorin III
Degree:	Doctor of Philosophy
Year this Degree Granted:	2001

Permission is hereby granted to the University of Alberta Library to reproduce single copies of this thesis and to lend or sell such copies for private, scholarly, or scientific research purposes only.

The author reserves all other publications and other rights in association with the copyright in the thesis, and except as hereinbefore provided, neither the thesis nor any substantial portion thereof may be printed or otherwise reproduced in any material form whatever without the author's prior written permission.

Daisy Sahoo

38 Bateman Drive
Nepean, Ontario
K2G 5H4

Oct 20, 2000
Date

University of Alberta

Faculty of Graduate Studies and Research

The undersigned certify that they have read, and recommend to the Faculty of Graduate Studies and Research for acceptance, a thesis entitled *Probing the Lipid-bound Conformation of Apolipophorin III* submitted by Daisy Sahoo in partial fulfillment of the requirements for the degree of Doctor of Philosophy.

Robert O. Ryan
Dr. Robert Ryan

D. E. Vance
Dr. Dennis E. Vance

Dr. Robert S. Hodges

Dr. Elena Posse de Chaves

Dr. Shinji Yokoyama

Dr. Mary Sorci-Thomas

October 16, 2000
Date Thesis Approved

ABSTRACT

Exchangeable apolipoproteins belong to a class of α-helical proteins that play a key role in lipoprotein metabolism. The reversible binding of exchangeable apolipoproteins to lipoprotein surfaces is consistent with their ability to exist in both lipid-free and lipid-bound states. It has been hypothesized that lipid interaction occurs following a conformational opening of the protein. Although we have a reasonable understanding of how exchangeable apolipoproteins interact with various lipid systems, key issues remain unresolved, including the structural basis of conformational opening and the conformation of the lipid-bound form.

Apolipophorin III, from the Sphinx moth, *Manduca sexta*, is an 18-kDa hemolymph exchangeable apolipoprotein that functions in lipoprotein binding and particle stabilization. Apolipophorin III shares a common functional and molecular architecture with mammalian apolipoproteins, thus, the insect system serves as a valuable model for studies of protein-lipid interactions and structure-function relationships. In the lipid-free state, apolipophorin III exists as a globular bundle consisting of five amphipathic α-helices. However, like most apolipoproteins, apolipophorin III exerts its biological function in the lipid-bound state.

The goal of my research was to elucidate the lipid-bound conformation of apolipophorin III. In the first part of my thesis, making use of an isotopic-labeling strategy for NMR spectroscopy, I have shown that hydrophobic residues interact initially with lipid micellar surfaces followed by hydrophilic residues. In the second part, cysteine residues were introduced into apolipophorin III by site-directed mutagenesis and labeled with an extrinsic fluorophore that acts as a probe for different regions of the

protein. Using aqueous and lipophilic quenchers, I (i) monitored the change in microenvironment of fluorophore-labeled cysteine residues on apolipophorin III upon lipid binding; (ii) provided evidence for the superficial association of apolipophorin III with a lipoprotein surface and (iii) obtained information regarding the relative spatial disposition of helices 1, 2, 3 and 5 on discoidal phospholipid bilayer complexes. Using pyrene excimer fluorescence, I showed lipid-induced helical repositioning of apolipophorin III in terms of (i) helices 2 and 3 and helices 1 and 5 moving away from one another upon lipid binding and (ii) apolipophorin III molecules adopting a precise, non-random orientation around the periphery of discoidal complexes.

Based on the data obtained from these studies, I present a new lipid-bound conformation of apolipophorin III around the circumference of phospholipid bilayer complexes. In this model, I propose that helices 1, 2 and 5 move away from helices 3 and 4, with helix 1 extending away from helix 2, thus forming the basis for a "partially-extended" lipid-bound conformation of apolipophorin III.

ACKNOWLEDGEMENTS

I wish to extend my gratitude to those who have contributed to my happiness and well-being during my time as a graduate student. First and foremost, I must thank my supervisor, Dr. Robert Ryan. His constant enthusiasm, encouragement and support have motivated me and given me the confidence to believe that I can succeed in any path I choose to follow. Bob, you are truly an inspiration. I would also like to thank the members of my Graduate Committee, Dr. Dennis Vance and Dr. Robert Hodges, as well as Dr. Cyril Kay, for their helpful suggestions, encouragement and kind words over the past five years.

The work presented in this thesis would not have been possible without the generous help and support of several individuals. I am extremely grateful to Kim Oikawa and Robert Luty for performing CD studies and providing assistance with GdnHCl/temperature denaturation studies. I thank Paul Semchuk for electro-spray mass spectrometric analyses and Roger Bradley for help with electron microscopy. I must also acknowledge Perry d'Obrenan and Leslie Hicks for their excellent work with graphics and figures, especially during "the last moment". I also thank the Medical Research Council of Canada and the Alberta Heritage Foundation for Medical Research for providing me with financial support for the past four years.

It has truly been a pleasure and an experience to meet the people that I have during my years at the University. Vasanthy, we sure have had our share of moments! I have learned so much from you, in more ways than you know...and for that, I can not thank you enough. To Scott and Carl, I am so lucky to have you both as my friends. We

may have gone our separate ways, but I know we will always remain together. Thanks for being there in times of joy and sadness. Most importantly, thanks for making me laugh. To Vincent, Darrin, Mike, Paul, Jianjun, Dean, Elena, Sukhinder, Eric, Jody and Priscilla…you have all been there for me, both scientifically and personally... and you've all made it worth coming into work, even on the bad days.

Mom and Dad, I only wish I had the words to express my love and gratefulness towards you. You have always done so much for me. But, what matters the most is the support you have given me with respect to my decisions in life and the pursuit of my dreams. I know I am who I am today because of you…and for that, I am proud to have you as my parents.

And, to Victor… My life feels complete now that I am showered with your love, support, warmth, care and affection. I am so glad that you were the one to open my eyes and allow me to feel what I never knew was possible. I am thankful for the times we have shared and await the adventures that lie ahead in our future together.

TABLE OF CONTENTS

CHAPTER 1: INTRODUCTION 1

1.1 Mammalian lipoproteins 2

1.2 Insect lipophorin 4
- A) Composition of lipophorins 4
  - i) Lipids 4
  - ii) Non-exchangeable apolipoproteins 5
  - iii) Exchangeable apolipoproteins 6
- B) Structural organization of lipophorins 7
- C) Biosynthesis of lipophorins 8
  - i) Larvae 8
  - ii) Pupae 9
  - iii) Adults 10
- D) Variation of lipophorin metabolism with development 10

1.3 The role of lipophorin in lipid transport 11
- A) Activation of adipokinetic hormone 12
- B) Formation of LDLp 13
- C) Delivery of fatty acids to flight muscle 14
- D) Involvement of a basic matrix particle in the lipid shuttle 16

1.4 Exchangeable apolipoproteins 17

1.5 Apolipophorin III 18
- A) Purification 19
- B) Gene analysis and primary structure 20
- C) Physical properties of apolipophorin III 21

1.6 Functional characterization of apolipophorin III 25
- A) Lipid binding properties 25
  - i) Lipid binding affinity of apoLp-III 25
  - ii) Binding of apoLp-III to diacylglycerol 26
- B) Other functional properties 27

1.7 A common lipid-free molecular architecture among exchangeable apolipoproteins 28
A) NMR solution structure of *M. sexta* apolipophorin III 30
B) X-ray crystal structure of *L. migratoria* apolipophorin III 34
C) X-ray crystal structure of the N-terminal domain of apolipoprotein E 35
D) X-ray crystal structure of apo Δ(1-43)A-I 36

1.8 Lipid-bound conformation of apolipophorin III 36
A) Behaviour of apoLp-III at an air-water interface 37
B) "Conformational Opening" hypothesis 38
C) Discoidal complexes: a model protein-lipid complex 39
D) Initiation of apoLp-III-lipid interactions 41
i) Initiation by ionic interactions 41
ii) Initiation by hydrophobic interactions 42
iii) Correlation of binding activity with a partially folded conformation 46
E) Spectroscopic evidence for a conformational change in apoLp-III 47
i) Studies by circular dichroism spectroscopy 47
ii) Fluorescence studies 49
iii) FTIR studies 50
F) Disulfide bond engineering: further evidence for a conformational change 51

1.9 Specific aims 51

CHAPTER 2: MATERIALS AND METHODS 54

2.1 Materials 55

2.2 Methods 56

CHAPTER 3: NMR EVIDENCE FOR A CONFORMATIONAL ADAPTATION OF APOLIPOPHORIN III UPON LIPID ASSOCIATION 66

3.1 Introduction 67

3.2 Results 68
^{15}N Isotope labeling strategies 68
Rationale for experimental design 71
Behaviour of resonances corresponding to hydrophobic residues in apoLp-III 73
Behaviour of resonances corresponding to hydrophilic residues in apoLp-III 77

3.3 Discussion 80

CHAPTER 4: FLUORESCENCE QUENCHING STUDIES OF EXCHANGEABLE APOLIPOPROTEIN-LIPID INTERACTIONS 85

4.1 Introduction 86

4.2 Results 87
Structural characterization of pyrene-labeled N40C- and L90C-apoLp-III 87
Functional characterization of pyrene-labeled N40C- and L90C-apoLp-III 90
Potassium iodide quenching 92
Lipophilic quenchers 94

4.3 Discussion 99
Use of fatty acid spin labels to study lipid-bound protein conformations 101
Fluorescence quenching of apoLp-III-phospholipid disc particles 102
Shallow penetration of apoLp-III with lipoprotein surfaces 103

CHAPTER 5: PYRENE EXCIMER FLUORESCENCE: A SPATIALLY SENSITIVE PROBE TO MONITOR LIPID-INDUCED REPOSITIONING OF HELICES 2 AND 3 IN APOLIPOPHORIN III 105

5.1 Introduction 106

5.2 Results 106
Characterization of pyrene-labeled apoLp-III 106
Pyrene excimer fluorescence 108
Fluorescence properties of lipid-free pyrene-labeled apoLp-III 110
Effect of apoLp-III unfolding on pyrene excimer fluorescence 111
Interaction of pyrene-labeled N40C/L90C apoLp-III with trifluoroethanol 116
Helical repositioning of pyrene-labeled apoLp-III on discoidal complexes 118
Relative orientation of apoLp-III molecules on discoidal complexes 121

5.3 Discussion 123
Pyrene rings proximal in the lipid-free helix bundle state 125
Unfolding of pyrene-labeled apoLp-III 125
Lipid-induced tertiary structural reorganization 127
Relative orientation of neighboring apoLp-III molecules in disc particles 129

CHAPTER 6: ELUCIDATION OF THE LIPID-ASSOCIATED CONFORMATION OF APOLIPOPHORIN III AROUND DISCOIDAL PHOSPHOLIPID COMPLEXES 131

6.1 Introduction 132

6.2 Results 132
Characterization of single-cysteine apoLp-III mutants 133
Fluorescence quenching studies 134
Characterization of double-cysteine mutant apoLp-III 137
Pyrene excimer fluorescence 140

6.3 Discussion 145
Spatial disposition of helices 1 and 5 146
Repositioning of helices 1 and 5 by pyrene excimer fluorescence 147
A new DMPC-bound conformation of apoLp-III 148

CHAPTER 7: GENERAL DISCUSSION 152

7.1 Lipid-induced conformational adaptation of apoLp-III 155

7.2 Rationale for use of pyrene fluorescence spectroscopy 157

7.3 Change in microenvironment upon binding of apoLp-III to lipid surfaces 158

7.4 Mode of interaction of apoLp-III with a lipoprotein surface 160

7.5 Spatial disposition of apoLp-III helices on DMPC phospholipid bilayers 162

7.6 Lipid-induced helical repositioning of apoLp-III on DMPC phospholipid bilayers 163

7.7 Relative orientation of apoLp-III around phospholipid bilayer complexes 165

7.8 Applicability of lipid-bound apoLp-III model to other lipid-bound Models **165**
A) Human apoA-I 166
B) N-terminal domain of human apoE 168
C) Apolipophorin III 171

7.9 Future studies on the "partially-extended" lipid-bound model of apoLp-III **173**
A) Disulfide bond engineering 173
B) Pyrene excimer fluorescence spectroscopy 174
C) Crosslinking studies 174
D) Fluorescence resonance energy transfer (FRET) 175

7.10 Binding of apoLp-III to discoidal vs. spherical particles **176**

7.11 Concluding remarks **177**

BIBLIOGRAPHY **179**

LIST OF TABLES

Table 1-1. Major human plasma exchangeable apolipoproteins 17

Table 4-1. Effective Stern-Volmer quenching constants (K_{SV}) for pyrene-labeled N40C- and L90C-apoLp-III using KI 93

Table 4-2. Apparent Stern-Volmer constants (K_{app}) for wild-type and pyrene-labeled apoLp-III using spin-labeled fatty acids 97

Table 6-1: Effective Stern-Volmer quenching constants (K_{sv}) for pyrene-labeled A8C- and A138C-apoLp-III using KI 135

Table 6-2. Apparent Stern-Volmer constants (K_{app}) for pyrene-labeled A8C- and A138C-apoLp-III using spin-labeled fatty acids 137

Table 7-1. Cysteine-containing apoLp-III mutants and their helical designations 158

LIST OF FIGURES

Figure 1-1. Model of lipid mobilization and transport by lipophorin in insects 15

Figure 1-2. Amino acid sequence of *Manduca sexta* apoLp-III 20

Figure 1-3. Ribbon diagram of NMR solution structure of lipid-free apoLp-III 31

Figure 1-4. Helical wheel representation of *M. sexta* apoLp-III 32

Figure 1-5. "Open conformation" model of apoLp-III upon lipid binding 39

Figure 3-1. ^{1}H-^{15}N HSQC spectra of apoLp-III 68

Figure 3-2. Location of ^{15}N-labeled residues in *M. sexta* apoLp-III 72

Figure 3-3. ^{1}H-^{15}N HSQC spectra of ^{15}N-valine specific-labeled apoLp-III in the presence and absence of D_{38}-DPC 74

Figure 3-4. Effect of DPC concentration on the amide proton chemical shift of valine resonances in ^{15}N-valine apoLp-III 75

Figure 3-5. ^{1}H-^{15}N HSQC spectra of ^{15}N-leucine specific-labeled apoLp-III in the presence and absence of D_{38}-DPC 76

Figure 3-6. Effect of DPC concentration on the amide proton chemical shift of leucine resonances in ^{15}N-leucine apoLp-III 77

Figure 3-7. ^{1}H-^{15}N HSQC spectra of ^{15}N-lysine specific-labeled apoLp-III in the presence and absence of D_{38}-DPC 78

Figure 3-8. Effect of DPC concentration on the amide proton chemical shift of lysine resonances in ^{15}N-lysine apoLp-III 79

Figure 3-9. Ribbon representation of *M. sexta* apoLp-III NMR solution structure in buffer 81

Figure 4-1. Electrospray mass spectrometric profiles of N40C-apoLp-III 88

Figure 4-2. N-(1-pyrene)maleimide labeling of N40C-apoLp-III 89

Figure 4-3. Fluorescence excitation and emission spectra of pyrene-labeled apoLp-III 90

Figure 4-4. Electron micrographs of apoLp-III/DMPC complexes 91

Figure 4-5. Effect of apolipoproteins on phospholipase-C-induced turbidity of LDL 92

Figure 4-6. Estimation of the transverse disposition of helix 5 in phospholipid disc complexes 95

Figure 4-7. Estimation of transverse disposition of helices 2 and 3 in phospholipid disc complexes 96

Figure 4-8. Estimation of spatial disposition of apoLp-III on a lipoprotein surface 99

Figure 5-1. Electrospray mass spectrometry profile of pyrene-labeled N40C/L90C-apoLp-III 107

Figure 5-2. Schematic representation of pyrene fluorescence properties 108

Figure 5-3. Fluorescence excitation and emission spectra of lipid-free pyrene-labeled N40C-, L90C- and N40C/L90C-apoLp-IIIs 110

Figure 5-4. Effect of GdnHCl on the secondary structure content and fluorescence of pyrene-N40C/L90C-apoLp-III 112

Figure 5-5. Effect of GdnHCl on the monomer fluorescence of pyrene-N40C-apoLp-III 113

Figure 5-6. Excitation spectra of pyrene-labeled N40C/L90C-apoLp-III in the absence and presence of GdnHCl 114

Figure 5-7. Effect of heat on pyrene excimer fluorescence 115

Figure 5-8. Excitation spectra of pyrene-labeled N40C/L90C-apoLp-III at low and high temperature 116

Figure 5-9. Effect of TFE on fluorescence of pyrene-labeled apoLp-III 117

Figure 5-10. Fluorescence emission spectra of pyrene-N40C/L90C-apoLp-III bound to phospholipid bilayer discs 119

Figure 5-11. Crosslinking of apoLp-III around DMPC discoidal complexes 121

Figure 5-12. Fluorescence emission spectra of single pyrene-labeled apoLp-III/DMPC discs 122

Figure 5-13. Schematic representation of apoLp-III in association with DMPC discoidal complexes 130

Figure 6-1. Bacterial expression of A8C-apoLp-III and A138C-apoLp-III 133

Figure 6-2. Fluorescence excitation and emission spectra of pyrene-labeled A8C- and A138C-apoLp-III 134

Figure 6-3. Estimation of transverse disposition of helices 1 and 5 in phospholipid disc complexes 136

Figure 6-4. Bacterial expression of A8C/A138C-apoLp-III 138

Figure 6-5. Disulfide bond formation determined by electrophoretic mobility 139

Figure 6-6. Crosslinking of sulfhydryls in A8C/A138C-apoLp-III 140

Figure 6-7. Fluorescence excitation and emission spectra of pyrene-labeled A8C/A138C-apoLp-III 141

Figure 6-8. Fluorescence emission spectra of pyrene-labeled A8C/A138C-apoLp-III bound to DMPC phospholipid bilayer disc complexes 143

Figure 6-9. Model depicting a "partially-extended" lipid-bound conformation of *M. sexta* apoLp-III 149

Figure 7-1. Schematic representation of the loose association of apoLp-III with a lipoprotein surface 161

Figure 7-2. Schematic representation of the "open conformation" model of apoLp-III around discoidal complexes 162

Figure 7-3. Schematic representation of "belt" conformations of apoLp-III around discoidal complexes 167

Figure 7-4. Schematic representation of "partially-extended" conformations of apoLp-III around discoidal complexes 170

Figure 7-5. Emission spectrum of DMPC discoidal complexes associated with two different pyrene-labeled apoLp-IIIs 171

Figure 7-6. Schematic representation depicting the location of disulfide bonds in the "open conformation" model of apoLp-III around discoidal complexes 173

LIST OF ABBREVIATIONS

AKH	adipokinetic hormone
Apo	apolipoprotein
ApoA-I	apolipoprotein A-I
ApoA-II	apolipoprotein A-II
ApoB	apolipoprotein B
ApoE	apolipoprotein E
ApoE(NT)	N-terminal domain of apolipoprotein E
ApoLp-I	apolipophorin I
ApoLp-II	apolipophorin II
ApoLp-III	apolipophorin III
BMH	bis-maleimidohexane
ATR-FTIR	Fourier transform attenuated total reflection infrared spectroscopy
CD	circular dichroism
CE	cholesteryl ester
CMC	critical micelle concentration
DAG	diacylglycerol
DMPC	dimyristoylphosphatidylcholine
DMPG	dimyristoylphosphatidylglycerol
DPC	dodecylphosphocholine
DSA	doxyl stearic acid
DSS	2,2-dimethyl-2-silapentane-5-sulfonate
FRET	fluorescence resonance energy transfer
GdnHCl	guanidine hydrocholoride
HDL	high density lipoprotein
HDLp-A	high density lipophorin-adult
HDLp-L	high density lipophorin-larval
HDLp-P	high density lipophorin-pupal
HDLp-W1	high density lipophorin-wanderer 1
HDLp-W2	high density lipophorin-wanderer 2
HPLC	high performance liquid chromatography
HSQC	heteronuclear single quantum correlation
IAEDANS	N-iodoacetyl-N'-(5-sulfo-1-naphthyl)ethylenediamine
IPTG	isopropyl β-D thiogalactopyranoside
KI	potassium iodide
LDL	low density lipoprotein
LDLp	low density lipophorin
LTP	lipid transfer particle
PC	phosphatidylcholine
PE	phosphatidylethanolamine
Pyrene	N-(1-pyrene)maleimide
SDS-PAGE	sodium dodecyl sulphate polyacrylamide gel electrophoresis
S.E.M.	standard error of mean
TAG	triacylglycerol

TFE	trifluoroethanol
UV	ultra-violet

Amino acid nomenclature:
Amino acids are referred to either by their full name, their three-letter code, or their one-letter designation.

Glycine	Gly	G
Nonpolar		
Alanine	Ala	A
Cysteine	Cys	C
Valine	Val	V
Leucine	Leu	L
Isoleucine	Ile	I
Methionine	Met	M
Phenylalanine	Phe	F
Proline	Pro	P
Tryptophan	Trp	W
Tyrosine	Tyr	Y
Uncharged polar		
Asparagine	Asn	N
Glutamine	Gln	Q
Serine	Ser	S
Threonine	Thr	T
Charged		
Arginine	Arg	R
Aspartic Acid	Asp	D
Glutamic Acid	Glu	E
Histidine	His	H
Lysine	Lys	K

CHEMICAL STRUCTURES

The following probes or crosslinking agents are used in experiments described in this thesis.

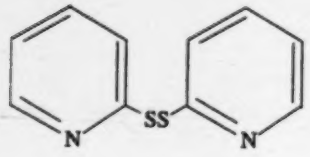

2,2'-dithiodipyridine (Aldrithiol™)

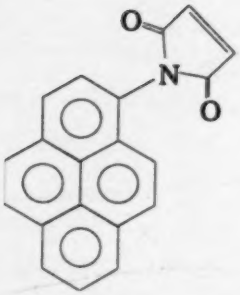

N-(1-pyrene)maleimide

5-doxyl stearic acid

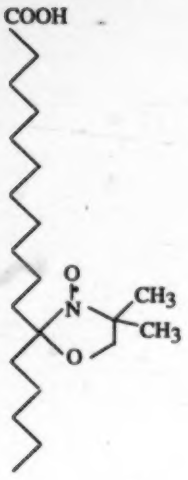

12-doxyl stearic acid

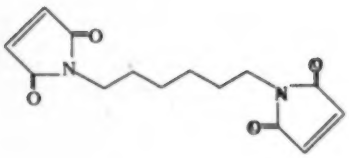

Bis-maleimidohexane

CHAPTER 1

Introduction

Apolipophorin III (apoLp-III) from the Sphinx moth, *Manduca sexta*, is a prototypical exchangeable apolipoprotein that serves as a valuable model for structure-function studies due to its similarity with mammalian exchangeable apolipoproteins at the level of its amino acid sequence (1), its physical properties (2, 3) and its amphipathic α-helices (1, 4). The amphipathic nature of apoLp-III allows it to exist in the hemolymph in both a soluble, lipid-free state and a lipid-bound state whereby it exerts its functions in lipophorin binding and particle stabilization during the transport of diacylglycerol from the fat body to flight muscles during prolonged flight. The lipid-free structure of apoLp-III has been determined (5, 6), yet little information is available regarding its structure in the lipid-bound state. Since most exchangeable apolipoproteins exert their biological effects in association with lipid, I sought to probe the lipid-bound conformation of apoLp-III using NMR and fluorescence spectroscopy. Based on my research, I present a model depicting the conformation of *M. sexta* apoLp-III on the surface of phospholipid bilayer complexes and discuss how it compares to currently-available models of lipid-bound conformations.

1.1 MAMMALIAN LIPOPROTEINS

Lipids such as triacylglycerol (TAG) and cholesterol are required for many cellular processes such as energy production and membrane and steroid biosynthesis. These water-insoluble lipids require a means by which they can be transported through the plasma in order to be delivered to tissues for storage or utilization. Mammals have devised a system whereby hydrophobic lipids are carried through the aqueous environment of the plasma via macromolecular structures called lipoproteins. Plasma

lipoproteins are spherical and consist of a neutral lipid core composed of TAG and cholesteryl esters, surrounded by a monolayer of amphipathic phospholipids and unesterified cholesterol. The surface monolayer also contains proteins called apolipoproteins, which, among other functions, serve to solubilize and stabilize the insoluble lipids of the lipoprotein particles. Only two apolipoproteins exist as integral components of lipoproteins (apolipoprotein (apo) B-100 and apo B-48). The other apolipoproteins have the additional ability to exist free of lipid in the plasma and are referred to as exchangeable apolipoproteins (apo A's, apo C's and apo E).

Plasma lipoproteins are classified according to density. Chylomicrons (density ~ 0.95 g/mL) are secreted by the intestine after a meal and are responsible for transport of dietary lipid. They are large lipid-rich particles, primarily composed of TAG. Meanwhile, the liver secretes TAG-rich particles called very low density lipoproteins (VLDL; density < 1.006 g/mL) which are known to transport TAG to peripheral tissues for storage or energy utilization. Chylomicrons are lipolysed in the capillaries to form chylomicron remnants. VLDL is lipolysed to form CE-rich low density lipoproteins (LDL; density range 1.019-1.063 g/mL) that deliver cholesterol to the peripheral tissues. Both chylomicron remnants and LDL are subsequently removed from circulation by the liver, primarily via LDL receptor-mediated endocytosis (7). High density lipoproteins (HDL; density range 1.063-1.21 g/mL) are small, dense particles composed primarily of CE. HDL is believed to play a role in the reverse cholesterol transport pathway by delivering cholesterol from the peripheral tissues back to the liver (8).

1.2 INSECT LIPOPHORIN

Like mammals, insects, possess a similar mechanism whereby dietary fat and mobilized stored fat are transported within their open circulatory system. While mammals have several different types of lipoproteins, insects rely on a single type of lipoprotein termed lipophorin (9) for most lipid transport. With the exception of Crustaceans, lipophorins are ubiquitous among arthropods (10). During different stages of lipid transport, the lipophorin particle varies in size and density. Lipophorin from each stage of lipid transport has been isolated and characterized from the hemolymph (blood) of the Sphinx moth or Tobacco hornworm, *Manduca sexta* (11-14). These forms vary with respect to lipid content and protein composition, and may be correlated to the physiological or developmental state of the insect. For example, high density lipophorins (HDLp; density range 1.09-1.18 g/mL) are the forms found in larvae and resting adults, while low density lipophorins (LDLp; density range 1.02-1.07 g/mL) are found only in adults during flight and carry large amounts of lipid from the fat body to the flight muscle. Very high density lipophorins (VHDLp; density range 1.24-1.28 g/mL) have been identified in the hemolymph of *M. sexta* during developmental stages (15) and in other species during their larval stages (16, 17). These particles represent a form which is released from the gut to produce HDLp [discussed in Law and Wells (18)].

A) Composition of lipophorins

*i) **Lipids***. Lipids comprise 40-50% of the lipophorin mass (19). In contrast to mammalian lipoproteins which contain high amounts of TAG, the core of lipophorins is predominantly composed of diacylglycerol (DAG), and much lower levels

of monoacylglycerol (MAG) and TAG. Similar to mammals, however, phospholipids are present on the surface monolayer of the particle and are the only common lipid component of insect lipophorins. While phosphatidylethanolamine (PE) makes up the majority of the phospholipids on the lipophorin surface, significant amounts of phosphatidylcholine (PC) are also present, along with smaller amounts of sphingomyelin, phosphatidylserine, phosphatidylinositol and cardiolipin (11, 20). The high PE:PC ratio found in lipophorins distinguishes them from mammalian lipoproteins wherein PC is the predominant polar lipid (21). The presence of long-chain (C_{20}-C_{40}), normal and methyl-branched aliphatic hydrocarbons contributes a major proportion of the non-polar lipid components, and represents an unique characteristic of lipophorins (22, 23). Interestingly, unlike mammals, insects are unable to synthesize cholesterol de novo. Since free cholesterol is an essential component of membranes, as well a precursor of ecdysone, a steroid molting hormone required for proper development and metamorphosis (24), the transport of dietary cholesterol by lipophorins appears to be a critical process for the survival of the insect species.

*ii) **Non-exchangeable apolipoproteins**.* Proteins account for 50-60% of the lipophorin mass (19). Upon examination of lipophorins from various insects, it was found that all lipophorins consist of two integral, non-exchangeable apolipoproteins, apolipophorin I (apoLp-I) and apolipophorin II (apoLp-II), that are present in a 1:1 ratio (25, 26). With an apparent molecular weight of ~ 250,000, apoLp-I is the largest apolipoprotein on lipophorin. Close examination of apoLp-I amino acid composition revealed similarities to mammalian apoB, the integral apolipoprotein associated with VLDL and LDL (26). Both apoB and apoLp-I (or apoLp-II) were insoluble in water

when separated from the lipoprotein. Furthermore, similar to mammalian apoB-containing lipoproteins, circular dichroism studies of native lipophorin revealed a secondary structure that is rich in β-sheet (27).

ApoLp-II, the other integral apolipoprotein present on the lipophorin particle, is smaller in size [apparent molecular weight ~ 78,000 (25)]. Lectin-binding studies on both apoLp-I and apoLp-II from several species provided evidence for the presence of mannose-containing oligosaccharide moieties (25).

Cross-linking studies by Kashiwazaki and Ikai (27) have shown that apoLp-I and apoLp-II are in close contact on a lipophorin particle. Furthermore, the higher susceptibility of *M. sexta* apoLp-I to trypsin cleavage than apoLp-II suggested that apoLp-II may be shielded from the aqueous environment of the lipophorin particle, whereas apoLp-I may be relatively exposed (11, 28).

Studies by Weers *et al.* (29) demonstrated that apoLp-I and apoLp-II originated from a common precursor protein. Immunoprecipitates from fat body homogenates yielded a 280-kDa protein which was recognized by monoclonal antibodies specific for either apoLp-I or apoLp-II. Pulse chase experiments confirmed that this 280-kDa protein was cleaved into apoLp-I and apoLp-II polypeptide components. This suggested that both these apolipophorins were products of the same gene.

iii) Exchangeable apolipoproteins. Apolipophorin III (apoLp-III) is the only water-soluble, exchangeable apolipoprotein that associates with lipophorin particles. Unlike in mammals, where most exchangeable apolipoproteins are bound to lipoproteins, apoLp-III usually exists as a lipid-free protein in the insect hemolymph (30, 31). ApoLp-III functions to facilitate transport of lipid from sites of storage in the fat body to sites of

utilization during metabolic situations (e.g. flight muscle). Both apoLp-III and its function in insect lipid transport will be discussed in greater detail in section 1.3.

B) Structural organization of lipophorins

Based on several pieces of data, the hydrophobic core model for human lipoproteins (32, 33) can be applied to insect lipophorin, whereby a globular core of neutral lipids is surrounded by a surface layer of amphiphilic lipids and proteins. Electron microscopy shows that lipophorins are spherical particles (11, 34, 35). ^{31}P-NMR spectroscopy and calorimetry experiments revealed that hydrocarbons are core components while phospholipids are surface components (36, 37). The surface localization of phospholipids was also confirmed by the susceptibility of lipophorin phospholipids to hydrolysis by phospholipase A_2 (23, 38). DAG is a major component of the lipophorin core, however, its active metabolism suggests that DAG may be partially exposed to the aqueous medium (11, 39-41). The presence of DAG on the lipophorin monolayer may be essential for transfer, enabling the lipophorin to act as a reusable shuttle (discussed in section 1.3). Katagiri *et al.* (42) used small-angle X-ray scattering analysis to propose a centrosymmetrical three layer model for HDLp from the African migratory locust (*Locusta migratoria*) and the cockroach (*Periplaneta americana*). Their studies suggested that lipophorin consists of an outer shell that contains apoLp-I and phospholipid; a middle layer contains apoLp-II and DAG and a core contains the apolar lipids such as hydrocarbons. The exact composition of each layer depends on the lipophorin under consideration. However, since apoLp-I and apoLp-II were both accessible in intact locust HDLp and LDLp to monoclonal antibodies specific for locust

apoLp-I and apoLp-II (43, 44), at least part of apoLp-II is located at the surface of the particle.

C) Biosynthesis of lipophorins

In mammals, upon entry into the intestine, dietary fat (in the form of TAG and CE) is packaged into chylomicron particles and transported via plasma to adipose tissue and the liver, while endogenously synthesized TAG is assembled into VLDL in the liver and secreted into circulation. In insects, the fat body combines many of the functions of the mammalian liver and adipose tissue. In addition, the fat body appears to be the sole site of lipophorin biosynthesis, serving as both a storage and biosynthetic organ. Therefore, in contrast to its mammalian counterparts, a single lipophorin species derived by the fat body functions as a transport vehicle for both dietary and endogenously synthesized fat.

i) Larvae. Lipophorin biosynthesis in feeding fifth instar larvae of *M. sexta* has been well-characterized by Prasad *et al.* (15). Their studies revealed that the fat body secretes nascent lipophorin consisting of apoLp-I, apoLp-II and phospholipid into the hemolymph as VHDLp. These nascent particles are thought to mature in the hemolymph, by accepting DAG derived from dietary lipid in the midgut tissue. Maturation of the lipophorin resulted in formation of HDLp (the circulating lipophorin of *M. sexta*), as detected by a shift in density to 1.15 g/mL, with no change in apolipoprotein content. It is believed that dietary glycerolipids are hydrolyzed into free fatty acids in the gut, and further taken up by the midgut tissue where they are converted to DAG prior to uptake by lipophorin.

While the above studies present a model whereby nascent lipophorin particles are produced in the fat body and derive their DAG from the midgut, Weers *et al.* (45) provided a different model for HDLp biosynthesis. Using *L. migratoria* as a model system in *in vitro* studies, the authors were able to show that, following synthesis, apoLp-I and apoLp-II were loaded with lipid in the fat body to form a lipophorin particle and released into the medium as HDLp (density of 1.12 g/mL). Therefore, both apolipoprotein synthesis and lipid loading occur in the fat body tissue. No evidence was obtained for the mechanism of biosynthesis proposed for *M. sexta* (15) since neither free apolipoproteins nor VHDLp were detectable and only HDLp was found in the medium.

Two separate studies provide further evidence for the model presented by Weers *et al.* (45). Using the common housefly, *Musca domestica* (46), or the southwestern corn borer, *Diatraea grandiosella* (47, 48), the authors showed that the density and lipid composition of the secreted lipophorin (from the fat body) were similar to that of circulating lipophorin, suggesting secretion of mature HDLp. However, in the case of the latter, it has been suggested that this mechanism may be related to the period of non-feeding (diapause) of the larvae, thus preventing lipid uptake in the midgut (19).

ii) Pupae. Once *M. sexta* completes its larval stage, it enters the pupal stage at which time metamorphosis occurs. During this stage, apolipoprotein mRNAs are absent from the fat body and lipophorin biosynthesis ceases (49). However, the existing lipophorin continues to transport lipid from fat body to developing adult tissues (50). Therefore, lipophorin produced in the larval stage appears to be important for lipid transport in the pupal stage, as well.

iii) Adults. Once in the adult stage, apolipoprotein mRNA reappears and lipophorin biosynthesis begins once again. The fat body secretes lipophorin with a density and lipid composition similar to that of mature lipophorin. There are, however, two differences between larval and adult lipophorin biosynthesis: i) the rapidly-growing larvae have a higher rate of biosynthesis (49); ii) the adult form of lipophorin (HDLp-A) contains two molecules of apoLp-III in addition to apoLp-I and apoLp-II (30, 51). Both apoLp-III molecules are integrated into the structure of the lipophorin since they do not exchange with free apoLp-III in the hemolymph (51). Interestingly, the resting larval and adult lipophorins of *L. migratoria* contain only apoLp-I and apoLp-II; association with apoLp-III only occurs during flight (as discussed in section 1.3).

D) Variation of lipophorin metabolism with development

As already described, the major hemolymph lipoprotein of the fifth instar larvae of *M. sexta* is the well-characterized HDLp (11, 26). Adult *M. sexta* lipophorin is very similar to larval lipophorin (26, 30) with the exception that it is distinguished by a higher lipid content and the presence of two molecules of apoLp-III.

When the *M. sexta* reach the end of the larval period, they enter a prepupal stage which is characterized by a behavioral pattern known as the "wandering stage". During this stage, the animals stop eating, void their midgut and move rapidly to look for a suitable place to undergo metamorphosis. Prasad *et al.* (12) isolated and studied the lipophorins from this 3- to 4-day prepupal period and noted some striking changes in lipophorin metabolism. Their investigations revealed that larval lipophorin (HDLp-L) was first converted to a higher density form which was relatively depleted of DAG (HDLp-W2), and then to a lower density form which was relatively enriched in DAG

(HDLp-W1). Since feeding ceases, the loss of DAG during the transition from HDLp-L to HDLp-W2 may be due to a continued delivery of DAG to fat body or other tissues. In addition, Tsuchida and Wells (50) provided experimental data to show that fat bodies from prepupae did not take up labeled DAG from lipophorin, thus supporting the notion that conversion of HDLp-W2 to HDLp-W1 may reflect a switch in metabolism in the fat body, whereby it changes from a fat-storing tissue to a fat-mobilizing tissue. Ultimately, *M. sexta* in the pupal stage possess pupal HDLp (HDLp-P). It was hypothesized that HDLp-P was derived from HDLp-L by alterations in lipid composition, since no new lipophorin was produced by the fat body in the prepupal or pupal stages. Of particular note, all lipophorin species isolated from different stages exhibited identical apolipoprotein components, consisting of apoLp-I and apoLp-II. In fact, when the proteins of HDLp-L were labeled with ^{3}H-amino acids during the transition from the fifth instar to the pupal stage, and HDLp-L, HDLp-W2, HDLp-W1 and HDLp-P were isolated, the radiospecific activity of the proteins did not significantly change during the transformation (12). These results confirm that HDLp-L is the precursor of HDLp-W2, HDLp-W2 is the precursor of HDLp-W1, and HDLp-W1 is the precursor of HDLp-P. In other words, the transition from one lipophorin species to another is a precisely controlled process which occurs solely by modification of preexisting lipophorin molecules.

1.3 THE ROLE OF LIPOPHORIN IN LIPID TRANSPORT

Mammals accumulate lipid reserves in the form of TAG. Under situations such as prolonged muscular exercise, TAG in the adipose tissue is hydrolyzed into long chain fatty acids and transported via the blood to provide metabolic fuel. The enzyme involved

in the hydrolysis of stored TAG and subsequent hydrolysis of DAG and MAG is hormone-sensitive lipase (52).

Insects, too, are highly active organisms that require efficient lipid transport for a variety of specialized purposes, with flight being the most strenuous of them all. In insects, DAG is mobilized from TAG stores in the fat body by TAG lipase (53) and released into the hemolymph. Upon reaching the flight muscles, DAG is hydrolyzed to free fatty acids which are taken up and oxidized to provide energy. Importantly, the vehicle used to transport DAG to the flight muscle is lipophorin.

A) Activation of adipokinetic hormone

In insects such as *M. sexta* and *L. migratoria*, species which use lipid as a fuel to power sustained flight, the initiation of flight activity entails secretion of adipokinetic hormone (AKH) from the corpus cardiacum (an endocrine gland found at the base of the brain) (54), resulting in mobilization of stored fat (55, 56). AKHs comprise a family of neuropeptides that possess lipid or carbohydrate mobilizing activities. *M. sexta* AKH is a nonapeptide (56), while in *L. migratoria*, there are three distinct AKHs: a decapeptide AKH-I and two octapeptides, AKH-II (57) and AKH-III (58).

Several experiments have confirmed the involvement of AKH in lipolysis of TAG. *In vivo* studies exhibit an enhanced level of DAG in hemolymph of insects which have been injected with AKH [reviewed in (59)]; incubation of isolated locust fat body tissue with AKH *in vitro* results in an accumulation of DAG (60, 61). It has been postulated that AKH binds to a fat body cell membrane receptor and, like hormone-sensitive lipase, AKH exerts its effects on lipolysis via a cAMP-dependent process, thus suggesting a role for protein kinase A in phosphorylation and activation of TAG lipase

(59, 62). As well, a recent study shows that injection of AKH-I into locust fat bodies results in an approximate two-fold increase in TAG lipase activity (63).

DAG released from the fat body into the hemolymph of *L. migratoria* (64, 65) or *M.sexta* (66) appears to be stereospecific and is in the *sn*-1,2-configuration. The pathway for stereospecific synthesis of this form of DAG appears to involve MAG acyltransferase in the fat body (67).

B) Formation of LDLp

TAG that is converted to DAG at the fat body is taken up by pre-existing circulating HDLp-A particles. In the resting *M. sexta* adult moth, HDLp-A (density of ~1.08 g/mL) (13) is composed of 48% protein (ratio of apoLp-I:apoLp-II:apoLp-III is 1:1:2) and 52% lipid, primarily phospholipid and DAG (26, 30). The transfer of DAG from fat body to HDLp-A most probably occurs with the assistance of lipid transfer particle (LTP) (68). LTP is a high molecular weight protein that facilitates net transfer and exchange of DAG between isolated lipophorins (13, 69, 70), as well as between fat body membranes and lipophorin in response to AKH (68).

Following LTP-mediated transfer of DAG, the HDLp-A particle [$M_r = 7.68 \times 10^5$ (51)], normally 16 nm in diameter (71), begins to expand. The capacity for HDLp to accept DAG is limited, since the expansion of the core volume would expose hydrophobic lipid to the aqueous environment. To circumvent this problem, several molecules of the exchangeable apolipoprotein, apoLp-III [which is normally found in a lipid-free state in the hemolymph of resting animals (30)], bind to the newly created lipid-water interface and stabilize the slowly expanding particle (51).

The fully loaded lipophorin is now a low density lipophorin (LDLp), approximately 23 nm in diameter (71), with a nearly doubled molecular mass [M_r = 1.56 x 10^6 (51)] and a lower density [1.03 g/mL; (51)]. In *M. sexta*, DAG accounts for 70% of the increase in mass, while apoLp-III molecules make up the remainder of the increase. In *L. migratoria*, however, LDLp increases its mass by 50%, with equal contributions from DAG and apoLp-III (34). Wells *et al.* (51) show that up to 16 molecules of apoLp-III can be found on a single LDLp particle in *M. sexta*. However, in *L. migratoria*, several reports suggest that 9 (72) or 14 (73) apoLp-IIIs can associate with LDLp. Further information about apoLp-III will be provided in section 1.5.

C) Delivery of fatty acids to flight muscle

In the mammalian system, lipoprotein lipase on the capillary endothelium acts on circulating TAG-rich lipoproteins to yield free fatty acids which enter adipose tissue cells and are converted to TAG. If we look more closely at VLDL, loss of TAG results in movement of surface apolipoproteins and phospholipids to HDL, ultimately resulting in the conversion of VLDL to LDL, which is cleared from circulation via receptor-mediated endocytosis and degraded (7). Flight muscles from *L. migratoria* (74-76) and *M. sexta* (77) have been shown to contain a membrane-bound lipoprotein lipase that not only hydrolyzes DAG to free fatty acids, but also has a higher activity against LDLp than against HDLp. Therefore, LDLp-associated DAG is hydrolyzed to yield free fatty acids that are presumed to diffuse into the flight muscle where they are oxidized to provide energy. It is worthy to note that fatty acid binding proteins have been identified in *L. migratoria* (78) and *M. sexta* (79), and these may play a role in fatty acid uptake/trafficking within the flight muscle cells.

Hydrolysis of DAG within LDLp ultimately produces a lipophorin particle with a diminished lipid content. Depletion of DAG results in the dissociation of apoLp-III, and hence, the recovery of lipid-free apoLp-III and regeneration of HDLp in the hemolymph. HDLp is, once again, free to begin another cycle of lipid transport by returning to the fat body for uptake of more DAG and consequent formation of LDLp. This cycle of DAG loading and unloading occurs many times in the lifetime of the particle (80) and validates the lipophorin reusable shuttle hypothesis first proposed by Chino and his colleagues (81) **(Figure 1-1).**

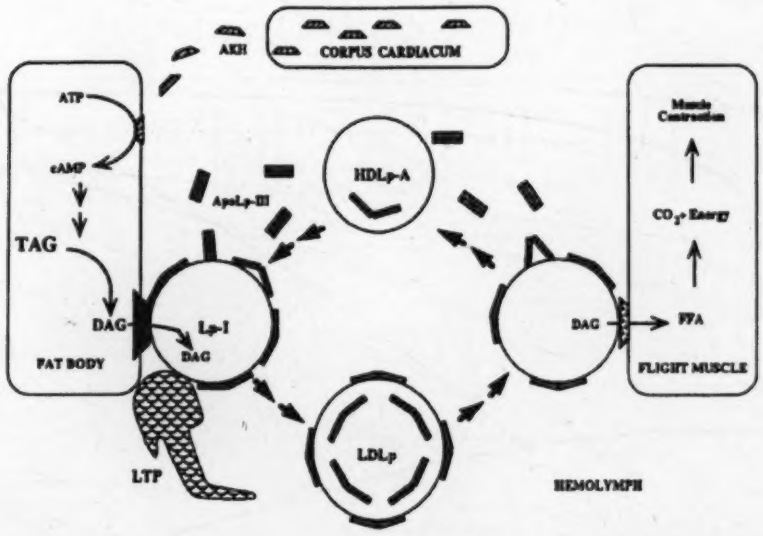

Figure 1-1. Model of lipid mobilization and transport by lipophorin in insects. As HDLp-A takes up DAG from the fat body, apoLp-III molecules are loaded onto the particle, concomitant with the increase in DAG. The resulting LDLp unloads DAG at the flight muscle, apoLp-III is released from the particle and HDLp-A is regenerated. Modified from Blacklock and Ryan (82) with permission.

D) Involvement of a basic matrix particle in the lipid shuttle

HDLp functions as a dynamic particle — it accepts and delivers lipids to tissues (e.g. fat body, muscle tissue) without being degraded (81). The lipophorin particle is a basic apolipoprotein-phospholipid matrix structure that represents an essential backbone (13, 36). In this regard, HDLp is visualized as a reusable shuttle wherein there exists a basic matrix structure in which lipid turnover (mainly DAG, cholesterol and hydrocarbon) can occur without turnover of protein components and without destruction of the particle (12, 13, 80, 81). In *M. sexta*, larval and pupal stages have one matrix lipoprotein which contains one molecule each of apoLp-I and apoLp-II; however, adults have a different matrix lipoprotein which contain two integral, non-exchangeable molecules of apoLp-III in addition to apoLp-I and apoLp-II (51). Strong evidence exists to support the concept that the basic matrix particle cycles between unloaded (HDLp) and lipid-loaded (LDLp) states during which apoLp-III can bind reversibly to the particle. Van Heusden and co-workers showed that after LDLp unloads DAG at the flight muscle, the apoLp-III that dissociates is then able to reassociate with HDLp-A to form new LDLp and continue the cycle (83). Studies using indirect immunofluorescence also provided evidence that entire lipophorin particles are not internalized by flight muscle cells (84). In addition, Kawooya *et al.* (38) analyzed lipophorin structure using a series of lipases. Their studies indicated that the basic matrix of lipophorin can maintain its structural integrity when largely depleted of DAG or PL. To complement their studies, Van Heusden *et al.* (85) demonstrated that this lipid-depleted lipophorin is able to accept DAG, *in vivo* and *in vitro*, and function in a manner similar to native lipophorin whereby it associates with apoLp-III under the influence of AKH to convert to LDLp. Therefore,

the reusable shuttle mechanism demonstrates the efficient use of a single lipophorin species, HDLp, to deliver lipid components to tissues in situations of energy-demand – a function which, in mammals, must be performed separately by chylomicrons, VLDL and LDL.

1.4 EXCHANGEABLE APOLIPOPROTEINS

Mammals and other species possess several exchangeable apolipoproteins, including apolipoprotein A-I (apoA-I), apolipoprotein A-II (apoA-II), apolipoprotein A-IV (apoA-IV), apolipoproteins C-II and C-III (apoC-II and apoC-III, respectively) and apolipoprotein E (apo E). The functions of these apolipoproteins are listed in **Table 1-1**.

Table 1-1. Major human plasma exchangeable apolipoproteins[a]

Apolipoprotein	Lipoprotein distribution	Function(s)
ApoA-I	All HDL classes	Cholesterol efflux; LCAT activation
ApoA-II	HDL-1, HDL-2, HDL-3	Inhibits apoA-I activity
ApoA-IV	Chylomicrons, HDL	Cholesterol efflux[b] LCAT activation[c]
ApoC-II	VLDL, HDLs	Activates lipoprotein lipase
ApoC-III	VLDL, HDLs	Inhibits apoC-II activity; VLDL uptake
ApoE	VLDL, IDL, HDL-1	Cholesterol efflux; LDL receptor ligand

[a]Adapted from (86)
[b]Taken from (87, 88)
[c]Taken from (89)

Exchangeable apolipoproteins are amphipathic in nature (see section 1.5) and share an inherent structural adaptability, thus providing them with the ability to reversibly associate with circulating lipoproteins. This property implies that such proteins can exist

in both lipid-free and lipid-bound states, hence forming the basis of their physiological role in lipoprotein metabolism. In fact, one of the best examples of the dual existence of exchangeable apolipoproteins is insect apoLp-III (90). As described above, apoLp-III is recovered as a lipid-free hemolymph protein in resting insects. However, via AKH-induced effects, or upon flight activity, apoLp-III associates with the surface of a lipophorin to stabilize DAG-enriched LDLp.

The remainder of this chapter will focus on the structure-function relationships of apoLp-III. The similarities and differences between apoLp-III and other members of this class of apolipoproteins will be discussed. It emerges that apoLp-III serves as an excellent model system through which we can gain information, not only with reference to structure, but also with respect to defining the nature and specificity of apolipoprotein-lipid interactions in all organisms.

1.5 APOLIPOPHORIN III

While HDLp in adult *M. sexta* can acquire 14 molecules of apoLp-III to form an LDLp particle (51, 73), larval HDLp does not associate with apoLp-III (15, 26), even though apoLp-III is present in the hemolymph (12, 30). Studies by Cole *et al.* (91) found that both adult and larval apoLp-III have the same amino acid composition and mRNA transcripts, suggesting that there is no difference in transcription of the gene. As well, neither adult nor larval hemolymph contains significant amounts of apoLp-III containing the propeptide AMVRR (1), suggesting that there is no difference in processing of the propeptide precursor between adults and larval fat body. Perhaps the reason for a lack of

apoLp-III associated with larval HDLp can be explained by mechanisms of lipophorin assembly. However, further studies are required to verify these suggestions.

A) Purification of apoLp-III

While *M. sexta* larval hemolymph contains almost 0.46 mg/mL apoLp-III, the amount of apoLp-III in adult hemolymph is about 17 mg/mL (30). Kawooya *et al.* (30) were able to isolate and purify this apoLp-III from adult *M. sexta.* Using gel permeation chromatography in the presence of guanidine hydrochloride, apoLp-III was successfully removed from the surface of lipophorin. In a parallel set of experiments, lipid-free apoLp-III was purified from hemolymph using a combination of gel permeation, ion exchange and lectin chromatography (30). Both preparations of apoLp-III are identical in electrophoretic mobility and both exhibit identical isoelectric points of 6.1. As well, unlike apoLp-I and apoLp-II, neither preparation is glycosylated.

After metamorphosis, adult *M. sexta* moths essentially contain HDLp, a form, which in adults, is known to contain two integral molecules of apoLp-III (51). Shapiro and Law (92) observed that the amount of LDLp in these adult insects increases when injected with synthetic locust AKH. This increase in LDLp is accompanied by an increased association of apoLp-III. Using this methodology, Wells *et al.* (93) purified apoLp-III from *M. sexta* moths with similar properties to those observed in Kawooya's study (30).

It is worth mentioning that apoLp-III has also been purified from organisms such as the locust, *L. migratoria* (31, 72), the grasshopper, *Gastrimargus africanus* (94), the flightless grasshopper, *Barytettix psolus* (95), a grasshopper which does not endure long-term flight, *Melanoplus differentialis* (95), the mesquite bug, *Thasus acutangulus* (93),

the southwestern corn borer, *Diatraea grandiosella* (96), the silkworm, *Bombyx mori* (97) and the greater wax moth, *Galleria mellonella* (98).

B) Gene analysis and primary structure

The sequence of the gene for *M. sexta* apoLp-III has been determined (99). The apoLp-III gene contains four exons: exon 1 codes for a relatively short 5' untranslated region and the first 15 amino acids of the signal sequence; exon 2 contains the remaining 3 amino acids of the signal sequence, the 5 amino acids of the prosequence and residues 1-64 of the mature protein; exon 3 codes for residues 65-118 of the mature protein; and exon 4 codes for residues 119-165 plus the 3' untranslated sequences.

Cole *et al.* (1) determined the primary structure of *M. sexta* apoLp-III. Mature apoLp-III is a single chain polypeptide of 166 amino acids with a molecular weight of 18, 380 Da (**Figure 1-2**).

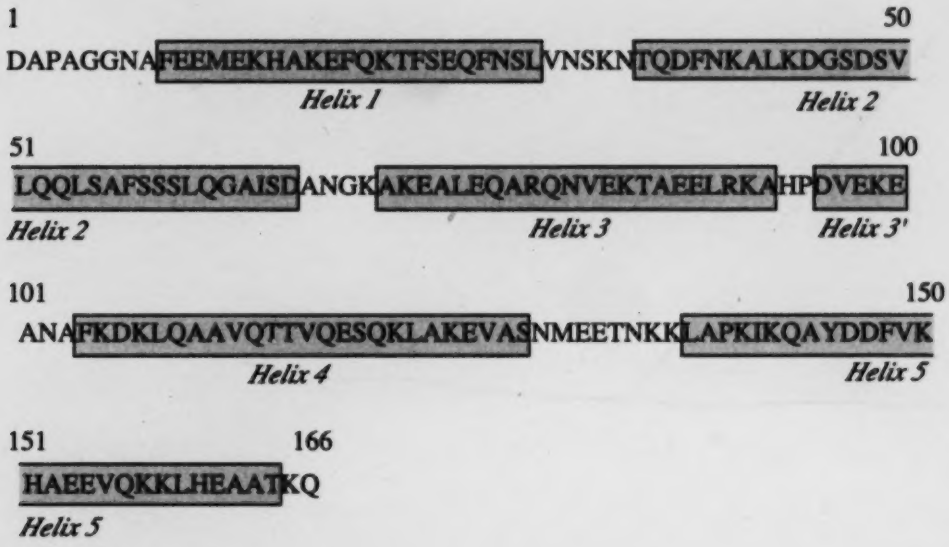

Figure 1-2. Amino acid sequence of *Manduca sexta* apoLp-III. Helices are shown in colour. The primary structure was determined by Cole *et al.* (1), while the helices were designated by Wang *et al.* (6).

Upon close analysis of the sequence, it was found that apoLp-III contains a prosegment (~2000 Da) before the mature protein, suggesting that apoLp-III undergoes both co- and post-translational proteolytic processing. Interestingly, the two Arg residues immediately preceding Asp1, the first amino acid of the mature protein, are a predominant feature of eukaryotic prosegments (100). Further, cotranslational cleavage between the signal and prosequences occurs between Ser (-6) and Ala (-5) (91), thus defining an amino-terminal pentapeptide prosegment (AMVRR) which bears striking sequence similarity to the pentapeptide prosegment of human apoA-II [ALVRR; (101, 102)].

The primary structure of apoLp-III was carefully examined using the computer program RELATE [described in Boguski *et al.* (103)]. ApoLp-III bears a remarkable resemblance to several human exchangeable apolipoproteins such as apo E, apoA-IV, apoA-I and apoC-I (1). Although there is little sequence identity between apoLp-III from *M. sexta* and mammalian apolipoproteins, there is considerable similarity based on common repeated sequences with amphipathic helical potential (1). And, as described in section 1.7, the shared amphipathic helix motif seems to represent the basis for the common functions of these apolipoproteins, especially in terms of their capacity to form a stable interaction with lipid surfaces for the execution of their various functions.

C) Physical properties of apoLp-III

The amount of apoLp-III bound to a lipophorin surface increases significantly upon the conversion of HDLp to LDLp, and the binding of apoLp-III to LDLp is linked to DAG loading. Thus, determination of the molecular properties of apoLp-III would enable us to understand how this protein carries out its key role in stabilization of the expanding lipid-water interface that results from DAG uptake.

Using circular dichroism (CD) spectroscopy, or by sedimentation equilibrium studies, it has been shown that apoLp-III is monomeric [(2, 3). In this regard, apoLp-III differs from apolipoproteins such as apoA-I, apoA-II and apoE since they have been shown to self-associate (104-106). Kawooya *et al.* (2) demonstrated that apoLp-III is a prolate ellipsoid with an axial ratio of 3.3. This corresponds to a minor axis of 12.5 Å and a major axis of 40 Å (107). CD spectroscopy also revealed that apoLp-III's secondary structure consists of 50% α-helix, 20% β-sheet and 30% random coil (2).

The primary structure of *M. sexta* apoLp-III lacks cysteine and tryptophan (1, 30). A UV absorption spectrum of apoLp-III reflects the contribution of 8 Phe residues per molecule of protein by characteristic fine structure peaks at 259 and 264 nm; another peak at 281 nm represents the single tyrosine residue in the protein (3). The low molar extinction coefficient for apoLp-III at 280 nm [1420 $M^{-1}cm^{-1}$; (3)] reflects the lack of tryptophan in the amino acid sequence.

Troughs at 208 and 222 nm in CD spectra indicate a high percentage of α-helical structure in apoLp-III between pH 5.9 and pH 8.1 (3), consistent with α-helix predictions based on its amino acid sequence (1) and Provencher-Glöckner (108) analysis. However, at very low or very high pH, analysis of CD spectra reveal that the protein denatures and assumes a random structure with loss in α-helicity.

The effect of temperature on apoLp-III secondary structure content was determined by CD in order to study the stability of this protein in solution (3). The midpoint of denaturation was found to be 52 °C. ApoLp-III is completely denatured at 67.5 °C, as determined by the high percentage of random coil. However, thermal-induced denaturation appears to be reversible, since after cooling, the protein regains

~95% of its α-helical structure. In comparison, human apoA-I has a temperature-induced denaturation midpoint of ~60 °C when determined by CD (109) or of 54 °C when determined by calorimetry (110). Guanidine hydrochloride (GdnHCl) was used to further study the stability of apoLp-III in solution (3). The midpoint of denaturation was achieved at 0.4 M GdnHCl, with most helical structure being lost around 0.5 M GdnHCl. Based on fluorescence intensity of the lone tyrosine residue, apoLp-III has a GdnHCl midpoint of denaturation of 0.3 M. Since this value is notably less as compared to the value of 0.4 M obtained by ellipticity at 222 nm, it is possible that the stability of the carboxyl terminal region of apoLp-III that contains the tyrosine residue (Tyr145) is relatively weak compared to forces that maintain the overall protein structure in its native conformation. The only other exchangeable apolipoproteins known to have such a low midpoint of GdnHCl denaturation are apoA-IV [0.4 M; (111)] and apoA-II [0.6 M; (112)]. With regard to the more stable proteins, the midpoints of denaturation for apoA-I and the N-terminal domain of apoE are 1.1 M (113, 114) and 2.5 M (115, 116), respectively, while that for apoC-II is 1.1 M (117).

From these same CD data, the free energy of unfolding of apoLp-III (ΔG^{H_2O}) was calculated to be 1.3 kcal/mol. Since this value compares well with values obtained from other apolipoproteins (115), further support is obtained for the idea that the structure of apoLp-III is labile. ApoA-II (1.0 kcal/mol) and apoA-IV (0.02 kcal/mol) are the only two apolipoproteins with ΔG^{H_2O} values lower than that of apoLp-III.

Using fluorescence spectroscopy, Ryan *et al.* (3) exploited the presence of the lone tyrosine residue in the C-terminal region of apoLp-III [Tyr145; (1)]. Excitation spectra (emission at 300 nm) and emission spectra (excitation at 277 nm) reveal that

tyrosine fluorescence in apoLp-III is much less than expected [quantum yield of Tyr in lipid-free apoLp-III is 0.012 compared to quantum yield of 0.07 for free Tyr (118)]. However, the spectral properties of the protein are dramatically altered in the presence of GdnHCl, as reflected by a significant enhancement in both the tyrosine excitation and emission spectra (3). These results suggest that tyrosine fluorescence is normally quenched to a large extent in native apoLp-III, but this quenching is abolished by denaturation of the protein. In an effort to explain the quenching of this tyrosine moiety, it was initially suggested that there may be energy transfer from Tyr145 to Phe148. These two residues exist in an *i, i+3* sequence configuration (present one turn away in the same helix), thus aligning in such a way as to stabilize the secondary structure through hydrophobic side chain stacking interactions. This hypothesis was proven invalid following site-directed mutagenesis of apoLp-III whereby Phe148 was substituted by Leu (119). In this case, fluorescence emission of Tyr145 remained partially quenched. However, the mutation also seemed to result in an altered tertiary organization of apoLp-III, as reflected by decreased inherent stability from denaturation experiments. Therefore, Phe148 may actually play a structural role by contributing to the overall stability of the protein: its aromatic side chain may interact with other residues in the protein via aromatic-aromatic interactions (120) in such a way that maintains the protein in an orientation that is optimal for interaction of Tyr145 with the quenching moiety. Further, studies on an isolated C-terminal helix of apoLp-III (118) show that there is increased fluorescence upon increasing the α-helicity of the peptide (121), thereby diminishing the possibility that the quenching moiety resides on the same helix as proposed earlier (3).

1.6 FUNCTIONAL CHARACTERIZATION OF APOLIPOPHORIN III

A) Lipid binding properties

i) Lipid binding affinity of apoLp-III. Previous studies have defined a range of lipid-binding affinities for several mammalian exchangeable apolipoproteins (122, 123). These studies have determined the following order for apolipoproteins from the highest lipid binding affinity to the lowest lipid binding affinity: apoA-II > apoC-III > apoC-I > apoA-I > apoA-IV.

Liu *et al.* (124) showed that human apoA-I can displace apoLp-III from the surface of LDLp. In these experiments, control LDLp has an apoLp-I:apoLp-II:apoLp-III molar ratio of 1:1:16; however, upon incubation of LDLp with apoA-I, the molar ratio changes to 1:1:2:7 for apoLp-I;apoLp-II:apoLp-III:apoA-I, with the lost apoLp-III being replaced by 7 molecules of apoA-I. The displacement of apoLp-III does not disrupt the structural properties of the LDLp in terms of size, density or lipid content. These experiments not only demonstrate that apoA-I has a higher lipid binding affinity than apoLp-III, but also that, consistent with previous findings (51), the stoichiometry proves that two molecules of apoLp-III remain on the lipophorin particle as non-exchangeable moieties.

In a more recent study (125), the N-terminal domain of human apoE was shown to displace apoLp-III from the surface of LDLp. Incubation of the hybrid particle with excess apoLp-III, however, could not displace the N-terminal domain of apoE off the particle surface. On the other hand, human apoA-I was able to displace the N-terminal domain of apoE from the lipophorin particle. Therefore, from the above experiments, we

can conclude that the lipid-binding affinity of apoA-I > N-terminal domain apoE > apoLp-III.

ii) Binding of apoLp-III to diacylglycerol. Like cholesterol in mammalian lipoproteins (126), DAG in insect lipophorin has been postulated to partition between the hydrophobic core and the surface monolayer in response to situations such as hormone-stimulated lipoprotein conversions (38, 127). Soulages and Brenner (128) have shown that in HDLp, DAG resides primarily in the core of the particle. In another study, lipophorin DAG is rapidly hydrolyzed by TAG-lipase, showing that some DAG is readily accessible to the enzyme, and must be localized at the particle/water interface (38). Recently, however, Wang *et al.* (129), used ^{13}C-NMR to provide direct evidence that DAG is found both in the core and on the surface of an LDLp particle. Due to its smaller and far less polar head group, the accumulation of DAG at the surface monolayer would be expected to result in particle instability. As such, it is postulated that partitioning of DAG molecules from the core to the surface of lipophorin creates binding sites for apoLp-III (127). In this way, apoLp-III serves to stabilize the newly-exposed DAG surface (51). Two separate studies described below provide support for this hypothesis.

a) Diacylglycerol enrichment by lipid transfer particle. As previously mentioned, hemolymph LTP has been shown to transfer neutral lipid from HDLp to LDLp. LTP has also been shown to catalyze the transfer of DAG from lipophorin to human LDL, without transfer or exchange of apolipoproteins (130). Singh *et al.* (131) clearly showed that LTP-mediated lipid-enrichment of LDL results in continued accumulation of DAG, thus leading to particle destabilization and aggregation. This aggregation is probably due to the creation of large lipid/water interfaces on the surface

of the lipoprotein. However, when apoLp-III is included in the incubation mixture, aggregation of LDL is prevented. Therefore, apoLp-III serves to stabilize the increased lipid content of LDL in a manner analogous to that postulated for LDLp (2, 5, 51).

b) Creation of diacylglycerol surfaces by hydrolysis with phospholipase C. Phospholipase C acts by hydrolytically cleaving the phosphocholine head group of phosphatidylcholine to create 1,2-DAG (132). Following hydrolysis of HDLp by phospholipase C, Wang *et al.* (129) performed ^{13}C-NMR studies to determine that phosphohydrolysis generated surface-associated 1,2-DAG. In fact, the resonance displayed a chemical shift very similar to the unique resonance present in LDLp, suggesting it corresponded to DAG located on the surface monolayer. Previous studies have shown that treatment of human LDL with phospholipase C (133) or sphingomyelinase (134) induces formation of LDL aggregates. Two separate studies (135, 136) demonstrated aggregation of either LDL or LDLp following phospholipase C treatment by measuring sample turbidity at 340 nm. As with experiments using LTP to create DAG surfaces, addition of exchangeable apolipoproteins such as apoA-I or apoLp-III into the incubation mixture prevent turbidity development, and hence, particle aggregation. Therefore, apoLp-III appears to play a role in the maintenance of particle (be it LDL or LDLp) integrity upon surface lipid depletion.

B) Other functional properties

Recent evidence suggests that apoLp-III may perform functions distinct from its role in lipid transport. Sun *et al.* (137) reported that *M. sexta* apoLp-III, may in fact, play a role in programmed cell death. Intersegmental muscles play an important role in the

emergence of the adult moth from its pupal casing. Three days before emergence, the intersegmental muscles of *M. sexta* begin to atrophy. Following the emergence process, the intersegmental muscles are no longer of use, and along with the motor neurons that innervate them, they die within 30 hours (138), triggered by the decline in the molting hormone, 20-hydroxyecdysone (139). Sun *et al.* (137) reported that, although apoLp-III is expressed at all stages of intersegmental muscle development, apoLp-III mRNA and protein levels are dramatically up-regulated coincident with intersegmental and motor neuron cell death. Further, it appears that apoLp-III is not associated with lipophorin before or during cell death. At this point, however, the actual function of apoLp-III in cell death remains unknown.

In unrelated studies, *G. mellonella* apoLp-III has been implicated in insect immune activation (140). It was shown that injection of recombinant apoLp-III into last instar *G. mellonella* larvae resulted in increased antibacterial activities against *E. coli*, as well as enhanced lysozyme-like activities. This new role for apoLp-III is rather interesting since larval hemolymph contains high levels of apoLp-III even though LDLp formation need not occur during this stage of development. Therefore, the role of apoLp-III may not be restricted to lipid transport alone.

1.7 A COMMON LIPID-FREE MOLECULAR ARCHITECTURE AMONG EXCHANGEABLE APOLIPOPROTEINS

The fact that exchangeable apolipoproteins have the ability to exist in alternate lipid-free and lipid-bound states implies that perhaps, these proteins possess an inherent

conformational flexibility. Several investigators suggested that these proteins may adopt a different conformation when in association with a lipid surface (5, 141). At the time, in the absence of three-dimensional structural information for apolipoproteins, several investigators relied on the use of amino acid sequence information to predict how the proteins might bind to a lipid surface (142, 143).

The amphipathic α-helix. As previously mentioned, apoLp-III bears remarkable sequence resemblance to many human apolipoproteins such as apoA-I, apo A-IV, apoE and apoC-I (1). Earlier studies reported that human apoA-I, apoA-IV and apoE are composed of tandemly repeated sequences that are multiples of 11 amino acids (103, 144-147). Cole *et al.* (1) examined the sequence of *M. sexta* apoLp-III and found multiple regions of internal homology or sequence periodicity . As well, repeating units ranging from 7 to 16 residues in length were defined, although most repeats consist of 14 or 15 residues. Moreover, closer examination of these repeating motifs reveals that the first 8 residues of each unit are highly conserved with respect to relative hydropathy and charge. The following depicts such a repeating motif:

hydrophobic—acidic—acidic—hydrophobic—hydrophilic—basic—basic—hydrophobic

1 2 3 4 5 6 7 8

Positions 9-11 of the motif contain weakly conserved basic/acidic/hydrophobic residues, while positions 12-14 are more highly variable. This motif is of particular interest since it has a high potential for forming amphipathic helical structures.

Indeed, in further experiments, a hydropathy profile obtained for *M. sexta* apoLp-III exhibits an amphipathic pattern that alternates regularly between hydrophobicity and hydrophilicity throughout the entire sequence of the protein. In addition, Cole *et al.* (1) determined that 63% of the protein may exist in α-helical conformation, a prediction which agrees well with earlier values obtained by Kawooya *et al.* (2).

Segrest was the first to suggest that amphipathic helices — helices that are defined by a segregation of hydrophobic and hydrophilic residues on opposite faces of the helix — may represent the structural basis for lipid-binding activity in apolipoproteins [(142); reviewed in (103)]. According to his theory, apolipoproteins contain specific amino acid sequences with amphipathic regions that have the propensity to assume an α-helical conformation such that the relatively apolar face of the helix can associate with the fatty acyl chains of phospholipids.

Therefore, the data suggest that perhaps it is not the primary sequence itself, but the common amphipathic structural motif which determines lipid-binding activity among exchangeable apolipoproteins. Certainly, in the years since, a great wealth of knowledge in the area of protein-lipid interactions has been obtained following determination of lipid-free structures of several exchangeable apolipoproteins.

A) NMR solution structure of *M. sexta* apolipophorin III

Development of an efficient bacterial expression system for *M. sexta* apoLp-III (119) facilitated structural insight towards the lipid-free conformation of this exchangeable apolipoprotein. Recombinant apoLp-III was isotopically labeled with ^{15}N or ^{13}C, thus facilitating the determination of the global fold and secondary structure

organization (6) and ultimately, the solution structure (Wang, Sykes & Ryan, unpublished results; PDB FILE #1EQ1) of lipid-free *M. sexta* apoLp-III by multidimensional NMR. As depicted in **Figure 1-3**, NMR data revealed that lipid-free *M. sexta* apoLp-III is a globular bundle consisting of five up-and-down amphipathic α-helices.

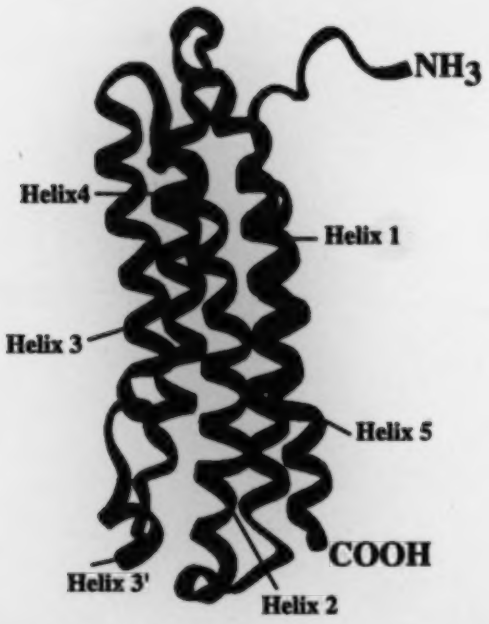

Figure 1-3. Ribbon diagram of NMR solution structure of lipid-free apoLp-III. The helices are indicated, as are the N- and C-termini. The global fold and secondary structural information is published (6). The solution structure is yet to be published (Wang, Sykes, Ryan; unpublished data). Coordinates are available in the Protein Data Bank (PDB#1EQ1).

Like cytochrome b_{562} (148) or cytochrome c' (149), apoLp-III appears to belong to the up-and-down helical bundle category described by Richardson (150). One of the most noticeable features of the apoLp-III solution structure is its elongated shape, consistent with previous hydrodynamic studies (2). Closer examination of the structure reveals the presence of a short helix, termed helix 3', that lies perpendicular to helices 3 and 4,

connecting them at the end of the elongated helix bundle (6). The other helices are connected to one another by short 5-7 residue flexible loop segments.

As previously mentioned, it has been suggested that amphipathic helices play a key role in protein-lipid interactions (142). **Figure 1-4** represents a helical wheel diagram for *M. sexta* apoLp-III based on secondary structure identified by specific NMR parameters (6).

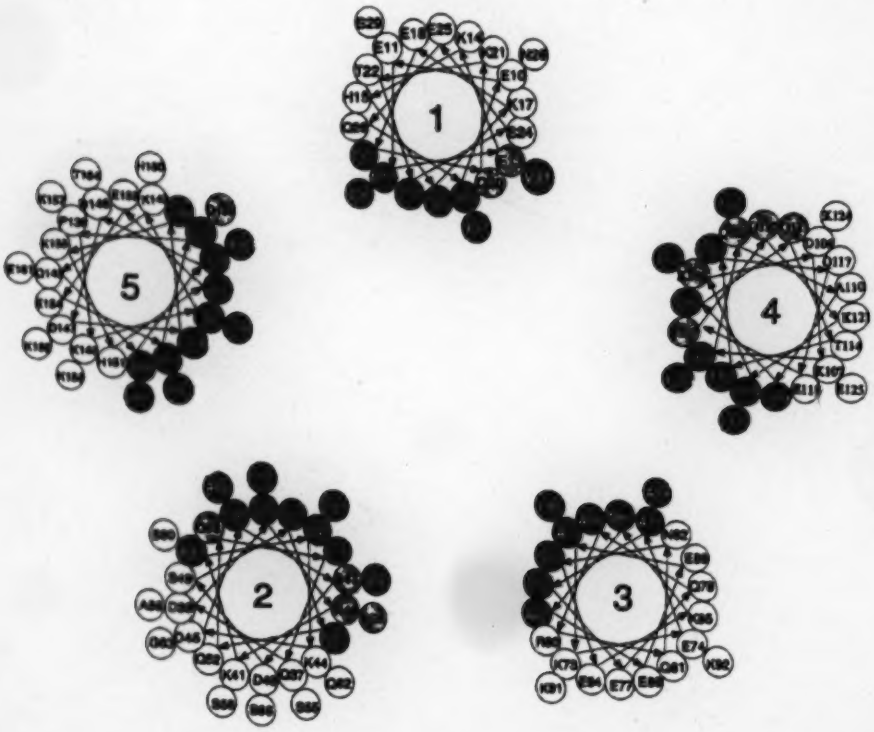

Figure 1-4. Helical wheel representation of *M. sexta* apoLp-III. The helical wheel diagram of the five-helix lipid-free bundle conformation of apoLp-III is based on the secondary structure of apoLp-III identified by the consensus NMR parameters described by Wang *et al.* (6). Residues making up the hydrophobic face (black circles) and hydrophilic face (clear circles) of each amphipathic helix are shown. Charged and polar residues (grey circles) located within the hydrophobic core of the helix bundle are indicated. This figure was reprinted from Wang *et al.* (6) with permission.

Indeed, each helix is amphipathic, with clearly defined hydrophobic and hydrophilic surfaces. The hydrophobic residues reside in the interior of the helix bundle, while charged residues lie on the surface of the bundle, facing the aqueous environment. Hydrophobic residues such as leucine, valine, isoleucine, phenylalanine and alanine are mainly responsible for the interhelical contacts among helices, consequently exerting a stabilizing force in terms of the globular fold of apoLp-III. Moreover, sequestration of the hydrophobic regions in the interior of the bundle explains the water solubility of apoLp-III in the absence of lipid. Charged residues make up 30% of the amino acids in apoLp-III (1). Ryan *et al.* (3) provide evidence for deprotonation of the 23 Lys residues above pH 10 and protonation of the side chain carboxylic groups of the 19 Glu residues and 9 Asp residues below pH 4. From this evidence, it was concluded that disruption of side chain charge-charge interactions may result in a notable loss of secondary structure. In fact, the presence of several oppositely charged residues that exist as *i, i+4* pairs suggests that side chain charge-charge interactions may represent a significant stabilizing effect in apoLp-III (3, 151). Interestingly, several charged residues (K105 and E13) and polar residues (Q20, N40, S47, Q53, S58, Q109, Q113, S119, Q120 and Q156) are buried within the hydrophobic core of the helix bundle, possibly contributing to the low intrinsic stability of the protein in the lipid-free state (6). Even though the amphipathic helices function as lipid-binding elements, it is critical that they exist within the context of the helix bundle when in the absence of lipid. In fact, several studies have shown that isolated peptides corresponding to helical segments in apoLp-III can neither adopt a helical conformation in buffer, nor are they able to interact with lipoprotein surfaces

(118, 152, 153). Therefore, interhelical contacts are essential for the maintenance and stabilization of the tertiary fold of the protein (153).

Determination of the solution structure of apoLp-III was a contributing step in the understanding of structure/function relationships of exchangeable apolipoproteins, especially with regard to protein-lipid interactions. Of particular interest, however, is the fact that *M. sexta* apoLp-III shares the same molecular architecture as both *L. migratoria* apoLp-III and the N-terminal domain of apoE, structures of which were solved almost a decade ago.

B) X-ray crystal structure of *L. migratoria* apolipophorin III

The cDNA sequence of *L. migratoria* apoLp-III has been determined (154). *L. migratoria* apoLp-III is a 161 amino acid protein lacking methionine, tyrosine and cysteine residues. Unlike *M. sexta* apoLp-III, *L. migratoria* apoLp-III is glycosylated, with carbohydrate moieties located at Asn 16 and Asn 83. Yet, despite a low 29% sequence identity (154), both *M. sexta* and *L. migratoria* apoLp-III are functionally equivalent (73). And, rather than amino acid sequence, the factor contributing to this common function appears to be the presence of amphipathic α-helical segments within the two proteins (154). *L. migratoria* apoLp-III was crystallized in a form suitable for high-resolution structural analysis (155) and the X-ray crystal structure was determined at a resolution of 2.5 Å (5). The protein has an overall length of 53 Å and a width of 22 Å. Similar to *M. sexta*, *L. migratoria* apoLp-III is a globular bundle consisting of five long up-and-down amphipathic α-helices connected by rather short loop regions.

C) X-ray crystal structure of the N-terminal domain of apolipoprotein E

At the same time, Wilson *et al.* (156) determined the X-ray crystal structure of the N-terminal domain of human apoE at 2.5 Å resolution. ApoE is a 299-amino acid exchangeable apolipoprotein that mediates the transport and uptake of cholesterol and lipid via a high affinity interaction with the LDL receptor (157). This protein is composed of a 22-kDa N-terminal domain (residues 1-191) and a 10-kDa C-terminal domain (residues 216-299) (115). The N-terminal domain is of particular interest since it houses the receptor binding region of apoE (158). Like apoLp-III, the N-terminal domain of apoE is related to other members of the apolipoprotein gene family (apoA-I, apoA-IV, apoC-I, apoC-II and apoC-III) (103, 145, 159). As well, like these other proteins, this domain contains internal sequence repeats that are predicted to form amphipathic α-helices (103, 159). CD spectroscopy also revealed that the protein is high in α-helical content (160). The fact that the N-terminal domain of apoE is monomeric in solution at high concentrations (115) enabled crystallographic analysis of this protein (161).

Similar to the apoLp-IIIs described above, the X-ray crystal structure revealed that, in the absence of lipid, the N-terminal domain of apoE (residues 23-164) contains elongated amphipathic α-helices linked by short loops. The four helices that make up the N-terminal domain form a globular helix bundle, with the hydrophobic face of the α-helices oriented inward and the hydrophilic faces exposed to the aqueous milieu. Leucine side chains occur about every seven residues and stabilize the interfaces between helix 1 and helix 4 and between helix 2 and helix 3. More than a third of the amino acids in this structure are charged, partially covering the surface of the helix bundle. Most of these charged residues participate in either intermolecular or intramolecular salt bridges in the

crystal structure. The combination of tight hydrophobic packing, leucine zippers and electrostatic interactions probably account for the high free energy of stabilization for this domain [ΔG^{H_2O} = ~10 kcal/mol (115, 162)].

D) X-ray crystal structure of apo Δ(1-43)A-I

Recently, *Borhani et al.* (163) determined the X-ray crystal structure of an N-terminal deletion mutant of human apoA-I at 4 Å resolution. The structure of apo Δ(1-43)A-I revealed an extended α-helical horseshoe-shaped or elliptical ring-like structure consisting of four truncated apoA-I molecules arranged as pairs of antiparallel dimers. The four molecules associate via the hydrophobic faces of their amphipathic helices to form a four-helix bundle. While the lipid-free structures of *M. sexta* apoLp-III, *L. migratoria* apoLp-III and the N-terminal domain of apoE are intramolecular helix bundles (5, 6, 156), the lipid-free structure of apo Δ(1-43)A-I is an intermolecular bundle.

1.8 LIPID-BOUND CONFORMATION OF APOLIPOPHORIN III

The lipid-free structures that are available to date indicate that apoLp-III (and the N-terminal domain of apoE) has its hydrophobic residues sequestered within the core of their helix bundle, while its hydrophilic residues face the aqueous environment. According to Segrest *et al.* (164), in the presence of lipid, these proteins must associate in such a way that the hydrophobic interior of the protein comes into contact with the hydrophobic surface of the lipid. Moreover, given the widespread occurrence of sequences in apolipoproteins with potential for forming amphipathic α-helices, numerous groups are studying the possible tertiary interactions and overall arrangements of secondary structural elements when such proteins are bound to lipid surfaces. The

remainder of this chapter will discuss the several pieces of evidence which have been obtained in support of the hypothesis that apoLp-III undergoes a conformational opening in the presence of lipid such that its hydrophobic interior is exposed to the lipid environment.

A) Behaviour of apoLp-III at an air-water interface

Kawooya *et al.* (2) performed monolayer studies which first shed light on the peculiar behaviour of *M. sexta* apoLp-III at an air-water interface. Their data revealed that apoLp-III could form a monolayer that can be alternately compressed and expanded. Upon compression of the monolayer, apoLp-III occupies a molecular area corresponding to 480 Å. But, at low surface pressures, apoLp-III covers an area of 3795 Å, the latter most probably representing the state of the protein when adsorbed to a fully-loaded lipoprotein particle. When apoLp-III was bound to phospholipid and DAG-coated polystyrene beads, it occupied a molecular area of 4300 Å. In general, when bound to a surface, a globular protein with a molecular weight of ~18, 000 Da can only occupy an area of about 2000 Å (2). Thus, it is evident that apoLp-III cannot maintain its lipid-free helix bundle structure when adsorbed to a lipid surface, but rather adopts a different conformation that allows the molecule to occupy the observed areas. On this account, the proposal arose that apoLp-III undergoes a conformational opening and thereby covers a larger area of lipid/water interface (2).

Wells *et al.* (51) studied the role of apoLp-III in *in vivo* lipoprotein interconversions in adult *M. sexta*. Their studies revealed that following injection of AKH, HDLp converts to LDLp due to loading of DAG. However, they noted the appearance of an "intermediate particle" during this loading process. They suggested that

this intermediate results from the fact that apoLp-III is added onto HDLp more rapidly than DAG, and that it changes its conformation on the surface as more DAG is added onto the lipophorin. From a series of calculations based on the number of apoLp-III molecules/particle as a function of surface area, molecular areas similar to those reported by Kawooya *et al.* (2) were obtained. Thus, their data suggested that initially apoLp-III binds with its minor axis parallel to the surface of the lipophorin particle. Further, as the surface of the particle expands during loading of DAG, apoLp-III unfolds to cover a greater area of hydrophobic surface.

B) "Conformational Opening" hypothesis

In biochemical terms, apoLp-III must exist in equilibrium between its lipid-free form and its lipophorin-bound form. In fact, the low stability of the helix bundle structure of apoLp-III is probably a requirement for its known reversible lipoprotein binding activity. Therefore, in order to readily convert from lipid-free state to a lipid-bound state and exert its biological function in the insect, both forms of apoLp-III must be thermodynamically similar. For this reason, it is unlikely that the protein adopts a completely different structure in the presence of lipid. Rather, it probably adopts a conformation that retains most of its secondary structural elements.

Breiter *et al.* (5) proposed a model for the lipid-bound conformation of apoLp-III, whereby helices 1, 2 and 5 move 180° away from helices 3 and 4 about "hinge" regions located in the loops between helices 2 and 3 and between helices 4 and 5 (**Figure 1-5**). Such an opening allows for exposure of the hydrophobic side chains of apoLp-III to the lipid surface.

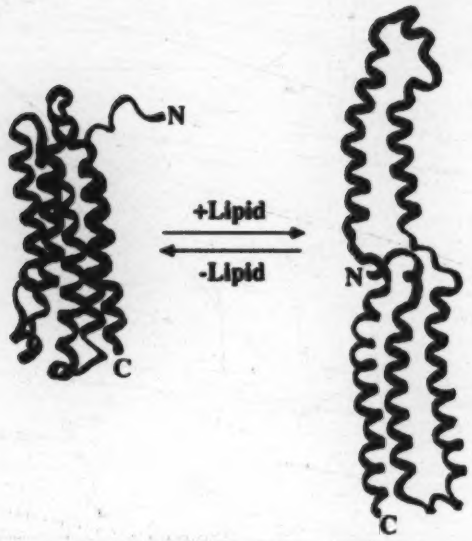

Figure 1-5. "Open conformation" model of apoLp-III upon lipid binding. In the presence of lipid, the apoLp-III helix bundle is proposed to open about hinge regions in such a way that helices 1, 2 and 5 move away from helices 3 and 4. This results in exposure of the hydrophobic residues that contact lipid. This conformation is based on a proposal presented by Breiter *et al.* (5).

A similar conformational opening for the N-terminal domain of apoE is proposed by Weisgraber (141) and will be discussed briefly in the Discussion section (Chapter 7).

C) Discoidal complexes: a model protein-lipid complex

A common property shared by all soluble apolipoproteins is their ability to transform phospholipid vesicles into discoidal-shaped particles. In most cases, the phospholipid in the discoidal complex is organized in a bilayer, with the apolipoprotein oriented around the periphery of the discoidal complexes (165, 166). Unless otherwise specified, the experiments described below use dimyristoylphosphatidylcholine (DMPC) as the phospholipid component of the complexes. The DMPC/apoLp-III complex serves as an useful model for studies involving the lipid-bound conformation of apoLp-III.

Electron micrographs revealed that the turbid suspension obtained by sonication of DMPC contains vesicles with diameters ranging from 30 to 137 nm. However, upon incubation with apoLp-III, the vesicles transform into a clear solution of discoidal complexes that are uniform in size and shape (167). On average, the disc structures are 18.5 nm in diameter with a thickness of 4.8 nm. The molecular mass of these complexes is calculated to be ~642,000 Da based on flotation equilibrium experiments. Compositional analysis revealed a phospholipid:protein ratio of 102:1. Using dimethyl suberimidate as a crosslinking agent, Wientzek *et al.* (167) determined that up to 6 molecules of apoLp-III are bound around the periphery of the disc complexes.

Orientation of apoLp-III around discoidal complexes. The amphipathic α-helices of apolipoproteins have been suggested to orient themselves around the periphery of the phospholipid bilayer, thus protecting the hydrophobic fatty acyl chains from the aqueous medium. However, the orientation of the helices on the edge of the disc has been a subject of constant debate. While some groups believe apolipoproteins align with their helices parallel to the fatty acyl chains (168, 169), others believe that helices align perpendicular to the fatty acyl chains [(165, 170, 171). Based on the dimensions of apoLp-III obtained by X-ray crystallography (5), as well as the results of their crosslinking studies, Wientzek *et al.* (167) proposed a model that supports the hypothesis presented by Breiter *et al.* (5) which suggests the opening of the protein about hinge regions located between helices 2 and 3 and between helices 4 and 5 (Figure 1-5). This model depicts the α-helices of elongated apoLp-III molecules binding around the periphery of the disc perpendicular to the fatty acyl chains of the phospholipids.

The perpendicular orientation of apoLp-III around the disc complex is further validated by evidence obtained from polarized Fourier transform attenuated total reflection infrared (ATR-FTIR) spectroscopy. Data was obtained from DMPC/apoLp-III complexes spread onto a germanium plate (172). Aside from determining that apoLp-III is highly α-helical in the presence of lipid, ATR-FTIR data show that the α-helices of apoLp-III orient parallel to the germanium plate. In other words, the α-helices are parallel to the lipid bilayer and perpendicular to the acyl chains of the phospholipid.

D) Initiation of apoLp-III-lipid interactions

Although it is generally accepted that the amphipathic α-helix motif is responsible for the interaction of exchangeable apolipoproteins with hydrophobic lipid surfaces, the molecular mechanisms involved in initiating this interaction are not well-resolved. To date, two proposals have been put forth with regard to the recognition and initiation of binding of apoLp-III with lipid: one involves ionic interactions, while the other involves hydrophobic interactions.

*i) **Initiation by ionic interactions.*** α-Helices such as those found in exchangeable apolipoproteins have been shown to interact with phospholipids (173, 174). Using a combination of differential scanning calorimetry and ^{31}P-NMR, Zhang *et al.* (175) investigated the interaction of apoLp-III with acidic, zwitterionic and uncharged lipids. Although it has been shown that apoLp-III has difficulty binding to lipoprotein particles whose surface is almost exclusively covered with phospholipid (128, 176), results of the studies of Zhang *et al.* (175) prompted them to propose that initial interaction of apoLp-III with lipids may occur via ionic interactions between charged residues on the protein exterior and the phosphate moieties of the phospholipid head

groups on the lipoprotein surface. Such an interaction would bring the protein into close proximity to the hydrophobic lipid surface (175). This, in turn, triggers a conformational change within apoLp-III, allowing exposure of its hydrophobic residues to the lipid surface.

The polar faces of the amphipathic helices of *M.sexta* apoLp-III possess many oppositely charged amino acids [27 negatively charged and 29 positively charged residues in its primary sequence (1)] that exist in *i*,(*i*+4) sequence configuration (3). It has been suggested that such a configuration has the potential to form intramolecular salt bridges which serve as a stabilizing force for maintenance of secondary structure (151) and, in the case of apoLp-III, confer stability to the helix bundle conformation (3). To assess the role of charged amino acid side chains in the initiation of lipid interaction, carboxylate side chains of apoLp-III were amidated, while lysine side chains were acetylated (177). CD analysis revealed that both modified proteins lose helical structure. Both acetylated and amidated apoLp-IIIs are non-functional with respect to lipoprotein binding and transformation of DMPC vesicles into discoidal complexes. Unfortunately, the data from this investigation remain inconclusive since the extent of protein modification may have been too extreme for the nature of these studies.

ii) Initiation by hydrophobic interactions. *In vivo*, DAG is loaded onto pre-existing HDLp particles, thus giving rise to LDLp particles. The appearance of DAG at the lipophorin surface disrupts phospholipid organization such that DAG molecules emerge at the surface monolayer, intercalating between phospholipid molecules to generate unstable hydrophobic gaps. Appearance of these new hydrophobic patches triggers recruitment and binding of up to 16 apoLp-III molecules per LDLp particle (51),

all in a manner whereby apoLp-III binds as a function of DAG content (51, 178, 179). Molecular modeling has shown that the hydrophobic face of an amphipathic α-helix from apoLp-III can fit between phospholipid head groups in the gap created by intercalation of DAG (127), resulting in stabilization of the lipophorin structure. Therefore, partitioning of DAG into the surface monolayer may represent the key step in initiating binding of apoLp-III to lipoprotein surfaces.

Soulages *et al.* (179) used surface plasmon resonance spectroscopy to investigate the mechanism of binding of *M. sexta* apoLp-III to egg phosphatidylcholine bilayers as a function of DAG concentration. Binding of apoLp-III reaches saturation at 2 mol% DAG in the bilayer. Under these conditions, apoLp-III forms a closely packed monolayer 55 Å thick, wherein each molecule occupies 500 Å at the membrane surface, the latter value being in good agreement with data previously obtained by surface monolayer balance studies (2). All together, this data is consistent with the conformational opening model. Following the appearance of hydrophobic defects caused by the appearance of DAG at the lipoprotein surface, the helix bundle orients on the lipid surface with its long axis normal to the membrane surface and parallel to the fatty acyl chains of the phospholipid monolayer.

Recognition by the "hydrophobic sensor". Based on the three-dimensional crystal structure of *L. migratoria* apoLp-III, Breiter *et al.* (5) noted that the loop regions connecting helices 1 and 2 and helices 3 and 4 (both at one end of the helix bundle) possess relatively exposed hydrophobic residues. Moreover, sequence alignment of apoLp-IIIs from different species indicates the presence of conserved leucine residues within these loops (4). This led to the proposal of the "hydrophobic sensor" hypothesis:

the end bearing the hydrophobic residues (and located directly opposite to the end which contains the putative hinge regions about which the helix bundle is postulated to open) would initiate contact with the hydrophobic gaps that develop on the lipoprotein particle (5). This initiation step would be followed by conformational opening of the protein in order to expose its hydrophobic interior, thus allowing it to spread along the lipid surface.

In order to test this "sensor" hypothesis, Weers *et al.* (180) used site-directed mutagenesis to substitute hydrophobic leucine residues within the proposed "sensor" with positively-charged arginine. Addition of the mutant apoLp-IIIs to phospholipid vesicles [DMPC or dimyristoylphosphatidylglycerol (DMPG)] caused rapid clearance of vesicle turbidity due to formation of discoidal complexes. It should be pointed out that the triple Leu → Arg mutant displayed the highest clearance rate compared to wild-type and the other single Leu → Arg mutant apoLp-IIIs when incubated with DMPG, suggesting that charge effects may be involved in facilitating electrostatic attraction of apoLp-III to the negatively charged DMPG vesicle surface. This observation is, in fact, in good agreement with previous studies which show that apoLp-III binds strongly to negatively charged lipid surfaces (175). In contrast, all mutant apoLp-IIIs displayed an impaired ability to initiate a binding interaction with spherical LDL particles. This contradictory behaviour can be explained by the fundamental difference in the mode of interaction of an apolipoprotein with either phospholipid vesicles or spherical lipoprotein particles. Unlike with phospholipid vesicles, apolipoprotein binding to lipoprotein surfaces is induced by the appearance of hydrophobic DAG in the surface monolayer. Therefore, the loss of hydrophobic character in the Leu → Arg mutant apoLp-IIIs may affect the

ability of these proteins to initiate interaction with hydrophobic binding sites generated on the surface of the modified LDL.

These results corroborate data obtained by Narayanaswami *et al.* (181) for *M. sexta* apoLp-III. A short helix, namely helix 3', was first identified following three-dimensional heteronuclear NMR studies on the secondary structure and global fold of *M. sexta* apoLp-III (6). Helix 3' is a 6-residue α-helix (PDVEKE) that is located outside of the helix bundle, providing a link between helices 3 and 4. Alignment of the primary sequence of *M. sexta* apoLp-III with the sequences available from other Lepidopteran species indicates that the residues constituting helix 3' are highly conserved (70-80% identity) (181). The relatively solvent-exposed nature of helix 3', along with the presence of a single hydrophobic residue in the middle of its sequence led to the hypothesis that this short helix may be responsible for recognition and initiation of apoLp-III binding interactions with lipid (6). In an effort to determine the importance of this short helix, the authors replaced helix 3' with a β-turn (181). Although NMR studies reveal that the global fold of this mutant protein is not disrupted, it is quite evident that binding of the mutant apoLp-III to lipoproteins was defective. To dissect the mode of lipid interaction in more detail, V97 and its flanking charged residues, D96 and E98, were mutated to polar, uncharged residues. Mutagenesis of D96 and E98 had no effect on lipid binding. In contrast, mutation of V97 impaired the ability of this protein to compete with wild-type apoLp-III for binding sites created on the lipoprotein surface. Taken together, the data support the notion that V97 within helix 3' is required for initiation of the interaction of apoLp-III with hydrophobic surfaces.

In a recent study, Kahalley *et al.* (182) evaluated the importance of a conserved leucine residue (Leu30) in the binding of *M. sexta* apoLp-III to DMPC discoidal complexes. Following mutagenesis of this Leu30 to Cys, their results revealed that the mutant protein behaved identically to wild-type apoLp-III in terms of its lipid binding activity, thus suggesting that this conserved residue is not absolutely required for binding of apoLp-III to lipid surfaces. This result is in good agreement with results from the helix 3' study (181), since Leu30 is located at the end of helix 1 and opposite to the end of the molecule that appears to be essential for initiating lipid interaction.

Although we can not rule out the possibility that a combination of ionic and hydrophobic interactions are required for lipid interaction, the data agree with the notion that recognition and initial binding precede conformational opening of the helix bundle and formation of a stable binding interaction. Interestingly, a similar short helix (9 residues in length, spanning amino acids 44-53) is present in the N-terminal domain of apoE (156), connecting helices 1 and 2. Sequence analysis suggests that this region of apoE is the most conserved among species (141). As such, further studies are required to see if this mechanism of initiation is applicable to helix bundle apolipoproteins in general.

iii) Correlation of binding activity with a partially folded conformation.

Recent evidence showed that the lipid binding activity of *M. sexta* apoLp-III correlates with a partially folded conformation (183). Upon decreasing the pH from 8.0 to 4.0, binding of apoLp-III to DMPC discs increases approximately 40-fold. On the basis of this and other data, the authors proposed that apoLp-III can form a folding intermediate below pH 7. Near-UV spectral changes associated with changes in pH indicated that the

transition from a native to an intermediate state formation was accompanied by a loss of the packing constraints of Tyr145. Moreover, UV absorption spectroscopy denotes hydration of Tyr145 and approximately four Phe residues during formation of this intermediate state. The authors suggest that it is the internal hydration state of apoLp-III that increases its lipid binding activity. In fact, in many ways, this partially folded intermediate resembles a molten globule-like state, a conformation that has been previously described for human apoA-I (184). A more detailed role for this intermediate in the biological activity of exchangeable apolipoproteins remains to be determined.

E) Spectroscopic evidence for a conformational change in apoLp-III

i) Studies by circular dichroism spectroscopy. Using DMPC disc complexes as a model system for a lipid surface, Wientzek *et al.* (167) gathered several pieces of data in support of a conformational change in apoLp-III upon interaction with lipids. DMPC/apoLp-III complexes were examined by far-UV CD. When suspended in buffer alone, or in the presence of 50% trifluoroethanol (TFE), a known helix-inducing solvent, apoLp-III on the disc complexes had maximized its α-helical content. These results are in sharp contrast to data obtained earlier for lipid-free apoLp-III, where addition of 50% TFE increases the α-helical content from 60% to 81% (3). Therefore, it appears that binding to DMPC allows apoLp-III to adopt a stable conformation that has maximized its α-helical content. This lipid-induced stabilization has been reported for other mammalian apolipoproteins such as apoA-I (109), apoA-IV (185) and apoC-II (186).

DMPC/apoLp-III complexes were subsequently subjected to denaturation by GdnHCl. While lipid-free apoLp-III is quite sensitive to denaturation [midpoint of 0.4 M

GdnHCl; (3)], apoLp-III in complex with lipid seems quite resistant to denaturation. A biphasic pattern of denaturation is observed with midpoints of denaturation at 2.2 M and 3.7 M GdnHCl (167). The first midpoint may reflect a partial unfolding of the protein with full maintenance of secondary structure while on the lipid surface; the second midpoint may reflect complete denaturation of the protein following dissociation from the lipid. The two midpoints of denaturation corroborate results obtained by Reijngoud *et al.* (114) who demonstrated that denaturation of DMPC/apoA-I complexes is a two-step process.

Interesting CD spectra were obtained from *L. migratoria* apoLp-III in order to study conformational changes that accompany lipid association. *L. migratoria* apoLp-III lacks methionine, cysteine and tyrosine, yet contains two phenylalanine and two tryptophan residues (154). In the absence of lipid, a near-UV CD spectrum of locust apoLp-III reveals several well-resolved extrema which are assigned to the Phe and Trp residues (187). The crystal structure shows that side chains of both these residues orient toward the interior of the helix bundle (5). However, in complex with DMPC, the same extrema are reversed in sign and shifted to longer wavelengths, consistent with the concept that the bundle has opened and helical segments have repositioned themselves in such a way that the aromatic residues are now exposed to a less polar environment (i.e. DMPC). It is worth noting that similar observations from near-UV spectra have been made with human apoA-I in association with lipid, where the peaks observed for HDL are reversed in sign and shifted as compared to the peaks observed for lipid-free apoA-I (188).

ii) Fluorescence studies. Using the single tyrosine residue of *M. sexta* apoLp-III as an intrinsic probe, fluorescence studies were performed on DMPC/apoLp-III complexes. As mentioned earlier, Ryan *et al.* (3) have shown that tyrosine fluorescence emission in lipid-free apoLp-III is significantly quenched; however, upon GdnHCl denaturation, tyrosine fluorescence is enhanced. Tyrosine fluorescence is also significantly enhanced when apoLp-III is bound to DMPC discs. The increase in quantum yield of the lone tyrosine (0.015 for lipid-free apoLp-III and 0.110 for apoLp-III in complex with DMPC) without a change in fluorescence lifetime [7 ns; (121)] is in agreement with the enhancement in tyrosine fluorescence (167). Similar increases are observed when apoLp-III is in complex with 0.4% lysophosphatidylcholine mixed micelles or when apoLp-III is in the presence of 50% TFE (189). Further, both native and recombinant apoLp-III undergo a 7-to-10-fold enhancement of tyrosine fluorescence upon association with dodecylphosphocholine (119).

Due to the absence of tyrosine residues, fluorescence studies were performed on *L. migratoria* apoLp-III using the two tryptophans as the intrinsic probes (187). Trp115 is localized in the middle of the fourth helix, while Trp130 is found within the loop connecting helices 4 and 5 (5). Lipid-free locust apoLp-III emits maximal Trp fluorescence at 347 nm (excitation wavelength of 280 nm). However, in complex with DMPC, the Trp fluorescence emission maximum is blue-shifted to 321 nm, indicating that the Trp residues now reside in a more hydrophobic environment. Other apolipoproteins such as *Bombyx mori* apoLp-III (190), human apoC-I (191), human proapoA-I (192) and human apoE (162, 193) share similar observations. Weers *et al.* (194) took their studies one step further by creating two different locust apoLp-III

mutants, each possessing a single Trp residue. Major differences are found in the fluorescence properties of both single-Trp mutants in the lipid-free state. However, lipid association results in both fluorophores reorienting to a similar lipid environment. More importantly, this study demonstrated that the loop region containing the Trp residue interacts with the hydrophobic surface in a manner similar to the fourth helix that contains the other Trp residue. Taken together, fluorescence data are consistent with a conformational change occurring upon the complexation of apoLp-III with lipid.

iii) FTIR studies. Using hydrogen/deuterium exchange monitored by ATR-FTIR spectroscopy, Raussens *et al.* (195) endeavoured to study lipid-free and DMPC-bound apoLp-III in terms of their dynamically variable domains. Hydrogen/deuterium exchange is related to the solvent accessibility of the amide groups of the protein, and hence, the tertiary structure of the protein is based on stability of secondary structure elements. Therefore, this technique enables one to identify submolecular motional domains including i) fast exchanging protons of the solvent-exposed surface of the protein; ii) intermediate exchanging protons of the flexible (loop) regions partially buried in the protein; and iii) slowly exchanging protons buried in the protein core, formed by the most rigid clusters of amino acids [reviewed in (196)]. In lipid-free apoLp-III, 36, 12 and 52% of the total residues contribute to slow, intermediate and fast exchanging populations, respectively. However, in DMPC-bound apoLp-III, the respective distribution of these residues is 20, 16 and 64%. This is rather interesting, since 25 residues move from the core to a more solvent-accessible domain, thus, representing a 12% increase in the number of exposed residues. Therefore, a vast tertiary structural reorganization of the protein appears to take place, whereby apoLp-III loses its

tertiary fold in order to interact with lipids. This conformational adaptation likely maintains the helix boundaries present in the lipid-free globular protein, but involves a repositioning of the helical orientation such that helix-helix interactions, known to stabilize the bundle conformation, are replaced by helix-lipid interactions.

F) Disulfide bond engineering: further evidence for a conformational change

Narayanaswami *et al.* (197) pursued their testing of the conformational opening hypothesis and tethered the apoLp-III helix bundle via a disulfide bond. Site-directed mutagenesis was used to introduce cysteine residues into apoLp-III (which otherwise lacks cysteine) at the N40 (helix 2) and L90 (helix 3) positions. These two sulfhydryls are within disulfide bonding distance in the globular helix bundle. It was postulated that this disulfide bond would hamper opening of the helix bundle about hinge regions by preventing helices 1, 2 and 5 from moving away from helices 3 and 4. Indeed, under oxidizing conditions, the tethered protein is unable to bind to lipid in lipoprotein binding assays (135, 136). However, reduction of the disulfide bond restores full lipoprotein binding activity. Certainly, this set of experiments provides clear, direct experimental evidence that conformational opening of the apoLp-III helix bundle is an essential step for either initiation or a stable interaction with lipoprotein surfaces.

1.9 SPECIFIC AIMS

M. sexta apoLp-III is a prototype exchangeable apolipoprotein that reversibly associates with lipoprotein particles. The dual existence of this protein in water-soluble and lipid-bound forms suggests that apoLp-III possesses an inherent conformational adaptability. Contrary to most vertebrate apolipoproteins, apoLp-III shows no tendency to self-

associate in solution and this property has allowed extensive biophysical characterization of the protein in the lipid-free state. However, there still exists a gap in our understanding of the lipid-bound conformation of apoLp-III, as well as the mechanistic details involved in the interaction of such proteins with lipid surfaces.

Given the structural information available from X-ray crystallography and NMR studies of apoLp-III from different species in the absence of lipid, the aim of the studies in this thesis is to gain a better understanding of the tertiary organization of this protein in the lipid-bound state.

In the following chapters, I have combined site-directed mutagenesis with an efficient bacterial expression system and used NMR and fluorescence spectroscopy to probe the lipid-bound conformation of *M. sexta* apoLp-III. Each of the following chapters describes experiments which have been designed to reach a very specific goal — each relating to the lipid-bound conformation and arrangement of apoLp-III in different lipid systems. Specifically,

i) To monitor structural changes in specific ^{15}N-amino acid labeled apoLp-III samples upon titration with a micelle-forming lipid (dodecylphosphocholine) using ^{1}H-^{15}N heteronuclear single quantum correlation (HSQC) NMR spectroscopy (Chapter 3);

ii) To investigate apoLp-III helix topography and spatial arrangement in phospholipid disc complexes and intact spherical lipoprotein particles using fluorescence quenching techniques (Chapters 4 and 6);

iii) To address lipid-binding-induced helix repositioning in apoLp-III and the relative orientation of lipid-bound apoLp-III in model phospholipid disc complexes by exploiting the unique excimer fluorescence properties of N-(1-pyrene)maleimide (Chapters 5 and 6);

iv) To determine the relative orientation of apoLp-III molecules around the periphery of phospholipid bilayer complexes using pyrene excimer fluorescence spectroscopy (Chapter 5).

CHAPTER 2

Materials and Methods

2.1 MATERIALS

$^{15}NH_4Cl$, ^{15}N-Leucine, ^{15}N-Glycine, ^{15}N-Valine and ^{15}N-Lysine were purchased from Cambridge Isotope Laboratories (Andover, MA). ^{13}C-C_6-Glucose and ^{2}H-dodecylphosphocholine were obtained from Isotec. Inc. (Miamisburg, OH). Unlabeled amino acids, trifluoroethanol, dimyristoylphosphatidylcholine, dimethyl sulfoxide, dithiothreitol and phospholipase-C from *Bacillus cereus* were obtained from Sigma Chemical Co. (St. Louis, MO). 2,2'-dithiodipyridine (Aldrithiol™), 5-doxyl-stearic acid and 12-doxyl-stearic acid spin labels were obtained from Aldrich Chem. Co. (Milwaukee, WI). QuikChange™ Site-Directed Mutagenesis kit, XL1-Blue cells and *Pfu* Turbo polymerase were from Stratagene (La Jolla, CA). *Afl* III, *Nar* I and *Dpn* I were bought from New England Biolabs (Beverly, MA). N-(1-pyrene)maleimide and tris-(2-cyanoethyl)phosphine were purchased from Molecular Probes, Inc. (Eugene, OR). Isopropyl β-D-thiogalactopyranoside was bought from Chemica Alta (Edmonton, Canada). *Bis*-maleimidohexane was acquired from Pierce (Rockford, IL). Sepharose CL-6B, P6 Biogel and G75 column matrices were from Pharmacia (Uppsala, Sweden) and pET expression vector was from Novagen (Madison, WI).

2.2 METHODS

Analytical procedures

Sodium dodecyl sulfate polyacrylamide gel electrophoresis (SDS-PAGE) was performed according to Laemmli (198) on 12% or 18% acrylamide gels run at 30 mA constant current and stained with Coomassie Brilliant Blue R-250. In order to view fluorescence on gels under a UV-illuminator, the Coomassie staining protocol was omitted. Protein

concentrations were determined by the bicinchoninic acid assay (Pierce Chemical Co., Rockford, IL) while phosphatidylcholine concentration was determined using an enzyme-based colorimetric assay (Wako Pure Chemical Industries, Ltd. Osaka, Japan).

Site-directed mutagenesis

Site-directed mutagenesis of apoLp-III was performed as described earlier using synthetic oligonucleotides carrying specific mutations in the apoLp-III gene (197). In one mutation, the codon for Asn 40 [at the N-terminus of helix 2, close to the polar/nonpolar interface (6)] was replaced by the codon for Cys (N40C). In another experiment, the codon Leu 90 (at the C-terminus of helix 3, in the centre of the nonpolar face of the amphipathic helix) was replaced by the codon for Cys (L90C). The genes encoding full length apoLp-III bearing the mutations were cloned into the pET vector (119). A double-cysteine mutation, N40C/L90C, was created by ligation of the *Afl* II/*Hin*d III fragment bearing the L90C mutation into the *Afl* II/*Hin*d III-digested apoLp-III-pET vector containing the N40C mutation (197). All mutations were confirmed by dideoxynucleotide chain termination sequencing (199). A8C-apoLp-III, A138C-apoLp-III and A8C/A138C-apoLp-III were created by site-directed mutagenesis using the QuikChange™ system, with minor changes. Forward and reverse primers containing the desired mutations, each complementary to opposite strands of the pET vector containing wild-type apoLp-III plasmid, were extended by temperature cycling using *Pfu* Turbo polymerase [5 min at 96 °C, followed by 17 cycles of 96 °C (1 min), 58 °C (2 min), 72 °C (12 min)]. The reaction mixture also contained 5% dimethyl sulfoxide (v/v) and 50 mM $MgSO_4$. In order to digest the methylated parental DNA and select for the synthesized DNA containing the mutations, the amplified product was digested with *Dpn* I for 2 h at

37 °C and washed with sterile water using 30K Microsep™ Pall Filtron centrifugal concentrators (Pall Gelman Laboratory, Mississauga, ON). The product was transformed into XL1-Blue cells and the presence of the desired mutation in each plasmid was confirmed by restriction digest analysis (loss of *Afl*III site for A8C-apoLp-III and loss of *Nar*I site for A138C-apoLp-III). A8C/A138C-apoLp-III was created as described above using the A138C mutagenic primers and the pET-vector containing the plasmid for A8C-apoLp-III. The presence of both cysteine mutations was confirmed by the simultaneous loss of *Afl*III and *Nar*I sites during restriction enzyme digests. All apoLp-III/pET vector constructs were transformed into *Escherichia coli* BL21(DE3) cells for bacterial expression.

Bacterial expression apoLp-III

Expression of apoLp-III. Recombinant wild-type and cysteine-containing mutant apoLp-IIIs were expressed in *Escherichia coli* BL21(DE3) cells and purified as described earlier (119). Briefly, overnight cell cultures, grown in 2X yeast tryptone media, were diluted 1:100 (v/v) into M9 minimal media (200) supplemented with 2 mM $MgSO_4$, 13 mM glucose and 0.1 mM $CaCl_2$, and cultured at 37 °C. After 4 - 5 hours, when the OD_{600} reached 0.6 - 0.8, protein expression was induced by the addition of isopropyl β-D thiogalactopyranoside (IPTG; 1 mM final concentration) and the cells were incubated at 30 °C for another 4-5 hours. The cell culture was then centrifuged and the supernatant concentrated by ultrafiltration until the final volume of the medium was less than 50 ml. The concentrated medium was dialyzed against deionized water for 48 h and lyophilized.

Expression of isotopically-labeled apoLp-III. All isotopically-labeled apoLp-III samples were grown in M9 minimal medium containing a ^{15}N-labeled compound as the sole nitrogen source. Specifically, isotope-labeling of apoLp-III used M9 minimal media with $^{15}NH_4Cl$ for ^{15}N-uniform labeling; $^{15}NH_4Cl/^{13}C_6$-glucose for ^{15}N-/^{13}C uniform labeling; ^{15}N-leucine/$^{14}NH_4Cl$ for ^{15}N specific backbone nitrogen labeling; or a given ^{15}N-labeled amino acid of interest (^{15}N-leucine, ^{15}N-valine, ^{15}N-lysine, ^{15}N-glycine) together with unlabeled aliquots of the other 19 amino acids. The remainder of the expression protocol was as outlined above, with the exception that apoLp-III-expressing cells were grown at 30 °C before and after induction with IPTG.

Purification of apoLp-III

Wild-type, isotope-labeled apoLp-IIIs, N40C-, L90C- and N40C/L90C-apoLp-IIIs were purified by reversed phase HPLC as described previously (197). However, A8C-, A138C- and A8C/A138C-apoLp-IIIs were purified by gel filtration chromatography using a G75 matrix and lyophilized. Electrospray mass spectrometry (VG quattro electrospray mass spectrometer, Fisons Instruments, Manchester, UK) was used to characterize the molecular mass, purity and isotope-enrichment level of isolated recombinant apoLp-IIIs.

NMR spectroscopy

Protein samples for NMR experiments were dissolved in 95% H_2O/5% D_2O containing 250 mM phosphate, pH 6.4, and 0.5 mM NaN_3 (6). 2,2-Dimethyl-2-silapentane-5-

sulfonate (DSS) was used as an internal standard for proton chemical shifts. All NMR samples contained 0.1-0.2 mM ^{15}N-labeled apoLp-III. Per-deuterated dodecylphosphocholine (DPC) was dissolved in the same buffer at a concentration of 25 μg/μl. NMR experiments were performed on a Varian INOVA 500 NMR spectrometer equipped with four channels, a pulsed-field gradient triple resonance probe with an actively shielded z gradient and a gradient amplifier unit. Spectra were processed on a SUN workstation using VNMR software. Two-dimensional ^{1}H-^{15}N HSQC spectra (201) were acquired with the following number of complex points and acquisition times: F1(^{15}N) 128, 91.5 ms, F2(^{1}H) 512, 73 ms, 8-32 transients. The spectral widths of ^{1}H-^{15}N HSQC were 1398.8 Hz in F1 (^{15}N) and 7000 Hz in the F2 (^{1}H) dimension. Carrier positions used in ^{1}H-^{15}N HSQC spectra were as follows: ^{15}N, 119.0 ppm: ^{1}H, 4.71 ppm. Lipid titrations were carried out by sequential addition of aliquots of DPC in buffer until the apoLp-III:DPC molar ratio was > 1:60. A ^{1}H-^{15}N HSQC spectrum was recorded at each DPC titration point and analyzed to monitor amino acid chemical shift changes. Titration curves were generated by plotting the amide proton chemical shift of a given amino acid as a function of DPC concentration.

Pyrene-labeling of recombinant apoLp-III

To label the cysteine mutants with N-(1-pyrene)maleimide, the probe was solubilized in dimethyl sulfoxide (10 mM final concentration) and incubated in a 2:1 molar ratio with either N40C-, L90C-, A8C- or A138C-apoLp-III (in 100 mM sodium phosphate, pH 7.5) for 2.5 h at 37 °C in the dark. To label the double-cysteine mutants with pyrene, N40C/L90C-apoLp-III or A8C/A138C-apoLp-III was first incubated with a 2-fold molar

excess of dithiothreitol for 2 h at 37° C in order to maintain the sulfhydryls in a reduced state and avail them for labeling. Pyrene maleimide in dimethyl sulfoxide was incubated with the double-cysteine mutant apoLp-IIIs (in 100 mM sodium phosphate, pH 7.5) in the dark for 2.5 h at 37° C at a labeling ratio of 4 mol pyrene:1 mol protein. Unbound pyrene and pyrene-dithiothreitol complexes were removed by gel filtration chromatography using a P6 Biogel matrix. The proteins were analyzed by SDS-polyacrylamide gel electrophoresis and visualized under UV-light. Electrospray mass spectrometry was performed to confirm stoichiometry of labeling.

Structural characterization of pyrene-labeled apoLp-IIIs

The effect of pyrene modification on the secondary structure content of apoLp-III (in 50 mM sodium phosphate, pH 7.0) was evaluated by CD spectroscopy. Spectra were collected on a Jasco J-720 spectropolarimeter at 25 °C as previously described (3). The instrument was routinely calibrated with ammonium *d*(+)-10-camphor sulfonate at 290.5 and 192 nm and with *d*(-)-pantoyllactone at 219 nm. Protein concentrations were between 0.5 to 1.0 mg/mL. Guanidine hydrochloride (GdnHCl) samples were incubated 20 h prior to recording spectra to allow samples to attain equilibrium. Secondary structure content was analyzed using the Contin program of Provencher and Glöckner (108).

Functional characterization of pyrene-labeled apoLp-IIIs

The functional properties of the apolipoproteins were characterized by their ability to bind to lipoproteins as described elsewhere (197). Briefly, human LDL (50 μg of LDL

protein in 50 mM Tris-HCl, pH 7.5, containing 150 mM NaCl and 2 mM $CaCl_2$) was incubated with 160 milliunits of phospholipase C in the presence or absence of 50 μg of wild-type or pyrene-labeled apolipoproteins (135). All incubations (final volume of 250 μL) were carried out at 37 °C. Hydrolysis of the polar head groups of the LDL monolayer by phospholipase C generates a hydrophobic surface of diacylglycerol, thus causing aggregation with other LDL particles as monitored by an increase in absorbance at 600 nm. The presence of a functional exchangeable apolipoprotein inhibits LDL aggregation by binding to the hydrophobic surface of the modified LDL. Control incubations lacking apoLp-III or phospholipase C were also included.

The functionality of pyrene-labeled apoLp-IIIs was also assessed by their ability to transform DMPC vesicles into discoidal complexes. Preparation of DMPC discoidal complexes and their analysis by electron microscopy are described in the sections below.

Preparation of lipoprotein-associated apoLp-III

Lipoprotein-associated wild type, pyrene-N40C- or pyrene-L90C-apoLp-III was prepared according to Liu *et al.* (135). Wild type, pyrene-N40C- or pyrene-L90C-apoLp-III (1.5 mg) were incubated with human LDL (2 mg protein) in the presence of 6 U phospholipase-C (from *Bacillus cereus*) for 30 min at 37 °C. Unbound protein was separated by Sepharose CL-6B gel filtration chromatography.

Preparation of apoLp-III/DMPC complexes

DMPC vesicles were transformed into discoidal complexes by addition of recombinant wild-type or pyrene-labeled mutant apoLp-III as described (167). Briefly, apoLp-III

samples were dissolved in 100 mM sodium phosphate buffer, pH 7.5 and added to an equal volume of DMPC vesicles (lipid:protein ratio of 2.5:1(w/w) or molar ratio of 70:1) and incubated at 24 °C for 18 h. Phospholipid disc complexes with bound apoLp-III were isolated and separated from unbound apoLp-III by density gradient ultracentrifugation. The final lipid:protein molar ratio was ~150:1.

Electron microscopy

Samples for electron microscopy were adsorbed to carbon-coated grids, rinsed three times with buffer (10 mM Tris, 10 mM NaCl and1.5 mM $MgCl_2$) and negatively stained with 2% sodium phosphotungstate, pH 7.0, for 10 s. Grids were photographed in a Philips EM420 operated at 100 kV.

Crosslinking of N40C/L90C-apoLp-III and A8C/A138C-apoLp-III

Lipid-free N40C/L90C-apoLp-III and DMPC-bound N40C/L90C-apoLp-III were reduced with a 2-fold excess of 25 mM tris-(2-cyanoethyl)phosphine (in dimethyl sulfoxide) for 2 h at 37 °C. Phosphate-buffered saline (pH 7.0) and 25 mM *bis*-maleimidohexane (final concentration 1.25 mM) were added and the reaction mixtures (final volume of 25 µL) were incubated overnight at room temperature. Samples were dried under vacuum, resuspended in non-reducing sample treatment buffer, electrophoresed on a precast 8-25% SDS gradient gel on the PhastSystem (Amersham Pharmacia Biotech) and visualized using the Phast® silver staining protocol. Lipid-free A8C/A138C-apoLp-III were crosslinked using the same protocol for lipid-free N40C/L90C-apoLp-III. In this case, the final volume was kept at 150 µL and the

presence of crosslinks was examined by electrophoresis on 18% SDS-PAGE following staining with Coomassie blue.

Fluorescence spectroscopy

Fluorescence measurements were recorded on a Perkin-Elmer MPF-44B spectrofluorometer with the temperature maintained at 20 °C in a thermostatted cell holder. Unless otherwise specified, 100 mM sodium phosphate, pH 7.5, was used in all fluorescence experiments. Absorbance of samples was kept below 0.02 to minimize inner filter effects and corrections were made for light scattering. A slit width of 4-6 nm was used for both excitation and emission monochromators. Excitation spectra for pyrene-labeled samples were collected by setting the emission wavelengths at 375 nm or 460 nm for monomer and excimer, respectively. Emission spectra were collected by setting the excitation wavelength at 345 nm. For all calculations, the area under the monomer emission peak was calculated from 370 to 410 nm, while the area under the excimer emission peak was calculated from 440 to 510 nm. Monomer to excimer (m/e) ratios were calculated by dividing the monomer fluorescence emission intensity at 375 nm by the excimer fluorescence emission intensity at 460 nm. Tyrosine fluorescence in wild-type apoLp-III (which lacks tryptophan) was measured at excitation and emission wavelengths of 277 nm and 300 nm, respectively. Solvent background was subtracted and the spectra were corrected for variations in sensitivity.

Quenching studies. To measure the effect of aqueous quenchers, lipid-free pyrene-labeled apoLp-III, DMPC-bound or LDL-bound pyrene-N40C- and pyrene-L90C-apoLp-III were treated with increasing concentrations of potassium iodide in 50 mM sodium

phosphate, pH 7.5. KI solutions contained 1 mM sodium thiosulfate to suppress free iodine formation. Similarly, for depth-dependent quenching studies, aliquots of 5-doxyl-stearic acid or 12-doxyl stearic acid [5-DSA and 12-DSA, respectively (1.3 mM stock in ethanol)] were added to lipid-bound samples (final concentration of ethanol ≤ 1% by volume) and fluorescence intensities were measured following equilibration for 5 min. The effective quenching constants were determined according to the Stern-Volmer equation, $F_o/F = 1 + K_{SV}[Q]$, where F_O and F are fluorescence intensities in the absence and presence of quencher, respectively, and [Q] is the concentration of quencher. The slope of the plot of F_o/F vs. [Q] is the effective Stern-Volmer quenching constant, K_{SV} (202). When using spin labeled fatty acids as quenchers, the classic Stern-Volmer equation for free diffusion no longer applies since the quencher is not uniformly distributed over the corresponding space coordinate (203, 204). Therefore, for purposes of relative comparison within spin-labeled fatty acids, we have calculated an apparent quenching constant (K_{app}) in place of K_{SV}.

Denaturation studies. For GdnHCl denaturation experiments, 50 μg/mL solutions of pyrene-labeled N40C/L90C-apoLp-III were incubated with increasing amounts of GdnHCl (final concentrations ranging from 0 to 5 M GdnHCl) for 20 h at 4 °C prior to fluorometric analysis. Relative molar ellipticity at 222 nm (θ/θ_o) was calculated by dividing the molar ellipticity at each GdnHCl concentration (θ) by the molar ellipticity in the absence of GdnHCl (θ_o). M/M_o and E/E_o represent the area under the monomer or excimer emission at each GdnHCl concentration divided by the area under the monomer or excimer emission in the absence of GdnHCl, respectively. For temperature experiments, a circulating water bath was used to maintain the temperature in the cuvette

(ranging from 20 °C to 70 °C) of 50 μg/mL solutions of pyrene-labeled N40C- or N40C/L90C-apoLp-III. θ/θ_{20} was calculated by dividing θ at each temperature by θ at 20 °C. M/M_{20} and E/E_{20} were calculated by dividing the area at each temperature by the initial area at 20 °C.

TFE titration studies. For TFE experiments, 50 μg/mL solutions of pyrene-labeled N40C- or N40C/L90C-apoLp-III were incubated with increasing amounts of TFE [final concentrations ranging from 0% to 60% TFE (v/v)] for 1 min and then subjected to fluorometric analysis. M/M_o and E/E_o represent the area under the monomer or excimer emission at each TFE concentration divided by the area under the monomer or excimer emission in the absence of TFE, respectively.

CHAPTER 3

NMR Evidence for a Conformational Adaptation of Apolipophorin III upon Lipid Association*

*Parts of this chapter have already been published.

Wang, J., Sahoo, D., Schieve, D., Gagne, S. M., Sykes, B. D. and Ryan, R. O. (1997) Multidimensional NMR studies of an exchangeable apolipoprotein and its interactions with lipids in *Techniques in Protein Chemistry VIII* , Academic Press.

Wang, J., Sahoo, D., Sykes, B. D. and Ryan, R. O. (1998) NMR evidence for a conformational adaptation of apolipophorin III upon lipid association. *Biochem. Cell Biol.* **76**, 276-283.

3.1 INTRODUCTION

Using multidimensional heteronuclear NMR spectroscopy, we have recently determined the solution structure of *M. sexta* apoLp-III [(6, 205); Wang, Sykes and Ryan, in preparation], representing the first NMR structure of an intact exchangeable apolipoprotein. While the helix-bundle structural organization of apoLp-III and other exchangeable apolipoproteins (5, 156, 206) provides a rational explanation for their existence as monomeric, water soluble proteins, important questions remain about possible conformational adaptations that apolipoproteins undergo upon interaction with lipid surfaces. Although experimental evidence exists in favor of the proposed "open conformation" model, we still lack detailed structural information of lipid-associated apolipoproteins. Attempts to use X-ray crystallography have not been successful, owing to an inability to crystallize exchangeable apolipoproteins in complex with lipid. In the present chapter, we utilized our previously reported complete assignment of the NMR spectra of lipid-free *M. sexta* apoLp-III as a reference for NMR studies of the protein in the presence of lipid. Using the bacterial expression system available in our laboratory (119), we developed a useful method to incorporate ^{15}N specifically and exclusively into peptide backbone amide nitrogens. We carried out lipid-titrations with specific ^{15}N-amino acid labeled apoLp-III samples, and monitored spectral changes by ^{1}H-^{15}N heteronuclear single quantum correlation (HSQC) NMR spectroscopy. Consistent with the open conformation model, large spectral changes occurred in response to lipid interaction. Structural information obtained on a residue basis suggests apoLp-III initiates lipid-association in an oriented manner. Finally, the present approach has

yielded assignment information on lipid-bound apoLp-III HSQC spectra, an important step toward elucidation of its lipid-bound solution structure.

3.2 RESULTS

^{15}N Isotope-labeling strategies

In order to pursue heteronuclear multidimensional NMR experiments, a bacterial expression system for expression of apoLp-III has been developed which allows facile production of 150-200 mg/L ^{15}N-labeled apoLp-III or 100-125 mg/L ^{15}N/^{13}C-double labeled apoLp-III. **Figure 3-1, panel A** shows the ^{1}H-^{15}N HSQC spectrum of a 1 mM solution of lipid-free uniformly ^{15}N-labeled apoLp-III.

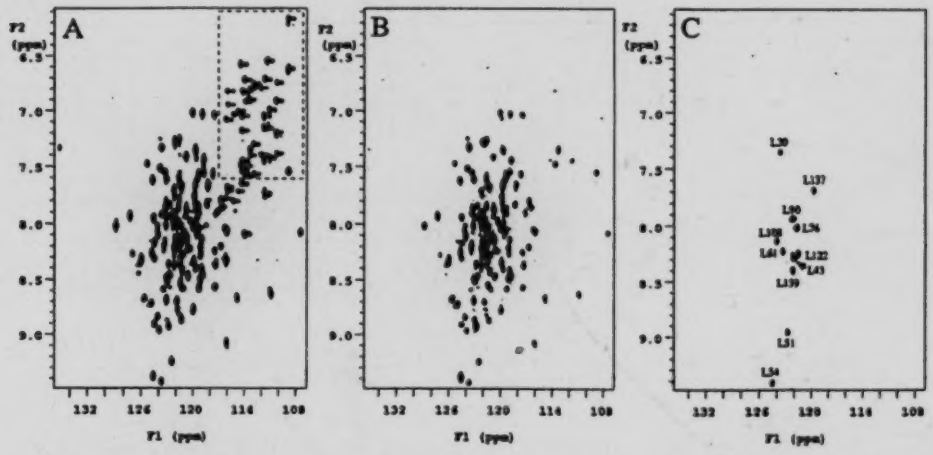

Figure 3-1. ^{1}H-^{15}N HSQC spectra of apoLp-III. *Panel A*, ^{15}N-uniformly-labeled apoLp-III; *panel B*, ^{15}N-backbone-labeled apoLp-III and; *panel C*, ^{15}N-leucine specifically labeled apoLp-III.

Panel A also indicates that, although the chemical shift dispersion in the ^{1}H-dimension is rather small (6.5 ppm to 9.5 ppm), it is generally upfield shifted, consistent with the fact that the protein secondary structure is predominantly α-helix (3). The chemical shifts in

the ^{15}N-dimension are well-dispersed which results in good separation of the overall crosspeaks. However, certain regions in the spectrum are still crowded as shown in Figure 3-1.

The upper right corner of the HSQC spectrum of ^{15}N-labeled apoLp-III shown in Figure 3-1, panel A contains numerous doublet crosspeaks which are derived from side chain amines of glutamine and asparagine residues. Since apoLp-III is rich in Gln and Asn (25 of the 166 amino acids), this region of the spectrum is crowded. In considering possible approaches to selectively label backbone amide nitrogens, we speculated that although bacteria efficiently and readily transaminate nitrogen to α-amino nitrogens of other amino acids, they may prefer NH_4Cl as a precursor of Gln and Asn side chain amine nitrogens. Interestingly, when bacteria were grown in media containing ^{15}N-leucine and unlabeled NH_4Cl, specific labeling of backbone amide nitrogens was achieved (**Figure 3-1, panel B**). The presence of unlabeled NH_4Cl is essential to this process because it provides an alternative, preferentially utilized, biosynthetic precursor of side chain nitrogen atoms. The isotope-labeling strategy shown in Figure 3-1, panel B, is the first report, to our knowledge, which allows for specific isotope-labeling of the backbone amide nitrogen atoms of a protein. As a reference control, bacteria harbouring the apoLp-III/pET plasmid were cultured in medium containing ^{15}N-leucine as the sole nitrogen source. ApoLp-III obtained by this isotope-labeling method gave a HSQC spectrum which was indistinguishable from the spectrum shown in Figure 3-1, panel A (data not shown). This result confirms that bacteria are capable of redistributing nitrogen derived from ^{15}N-leucine into all backbone and side chain nitrogens in this protein. Importantly, when the uniformly labeled spectrum is overlayed with the specifically

backbone labeled spectrum, it is apparent that several backbone amide resonances are masked by the abundant side chain amine nitrogen resonances. Thus, this labeling strategy simplifies HSQC spectra, enabling identification of crosspeaks from backbone amides that otherwise overlap with crosspeaks from side chain amines.

The metabolic labeling strategy described herein offers an attractive alternative method, permitting specific enrichment of backbone amide nitrogens with ^{15}N, effectively eliminating Gln and Asn side chain NH_2 resonance, and thus simplifying the spectrum. Mass spectrometric analysis of ^{15}N-backbone amide nitrogen-labeled apoLp-III indicated an isotope enrichment of 50%, demonstrating that unlabeled NH_4Cl competes with ^{15}N-leucine derived nitrogens for incorporation into the backbone nitrogen atoms in the protein. By contrast, an isotope enrichment of >95% was observed for uniformly ^{15}N-labeled apoLp-III using $^{15}NH_4Cl$ as the sole nitrogen source in M9 minimal media.

In order to examine the HSQC spectra in finer detail, we decided to attempt specific labeling of the 11 leucine residues in apoLp-III. To accomplish specific labeling of Leu, we cultured bacteria in M9 minimal media containing ^{15}N-leucine and the 19 other unlabeled amino acids. **Figure 3-1, panel C**, reveals a spectrum consisting of 11 well-separated resonances, consistent with the conclusion that specific labeling of the 11 Leu residues in apoLp-III has been achieved.

For $^{15}N/^{13}C$-double labeling of apoLp-III, the amount of $^{13}C_6$-glucose was optimized. Normally, minimal media contains 2.4-3.0 g glucose/L. However, it was found that efficient overexpression of $^{15}N/^{13}C$-double-labeled apoLp-III can be achieved with as little as 1.2 g/L of $^{13}C_6$-glucose, significantly reducing the cost of isotope-labeling.

Rationale for experimental design

In an effort to investigate structural changes in apoLp-III induced by lipid-binding, we used information gained from the spectral assignment and structure of lipid-free apoLp-III (6) to characterize NMR spectra obtained in the presence of lipid. It is not feasible to use naturally occurring lipoproteins for determination of the lipid-associated structure of apoLp-III since lipoprotein particle size is too large for heteronuclear multidimensional NMR studies. Instead, we have employed DPC as a model lipid since previous work has established that apoLp-III associates with DPC micelles (119, 205). DPC, which possesses a phosphocholine head group and a single C_{12} hydrocarbon chain, provides a good mimic of the phospholipid component of lipoprotein surfaces (207). DPC micelles contain about 56 lipid molecules, giving rise to a molecular weight of 22 kDa [molecular weight for D_{38}-DPC = 389; critical micelle concentration (CMC) = 1.1 mM; (208)]. Therefore, the apoLp-III/DPC micelle complex (assuming 1 protein molecule per micelle) will have a predicted molecular weight of about 40 kDa. In order to ensure a maximum of one apoLp-III per micelle complex, the final apoLp-III/DPC molar ratio should be at least 1:56.

^{1}H-^{15}N HSQC spectra of a uniformly ^{15}N-labeled apoLp-III sample at an apoLp-III/DPC molar ratio > 1:60 revealed significant linebroadening of crosspeaks versus those found with lipid-free protein. This is expected for apoLp-III/DPC complexes since their larger particle size causes slower tumbling which is manifest by a broader linewidth of the NMR signals. Linebroadening of apoLp-III resonances in the lipid-associated state contributes to severe resonance overlap that compromises interpretation of the spectra. As a result, direct analysis of the ^{1}H-^{15}N HSQC spectrum of uniformly ^{15}N-labeled apoLp-

III is difficult. To circumvent this problem, we used specific ^{15}N-amino acid labeled apoLp-III in place of uniformly ^{15}N-labeled protein. Using the bacterial expression system described, we prepared ^{15}N-valine apoLp-III, ^{15}N-leucine apoLp-III, ^{15}N-lysine apoLp-III and ^{15}N-glycine apoLp-III. The rationale for choosing these amino acids is their respective locations in the lipid-free helix-bundle conformation (6) (**Figure 3-2**).

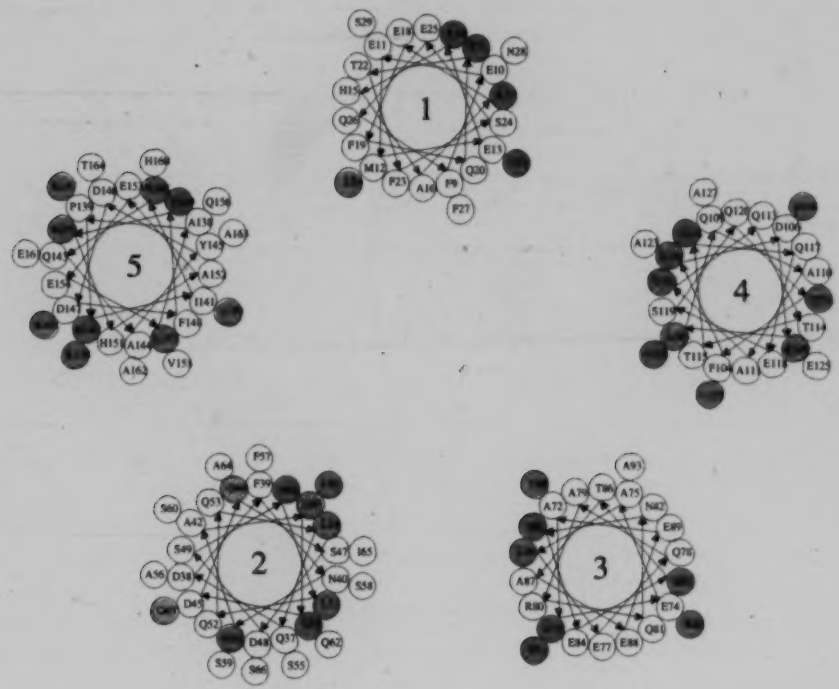

Figure 3-2. Location of ^{15}N-labeled residues in *M. sexta* apoLp-III. The helical wheel diagram shows the location of the ^{15}N-leucine residues (pink), ^{15}N-valine residues (blue), ^{15}N-lysine residues (green) and ^{15}N-glycine residues (orange) within the lipid-free helix bundle conformation.

While lysine (23 residues) is a hydrophilic residue which is mostly located on the exposed hydrophilic surfaces of amphipathic α-helices, leucine (11 residues) and valine (9 residues) are hydrophobic residues located on the opposite, buried hydrophobic surfaces in the helix-bundle conformation. On the other hand, glycine (5 residues) is mostly located in the loop regions which connect helical segments. By employing these four different amino acids, we were able to evaluate the effect of DPC titration on different regions of the protein, obtaining information on conformational adaptations of apoLp-III which accompany lipid-binding. Furthermore, the assignment of ^{1}H-^{15}N HSQC spectra of apoLp-III in the absence of lipid is useful as a reference standard to obtain the assignment of these residues in the presence of lipid.

Behavior of resonances corresponding to hydrophobic residues in apoLp-III

Typical ^{1}H-^{15}N HSQC spectra of ^{15}N-valine apoLp-III, obtained in the presence and absence of DPC micelles, are depicted in **Figure 3-3**.

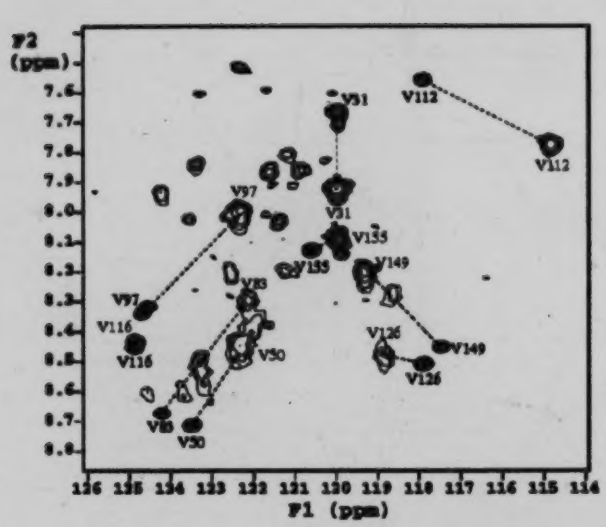

Figure 3-3. ^{1}H-^{15}N HSQC spectra of ^{15}N-valine specific-labeled apoLp-III in the presence (red crosspeaks) and absence (black crosspeaks) of D_{38}-DPC (1:60 apoLp-III:DPC molar ratio). Assigned resonances are labeled with the one letter code for residue name (red lettering indicates lipid associated resonances and black lettering represents resonances for lipid free state). Numbers indicate residue position in the protein sequence. The dotted arrows indicate crosspeak movement upon lipid-association. Note that isotope scrambling from ^{15}N-valine resulted in the appearance of several weak crosspeaks in the spectrum.

Note that some isotope scrambling was observed in ^{15}N-valine specific labeled apoLp-III since, in addition to the expected 9 strong crosspeaks, several additional weaker crosspeaks were present. Valine crosspeaks were easily distinguished by their stronger intensity and comparison with the known assignment of uniformly ^{15}N-labeled protein (6). Following addition of DPC, it is apparent that major changes in the chemical shift of apoLp-III valine residues occur, consistent with the concept that lipid association is accompanied by a major conformational change. The broader linewidths observed for crosspeaks in the presence of micellar concentrations of DPC indicate binding of apoLp-III to the lipid surface. Resonance assignment in the lipid-bound state was obtained by

following changes in apoLp-III valine residue chemical shift as a function of DPC titration.

^{1}H-^{15}N HSQC spectra shown in Figure 3-3 were taken at the beginning and end of a DPC titration experiment with ^{15}N-valine apoLp-III. To examine intermediate stages in this transition, spectra were collected at various DPC concentrations. Titration curves for five valine residues (V31, V50, V83, V97 and V112) are illustrated in **Figure 3-4**.

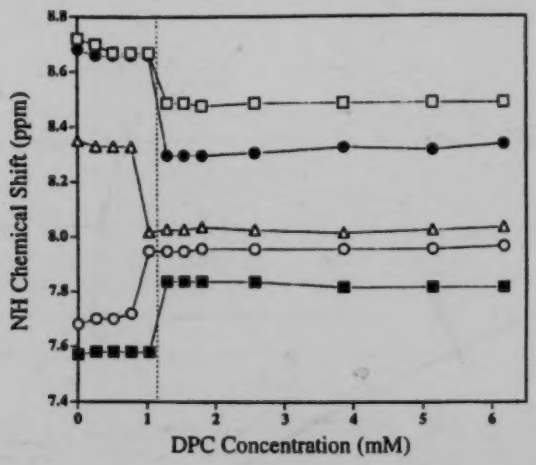

Figure 3-4. Effect of DPC concentration on the amide proton chemical shift of valine resonances in ^{15}N-valine apoLp-III. Spectral assignment in buffer is from Wang *et al.* (6). Filled squares: V112; open circles: V31; open triangles: V97; open squares: V50; and filled circles: V83. The dotted line corresponds to the CMC of DPC.

Below the CMC of DPC, crosspeaks corresponding to V50, V83 and V112 showed little or no chemical shift change. However, dramatic and abrupt changes in crosspeak chemical shift were observed for these residues when the DPC concentration reached its CMC. Similar abrupt changes in the chemical shifts of V31 and V97 were also noted, although their transitions occurred just below the CMC of DPC. Increasing the apoLp-III:DPC ratio (to a maximum of 1:100) did not cause further changes in the chemical shift of any of the valine crosspeaks. **Figure 3-5** shows ^{1}H-^{15}N HSQC spectra of ^{15}N-leucine

apoLp-III in the presence and absence of DPC. Using HSQC resonance assignments available for lipid-free apoLp-III (6) as a reference, we established the assignment of each of the 11 leucine resonances in the lipid-associated state. Consistent with lipid binding, spectra obtained in the presence of DPC micelles reveal dramatic linebroadening of all leucine crosspeaks.

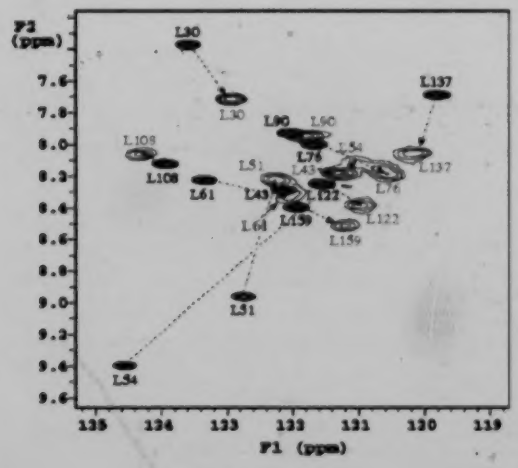

Figure 3-5. ^{1}H-^{15}N HSQC spectra of ^{15}N-leucine specific-labeled apoLp-III in the presence (red crosspeaks) and absence (black crosspeaks) of D_{38}-DPC (1:75 apoLp-III:DPC molar ratio). Assigned resonances are labeled with the one letter code for residue name (red lettering indicates lipid associated resonances and black lettering represents resonances for lipid free state). Numbers indicate residue position in the protein sequence. The dotted arrows indicate crosspeak movement upon lipid-association.

Figure 3-6 presents DPC titration curves for L30, L51, L54 and L137.

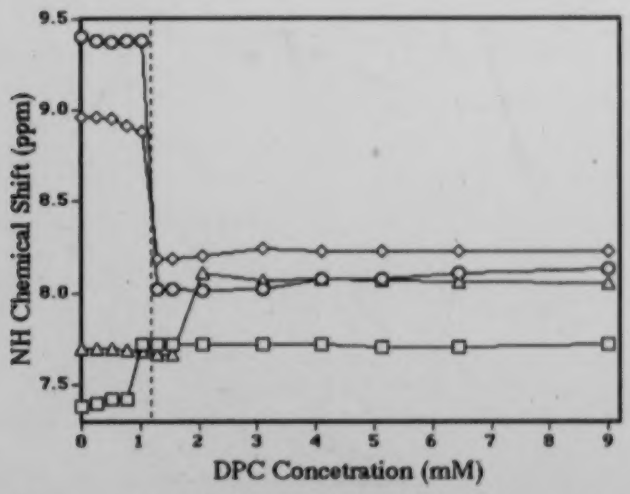

Figure 3-6. Effect of DPC concentration on the amide proton chemical shift of leucine resonances in ^{15}N-leucine apoLp-III. Spectral assignment in buffer is from Wang *et al.* (6). Squares: L30; diamonds: L51; circles: L54 and triangles: L137. The dotted line indicates the CMC of DPC.

While each of these four residues display a DPC dependent chemical shift transition, L51 and L54 shift at the CMC, L30 shifts below the CMC and L137 shifts above the CMC. Characterization of other leucine and valine residues revealed similar chemical shift transitions in response to DPC. In most cases the observed transition was abrupt and occurred at the CMC of DPC, although some residues underwent the transition slightly above or below the CMC.

Behavior of resonances corresponding to hydrophilic residues in apoLp-III

^{15}N-lysine apoLp-III ^{1}H-^{15}N HSQC spectra in the presence and absence of DPC micelles are shown in **Figure 3-7**. As with the spectra for ^{15}N-valine and ^{15}N-leucine apoLp-III,

the end point spectrum reveals a very different chemical shift pattern, with much broader linewidths. Employing the assignment of lysine resonances in lipid-free apoLp-III as a reference, chemical shift changes were followed as a function of DPC titration.

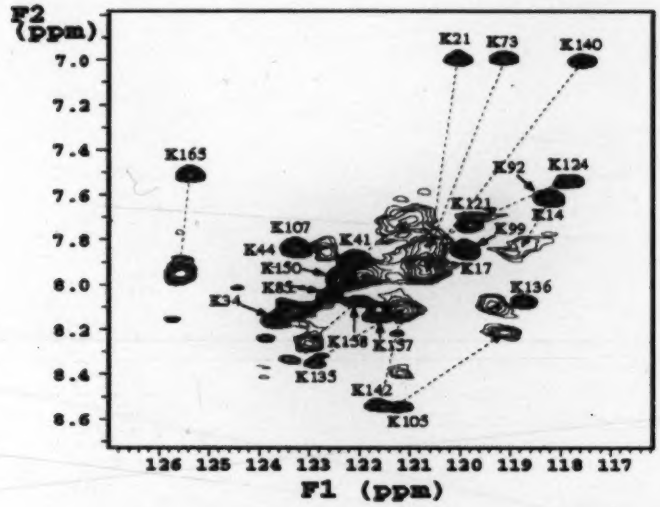

Figure 3-7. ^{1}H-^{15}N HSQC spectra of ^{15}N-lysine specific-labeled apoLp-III in the presence (red crosspeaks) and absence (black crosspeaks) of D_{38}-DPC (1:100 apoLp-III/DPC molar ratio) at pH 6.4. Assigned resonances are labeled with the one letter code for residue name. Numbers indicate residue position in the protein sequence. Due to significant overlap of lysine resonances in the presence of DPC, lipid-associated lysine residues are not labeled. The dotted arrows indicate crosspeak movement upon lipid-association. Note that the crosspeak corresponding to K71, which resonates at 9.14 ppm for NH, 127.97 ppm for N falls outside the spectral area shown in the figure.

Using this approach we were able to assign most lysine residues in spectra of lipid-bound apoLp-III. Visual inspection of spectra obtained at various DPC concentrations revealed different patterns in terms of the chemical shift transition behavior of lysine residues. Some lysine residues showed little chemical shift change in the proton dimension but a larger change in the ^{15}N dimension. **Figure 3-8** shows DPC titration curves for residues

K21, K73 and K135. K73 shows a dramatic chemical shift change below the CMC of DPC, similar to L30, V31 and L97. On the other hand, K21 and K135 undergo more gradual spectral changes in response to increasing DPC. As the DPC concentration increases, these two lysine crosspeaks undergo incremental chemical shift changes.

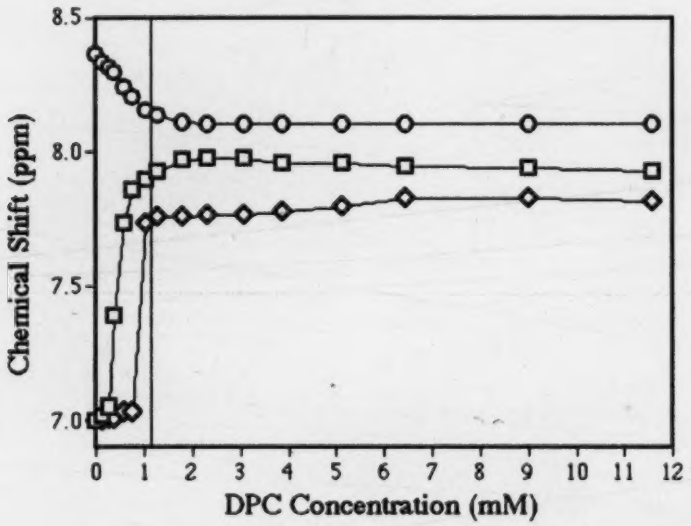

Figure 3-8. Effect of DPC concentration on the amide proton chemical shift of lysine resonances in ^{15}N-lysine apoLp-III. Spectral assignment in buffer is from Wang *et al.* (6). Squares: K21; diamonds: K73 and circles: K135. The solid vertical line corresponds to the CMC of DPC.

Unlike valine and leucine residues, DPC concentrations at the CMC did not cause major chemical shift changes. Also, the linewidths of the crosspeaks of lysine residues did not show significant broadening below the CMC of DPC. However, above the CMC, lysine residue crosspeaks were significantly broadened, indicating that apoLp-III binds to the newly formed DPC micelle surface to form mixed micelle complexes. DPC titration

experiments using ^{15}N-glycine apoLp-III yielded results similar to those obtained for lysine, except for G63 and G70 which behaved more like L137 (data not shown).

3.3 DISCUSSION

Using DPC micelles as a model lipid surface, we have performed titration experiments on specific ^{15}N-amino acid labeled apoLp-III samples. ApoLp-III binds to DPC micelles to form an ~ 40 kDa mixed micelle which gives rise to broader NMR signal linewidths. In addition, the binding interaction between apoLp-III and DPC micelles induces dramatic spectral changes in all four specific ^{15}N-amino acid apoLp-III samples, indicating a conformational change in apoLp-III upon lipid interaction. Collectively, valine, leucine, lysine and glycine include 48 residues, representing 29% of the amino acids in apoLp-III. They are distributed nearly equally along the primary structure, occupying both hydrophobic and hydrophilic faces of amphipathic helical segments (**Figure 3-9;** see also Figure 3-2).

Figure 3-9. Ribbon representation of *M. sexta* apoLp-III NMR solution structure in buffer (Wang, Sykes and Ryan, unpublished data). Sidechains indicated are from residues whose titration curves are shown in Figure 3-4 (valines), Figure 3-6 (leucines) and Figure 3-8 (lysines).

Since we have the complete assignment of NMR spectra of lipid-free apoLp-III (6), each HSQC crosspeak provides a unique probe to monitor conformational changes of the protein upon lipid-binding. Thus, this approach can provide structural details about conformational adaptation of apoLp-III upon lipid-association on a residue-by-residue basis. Furthermore, crosspeak assignment of labeled residues in lipid-bound apoLp-III can be obtained. It is worth noting, however, that observed dramatic and abrupt changes in crosspeak chemical shifts may result in ambiguity of the assignment. Thus, 3D/4D NMR experiments of uniformly labeled, lipid-bound apoLp-III are required to confirm these assignments.

The results obtained provide direct experimental support for the open conformation model. The differences observed between the titration behavior of leucine/valine residues and lysine residues indicate that hydrophobic residues and hydrophilic residues in the protein are affected differently by DPC titration. These differences may be explained by the overall organization of the protein, as shown in Figure 3-9. In the lipid-free helix-bundle structure, lysine residues are located on the hydrophilic face of the amphipathic α-helices, exposed to solvent, while valine and leucine residues are located on the hydrophobic face of the same α-helices, oriented toward the interior of the protein, shielded from the solvent. At concentrations below its CMC, DPC exists in solution as individual molecules. It appears that DPC molecules interact with exposed lysine residues, possibly through charge-charge interactions, to induce characteristic chemical shift changes, as shown in Figure 3-8 for K21 and K135. However, lysine residue chemical shift changes do not necessarily reflect a conformational change in the protein, since NMR spectra of the hydrophobic residues essentially showed no changes at these DPC concentrations, compared to the lipid-free apoLp-III spectrum. This indicates that DPC molecules are not able to interact with buried leucine and valine residues, presumably because DPC monomers are unable to penetrate the hydrophobic interior of the helix bundle. Thus, valine and leucine residues are likely shielded from non-micellar lipid by the helix-bundle organization since DPC molecules do not provide a continuous lipid surface suitable for stable apoLp-III interaction. No significant linebroadening was observed for apoLp-III crosspeaks below the CMC of DPC. At the CMC, however, DPC molecules form micelles which present a surface for interaction. Interaction between apoLp-III and the micelle surface triggers

structural changes in apoLp-III that are reflected in the observed spectral changes, including alterations in chemical shift and linebroadening. The data are consistent with the concept that apoLp-III adopts an open, "linear" α-helical structure, exposing its hydrophobic interior to the lipid surface. Once this conformational adaptation is complete and stable binding is established, no further spectral changes occur.

The structural details of the DPC micelle binding-induced conformational adaptation of apoLp-III can also be examined in terms of the initiation of lipid binding. From the NMR structure of lipid-free apoLp-III (see Figure 3-9), we identified that V50, L51 and L54 are located in the middle of helix 2, V83 is in the middle of helix 3 and V112 is in the middle of helix 4. Each of these valine and leucine residues make extensive hydrophobic contacts with neighboring residues, either on the same helix, or on different helices. Titration plots generated for these residues represent typical titration curves for hydrophobic residues located in the interior of the helix bundle. However, slight differences in lipid-titration behavior of other hydrophobic residues, including L30, V31, V97 and L137 were detected. Interestingly, L30, V31 and V97, which undergo a chemical shift transition at DPC concentrations just below the CMC, are located at one end of the helix-bundle (V97 is located in helix 3'). Based on structural comparison of exchangeable apolipoproteins, it is proposed that the "helix-short helix-helix" motif serves as a recognition site for initiation of lipoprotein binding (6). The data presented in this paper support the concept that this end of apoLp-III may initiate interaction with the lipid surface. This manner of interaction may be related to the observed chemical shift transition at DPC concentrations slightly less than its CMC in hydrophobic residues located at this end of apoLp-III, perhaps by seeding micelle formation. By contrast, in

the case of residues located at the other end of molecule (G63, G70, L76, V126 and L137), crosspeak chemical shift changes were retarded, occurring at DPC concentrations slightly above the CMC of this lipid.

In summary, NMR data from DPC titration experiments provide evidence in support of the open conformation model. These data also provide structural details of the conformational adaptation of apoLp-III upon lipid-binding, in terms of its recognition and binding interactions. Additional experiments need to be conducted to determine if this model is applicable to other exchangeable apolipoproteins. The present study clearly demonstrates the potential of elucidating a high resolution structure of lipid-bound apoLp-III using multidimensional NMR techniques.

CHAPTER 4

Fluorescence Quenching Studies of Exchangeable Apolipoprotein-Lipid Interactions*

*Parts of this chapter have already been published.

Sahoo, D., Narayanaswami, V., Kay, C. M. & Ryan, R. O. (1998) Fluorescence studies of an exchangeable apolipoprotein-lipid interactions. Superficial association of apolipophorin III with lipoprotein surfaces. *J. Biol. Chem.* **273**, 1403-1408.

4.1 INTRODUCTION

In the previous chapter, we were able to monitor the behaviour of different groups of amino acids upon interaction with a lipid surface. As an alternate approach towards probing the lipid-bound structure of apoLp-III, we decided to investigate individual fluorescently-labeled helices.

Fluorescence spectroscopy is a very sensitive technique that has been used to study protein structure and interactions of proteins with other molecules. Taking advantage of the fact that apoLp-III lacks cysteine residues, we introduced cysteine residues into various locations of the apoLp-III molecule using site-directed mutagenesis and exploited the use of extrinsic, thiol-reactive probes such as pyrene maleimide. The thiol (or sulfhydryl) functional group is present on cysteine residues and can be labeled with high selectivity. Furthermore, pyrene maleimide is essentially non-fluorescent until it has reacted with a sulfhydryl group.

The accessibility of pyrene maleimide to fluorescent quenchers in the lipid-free and lipid-bound states was used as an indicator of apoLp-III conformation. The quenching of the single tyrosine (Tyr145) was also used to examine the conformation of apoLp-III in the lipid-bound state. Although fluorescence from Tyr145 (located in helix 5) is negligible in the lipid-free state (3, 118), a significant enhancement is observed upon lipid binding (167), which facilitates quenching studies.

We used the aqueous quencher, potassium iodide, to quench tyrosine and pyrene maleimide fluorescence in order to gain information regarding the change in microenvironments as apoLp-III goes to lipid-free to DMPC- or LDL-bound states. By comparison of the relative effectiveness of different lipid-based quenchers such as doxyl

stearic acids, information about the spatial alignment and topography of apoLp-III α-helices complexed with phospholipids was obtained. Furthermore, we acquired information regarding the mode of interaction of apoLp-III with spherical lipoprotein surfaces.

4.2 RESULTS

Structural characterization of extrinsically-labeled N40C- and L90C-apoLp-III.

Two single-cysteine mutant apoLp-IIIs were created to probe the lipid-bound conformation of apoLp-III. In the first mutation, Cys was introduced into the N40 position, located at the N-terminus of helix 2 (close to the polar/nonpolar interface), while in the second mutation, Cys was introduced into the L90 position, located at the C-terminus of helix 3 (centre of the nonpolar face of the helix). Mass spectrometry yielded a mass of 18,371 ± 1.5 Da and 18,371 ± 1.5 Da for N40C-apoLp-III and L90C-apoLp-III, respectively, as compared to 18,381 Da for wild-type apoLp-III. Modification of N40C- and L90C-apoLp-IIIs by covalent attachment of pyrene maleimide resulted in labeling of the single engineered cysteine residue. The presence of a single attachment site on either protein and their availability for labeling was examined by two independent methods. **Figure 4-1** represents the mass spectrometric profiles of N40C-apoLp-III (**panel A**) as examined by these methods.

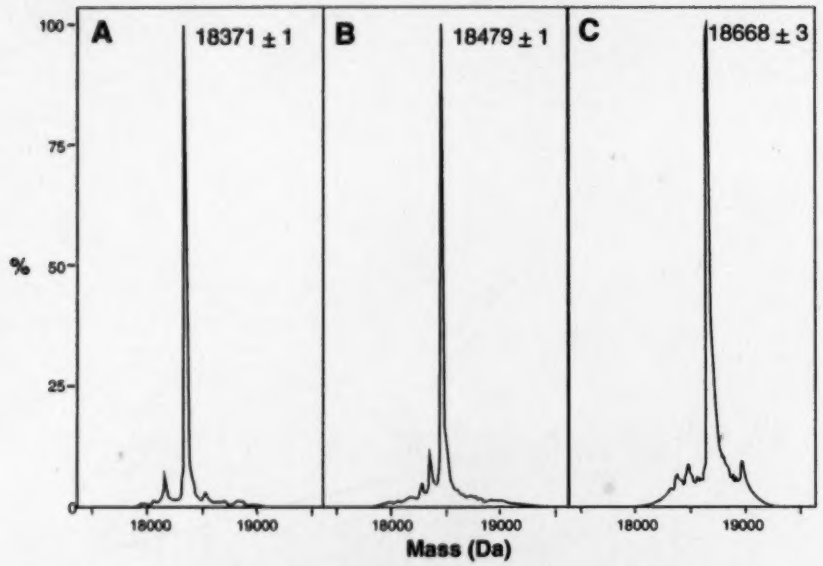

Figure 4-1. Electrospray mass spectrometric profiles of N40C-apoLp-III. *Panel A*, unlabeled recombinant N40C-apoLp-III; *panel B*, thiopyridyl-labeled N40C-apoLp-III and; *panel C*, pyrene-labeled N40C-apoLp-III.

The first method used 2,2′-dithiodipyridine labeling, which under native conditions, resulted in covalent linkage of the thiopyridyl moiety to the cysteine, yielding a product with a molecular weight increment of 108 Da (**Figure 4-1, panel B**). The second method employed pyrene maleimide which, upon covalent linkage to the free sulfhydryl, yielded a product with a molecular weight increment of 297 Da (**Figure 4-1, panel C**; 18,371 Da to 18,668 Da). It is worth noting that mass spectrometry confirmed the absence of labeling of wild-type apoLp-III upon treatment with pyrene maleimide. Taken together, these data indicate that there is a cysteine present in both recombinant proteins, and that under the conditions studied, neither cysteine is involved in intermolecular disulfide bond formation. N-(1-pyrene)maleimide has the unique property of becoming fluorescent only after covalent attachment to a sulfhydryl group. Following SDS-PAGE, N40C-apoLp-III

and pyrene-L90C-apoLp-III were fluorescent when viewed under a UV-illuminator. This fluorescence is depicted in **Figure 4-2**, using N40C-apoLp-III as an example.

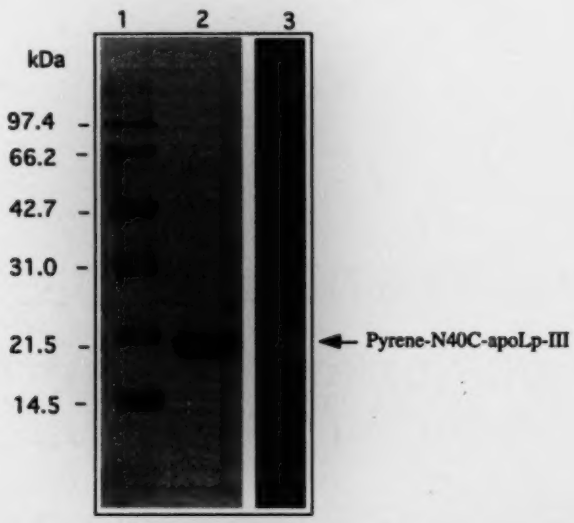

Figure 4-2: N-(1-pyrene)maleimide labeling of N40C-apoLp-III. N40C-apoLp-III was labeled with N-(1-pyrene)maleimide as described in Chapter 2.2 and electrophoresed on 12% SDS-PAGE. Lane 1, molecular weight standards; lane 2, Coomassie-stained pyrene-N40C-apoLp-III; lane 3, fluorogram of pyrene-labeled N40C-apoLp-III as viewed under an UV illuminator.

Fluorescence excitation and emission spectra of pyrene-N40C- and L90C-apoLp-III are shown in **Figure 4-3**. Typical fluorescence properties of pyrene, such as excitation maxima at 335 and 345 nm and emission maxima at 375 and 396 nm, confirming labeling of the cysteine residue on the proteins. Circular dichroism spectra revealed that the secondary structure content of pyrene-N40C- and pyrene-L90C-apoLp-III (60% α-helix) is very similar to that of wild-type apoLp-III (3).

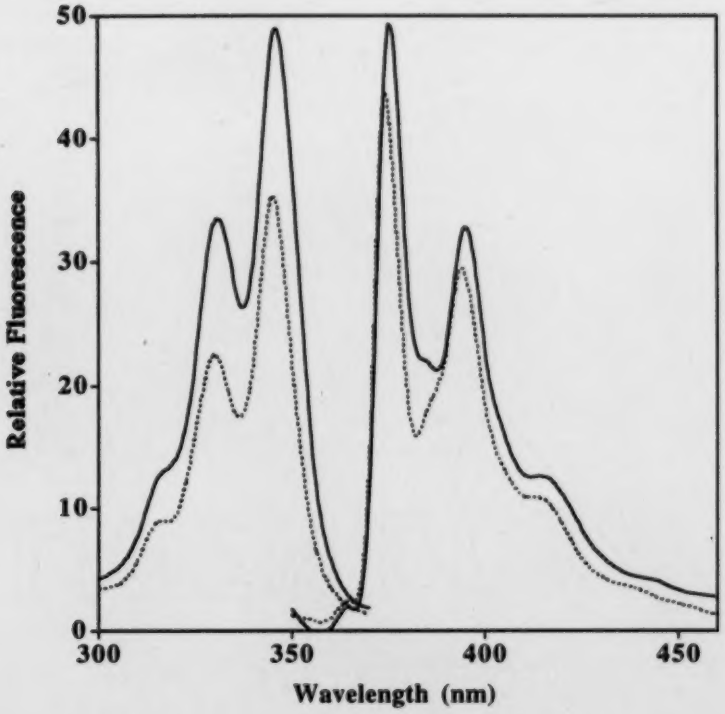

Figure 4-3. Fluorescence excitation and emission spectra of pyrene-labeled apoLp-III. Pyrene-N40C- (solid line) and L90C-apoLp-III (dashed line) in the lipid-free state were monitored at an emission wavelength of 375 nm for the excitation spectra, with excitation at 345 nm for the emission spectra. The excitation and emission slit widths were 4 nm.

Functional characterization of pyrene-labeled N40C- and L90C-apoLp-III

Formation of discoidal complexes. In order to ascertain that the functional characteristics of apoLp-III were not altered upon substitution with cysteine, the lipid-binding capability of the pyrene-labeled apoLp-IIIs was evaluated. One of the functional properties of exchangeable apolipoproteins is the ability to transform pre-formed multilamellar vesicular structures to disc-like complexes (164). As shown in **Figure 4-4**, incubation of DMPC vesicles (**panel A**) with wild-type or pyrene-labeled N40C-apoLp-III produced

discoidal complexes when mixed at a 2.5:1 ratio of phospholipid to protein (w/w) (**panels B and C**, respectively). On average, the disc complexes had a diameter of 18-22 nm.

Figure 4-4. Electron micrographs of apoLp-III/DMPC complexes. Discoidal complexes were isolated by density gradient ultracentrifugation (see Chapter 2.2) and stained with 2% phosphotungstate and photographed in the electron microscope. Panel A, DMPC vesicles; panel B, wild-type apoLp-III/DMPC complexes and panel C, pyrene-labeled N40C-apoLp-III/DMPC complexes. The solid bar represents 50 nm.

Stabilization of lipoprotein particles. Exchangeable apolipoproteins have the ability to stabilize human LDL under conditions where neutral glycerolipid is exposed on the particle surface (135). Upon treatment of LDL with phospholipase C, the polar head groups are cleaved from phosphatidylcholine moieties, resulting in the exposure of diacylglycerol on the monolayer surface (133). Creation of this hydrophobic surface induces aggregation of LDL particles, as seen by increased sample turbidity as a function of time (**Figure 4-5**). However, in the presence of wild-type apoLp-III, aggregation is prevented due to a stable binding interaction with the modified LDL. The observation that pyrene-N40C- and pyrene-L90C-apoLp-III were able to prevent phospholipase C-induced LDL aggregation, demonstrates that covalent attachment of the extrinsic fluorophore does not disrupt their lipoprotein binding ability and provides a useful system to study apolipoprotein interaction with the surface of a spherical lipoprotein.

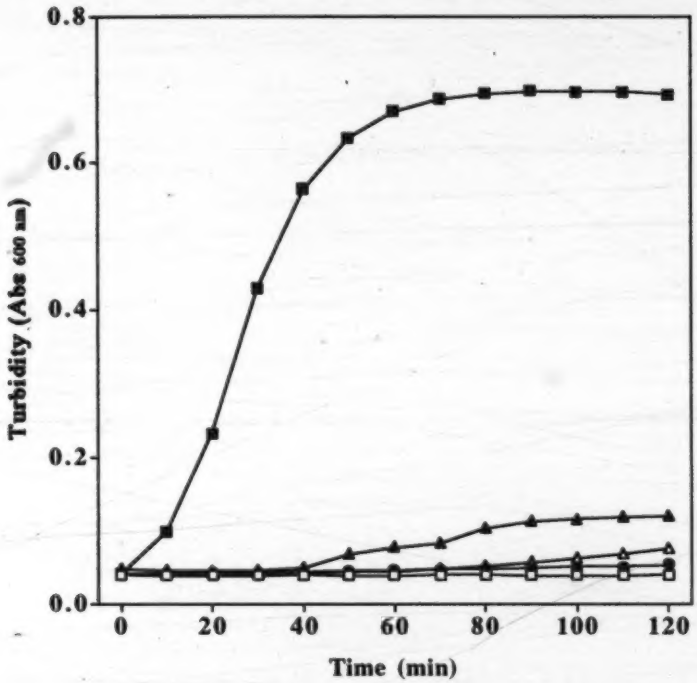

Figure 4-5. Effect of apolipoproteins on phospholipase-C-induced turbidity of LDL. Fifty µg of pyrene-N40C-apoLp-III (closed triangles), L90C-apoLp-III (open triangles) or wild-type apoLp-III (closed circles) were incubated with isolated human LDL (50 µg protein) in the presence of 160 mU phospholipase-C in a final volume of 250 µl in a microtiter plate at 37 °C. A negative control which had LDL but no phospholipase-C (open squares) and a positive control which had LDL in the presence of phospholipase-C but with no added apoLp-III (closed squares) were included. The reaction was initiated by the addition of phospholipase-C and the turbidity measured at 600 nm at the specified times. Values are average of three independent measurements ± S.E.M.

This novel, generally-applicable method was employed to induce a stable binding interaction between labeled apoLp-IIIs and spherical lipoprotein particles.

Potassium iodide quenching

Fluorescence properties of labeled apoLp-IIIs were used to investigate the effect of lipid interaction on specific apoLp-III helical segments. The aqueous quencher, KI, was used to probe the accessibility and alteration in the local microenvironment of pyrene-labeled

apoLp-IIIs in lipid-free and lipid-bound states (202). **Table 4-1** shows the effective Stern-Volmer quenching constants (K_{SV}) obtained for pyrene-N40C- and pyrene-L90C-apoLp-III.

Table 4-1: Effective Stern-Volmer quenching constants (K_{SV}) for pyrene-labeled N40C- and L90C-apoLp-III using KI

	K_{sv} (M^{-1})[a]		
	Lipid-free	DMPC-bound	LDL-bound
N40C-apoLp-III	27.1 ± 0.8	26.1 ± 1.2	2.2 ± 0.1
L90C-apoLp-III	19.8 ± 0.1	12.2 ± 0.1	2.8 ± 0.1

[a] K_{SV} values were calculated as described in Chapter 2.2; values shown are mean ± S.E.M. (n = 3)

Iodide, which quenches by a dynamic, collisional mechanism, was an efficient quencher of pyrene-apoLp-III fluorescence in the absence of lipid. When pyrene-labeled N40C-apoLp-III was unfolded in 2 M guanidine HCl, the observed K_{SV} (30.5 M^{-1}) was similar to that for the native protein, indicating the pyrene moiety in native N40C-apoLp-III is highly accessible to KI. With pyrene-N40C-apoLp-III/DMPC complexes, the extent of quenching by iodide was similar to that in the lipid-free state. On the other hand, with pyrene-L90C-apoLp-III/DMPC complexes, K_{SV} decreased by nearly 40%, compared to the lipid-free state. This reduced quenching efficiency may be due to a change in the microenvironment of the fluorophore upon interaction with the disc particles. Alternatively, it may be that the hydrophobic pyrene molecule is buried in the interior of the phospholipid bilayer, thereby denying access to iodide. Iodide was less effective at quenching pyrene-N40C- or pyrene-L90C-apoLp-III fluorescence when bound to the surface of LDL particles. The observed significant reduction in K_{SV} values indicates

sequestration of the fluorophore in both labeled proteins, away from the aqueous environment.

Lipophilic quenchers

Spin-labeled fatty acids, with the doxyl moiety located at different positions along the hydrocarbon backbone of the fatty acyl chain, serve as useful quenchers which operate within a lipid environment (209). These quenchers may be used as "molecular rulers" to characterize the interaction of a fluorophore with a given lipid surface. 5- and 12-DSA were incorporated into lipid particles and used to estimate the spatial disposition of Tyr145 in wild-type apoLp-III and the pyrene moiety on N40C- and L90C-apoLp-III, respectively. Upon binding DMPC, the globular apoLp-III helix bundle undergoes a conformational opening, aligning its helical segments around the perimeter of the disc complexes (167, 172). Quenching of tyrosine and pyrene fluorescence upon binding of apoLp-III to DMPC bilayer discs is shown in **Figures 4-6** and **4-7**, respectively. A plot of F_o/F vs. [Q] yields a straight line, the slope of which is equivalent to the apparent quenching constant, K_{app} (**inset** in Figures 4-6 and 4-7).

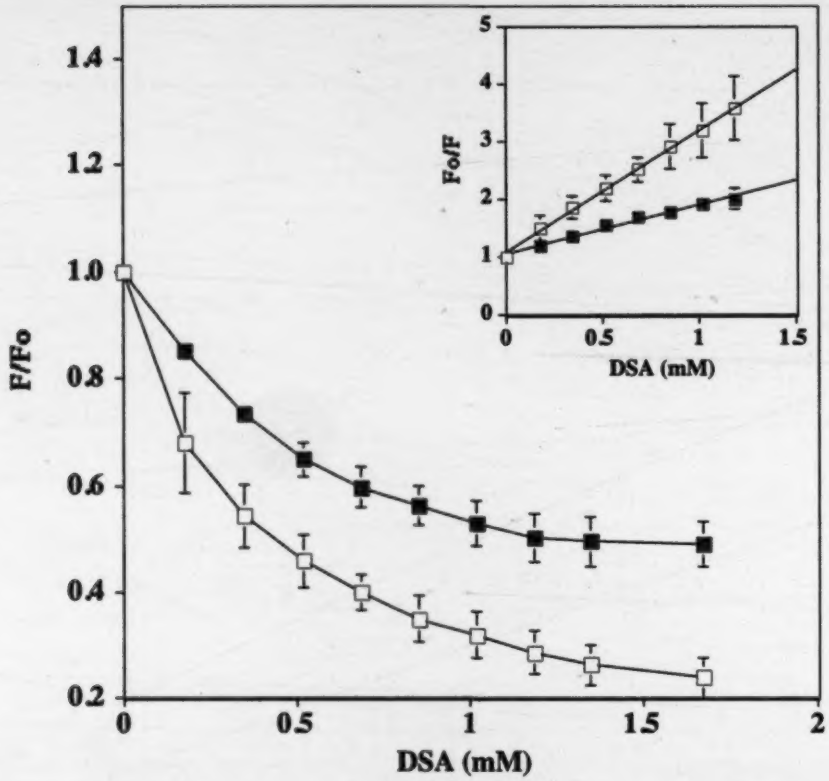

Figure 4-6. Estimation of the transverse disposition of helix 5 in phospholipid disc complexes. Plot of relative fluorescence *versus* concentration of spin-labeled fatty acid. 5-DSA (open squares) and 12-DSA (closed squares) were prepared as a stock ethanolic solution and were directly added to the lipid-bound wild-type apoLp-III samples, such that the final concentration of ethanol was always <1%. Fluorescence emission intensity of tyrosine was measured at 300 nm (excitation 277 nm). *Inset.* A Stern-Volmer plot of F_o/F vs. [Q] yields a straight line whose slope represents the apparent quenching constant. Initial values were used for calculations of K_{app}. Values are average of three independent measurements ± S.E.M.

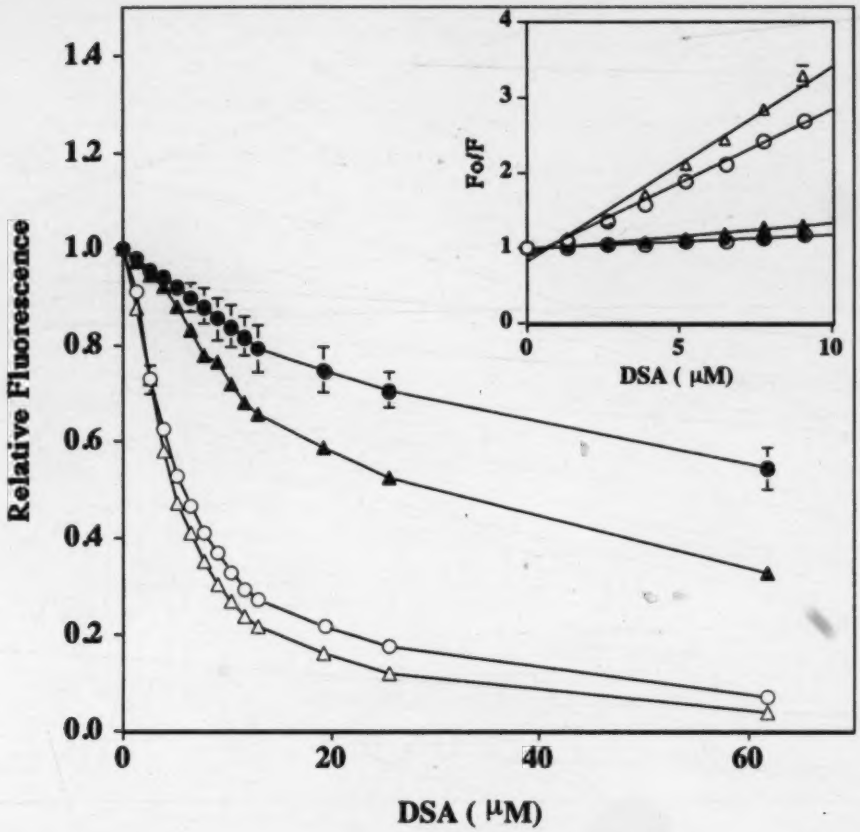

Figure 4-7. Estimation of transverse disposition of helices 2 and 3 in phospholipid disc complexes. Plot of relative fluorescence *versus* concentration of spin-labeled fatty acid. Pyrene-N40C- (circles) and pyrene-L90C-apoLp-III (triangles) disc complexes were quenched with 5-DSA (open symbol) and 12-DSA (filled symbol). Fluorescence emission intensity of pyrene was measured at 375 nm (excitation 345 nm). *Inset.* Stern-Volmer plot. Initial values were used for calculations of K_{app}. Values are average of three independent measurements ± S.E.M.

Table 4-2 shows that 5-DSA quenched tyrosine fluorescence to a significantly larger extent than 12-DSA. Similarly, in both pyrene-N40C-apoLp-III/DMPC and pyrene-L90C-apoLp-III/DMPC complexes, a greater extent of quenching was observed with 5-DSA.

Table 4-2. Apparent Stern-Volmer constants (K_{app}) for wild-type and pyrene-labeled apoLp-III using spin-labeled fatty acids.

	K_{app}[a] ($\times 10^{-4}$ M^{-1})					
	5-DSA			12-DSA		
	wild-type apoLp-III	pyrene-N40C apoLp-III	pyrene-L90C apoLp-III	wild-type apoLp-III	pyrene-N40C apoLp-III	pyrene-L90C apoLp-III
DMPC-bound	0.21 ± 0.04	19.6 ± 0.8	25.9 ± 1.4	0.09 ± 0.01	1.9 ± 0.6	3.6 ± 0.1
LDL-bound	ND[b]	15.6 ± 0.8	21.6 ± 2.0	ND	1.5 ± 0.2	3.6 ± 0.5

[a]Apparent K_{app} values were calculated as described in Chapter 2.2; values shown are the mean ± S.E.M. (n = 3).
[b]ND: Not determined due to interference of fluorescence from apoB-100.

In contrast to the location of apoLp-III in DMPC complexes, where it interacts with the phospholipid fatty acyl chains around the perimeter of the disc, apoLp-III likely binds to the surface monolayer of spherical lipoproteins with its helices intercalated between the head groups of phospholipids and interacting with diacylglycerol (127, 129). As shown above, apoLp-III interacts with spherical lipoprotein particles following treatment with phospholipase C. To evaluate whether apoLp-III associates weakly within the lipoprotein monolayer or if apoLp-III actually makes direct contact with the particle core, the ability of 5-DSA versus 12-DSA to quench pyrene-apoLp-III fluorescence was examined (**Figure 4-8**). This experimental approach could not be applied to wild-type apoLp-III, however, because its tyrosine fluorescence is masked by the extensive contribution of intrinsic fluorescence of the apoB-100 component of LDL. With both LDL-associated pyrene-N40C-apoLp-III and pyrene-L90C-apoLp-III, 5-DSA quenched to a much greater extent than 12-DSA, suggesting the fluorophore is located close to the water/lipid interface, thus suggesting a weak interaction between apoLp-III and the lipoprotein particle.

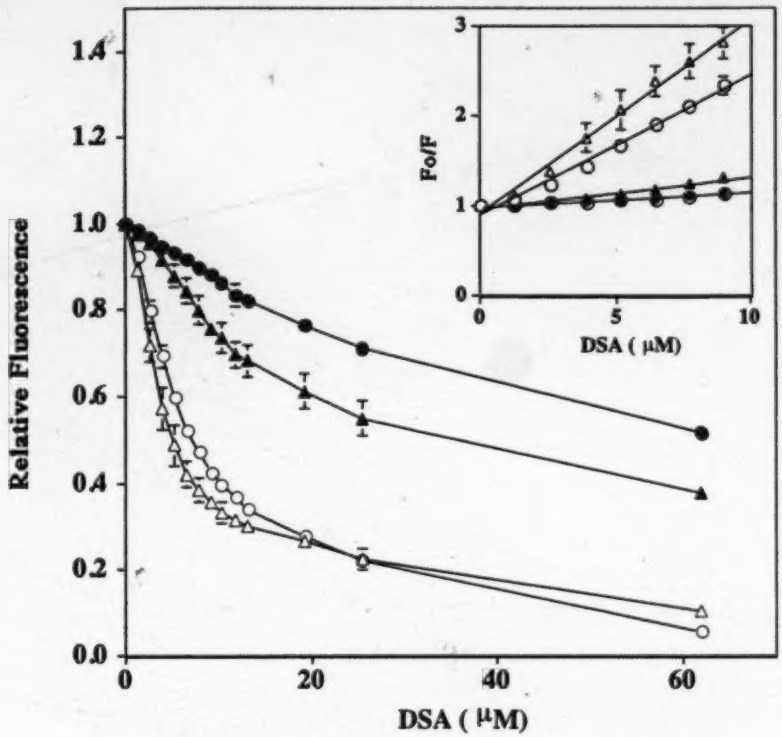

Figure 4-8. Estimation of spatial disposition of apoLp-III on a lipoprotein surface. Plot of relative fluorescence *versus* concentration of spin-labeled fatty acid. LDL-bound pyrene-N40C- (circles) and pyrene-L90C-apoLp-III (triangles) were quenched with 5-DSA (open symbols) and 12-DSA (closed symbols). Fluorescence emission intensity of pyrene was measured at 375 nm (excitation 345 nm). *Inset.* Stern-Volmer plot. Initial values were used for calculations of K_{app}. Values are shown as average of three independent measurements ± S.E.M.

4.3 DISCUSSION

The helix-bundle molecular architecture is a common structural motif of exchangeable apolipoproteins in their lipid-free state (5, 6, 156). Such an organization facilitates its existence as a soluble protein in an aqueous medium such as plasma or hemolymph, and permits binding to lipid surfaces through a conformational change. In order to obtain information about lipid-associated conformations of apoLp-III, the fluorescence properties of its unique tyrosine residue (located close to the centre of the non-polar face

at position 145 in helix 5) have been investigated (3, 118, 121, 167). In these studies Tyr145 served as a reporter of the conformational status of helix 5 in different environments. However, examining intrinsic tyrosine fluorescence has limited applications for the following reasons: 1) its quantum yield is low; 2) it cannot be selectively evaluated in the presence of other proteins and 3) the focus is limited to helix 5. To circumvent these problems and expand the versatility of the fluorescence approach to investigate structural aspects of lipid-associated apoLp-III, we have introduced single cysteine residues into the protein by site-directed mutagenesis at Asn40 (helix 2) or Leu90 (helix 3). Following covalent attachment of pyrene to the free sulfhydryl, fluorescence quenching was performed to evaluate the orientation of apoLp-III helical segments in DMPC disc complexes and the depth of penetration of the helices into the monolayer surface of intact spherical lipoprotein particles. The advantages of this approach include high quantum yield of the pyrene fluorophore, lack of interference from other proteins which may be present in the system under study and the ability to introduce the reporter fluorophore at specified locations in the protein.

Changes in accessibility to quenching by KI were measured to monitor alterations in the local microenvironment of the labeled cysteine residues. In the lipid-free globular form, high quenching constants were obtained for both pyrene-N40C- and pyrene-L90C-apoLp-III. This indicates that the pyrene moiety is readily accessible to the negatively-charged iodide. Examination of the structure of lipid-free apoLp-III (6) revealed several lysine residues in helices 3 and 4 in close proximity to N40C, as well as at *i*, *i* + 1 and *i*, *i* + 4 positions in helix 2. Similarly, lysines were found in helix 4, as well as at the *i*, *i* + 2 position to L90C in helix 3. Thus, a positively-charged microenvironment in the vicinity of the fluorophore likely enhances iodide quenching. Upon binding to model disc complexes, a 40% decrease in K_{SV} was noted for pyrene-L90C-apoLp-III, yet little or no change in K_{SV} was observed for pyrene-N40C-apoLp-III in these complexes. This result may be explained if helix 2 is located closer to the quarternary amine of choline head

groups of the phospholipids, promoting iodide quenching (210). When bound to the surface of spherical lipoprotein particles, K_{SV} for both pyrene-labeled apoLp-IIIs decreased by about 90% compared to the lipid-free state. A likely explanation for this large decrease in K_{SV} is burial of the hydrophobic pyrene moiety in the lipoprotein monolayer, which denies access to the hydrophilic iodide. Taken together, these results document clear differences in the microenvironment of the probe upon association with phospholipid disc complexes versus lipoprotein particles, indicating that these represent distinct lipid surfaces for binding of exchangeable apolipoproteins. Furthermore, apolipoprotein/lipoprotein complexes created using phospholipase C-modified LDL provide a useful, physiologically relevant alternative to phospholipid discs for studying the properties of lipid-associated exchangeable apolipoproteins. Indeed, these particles are amenable to studies of the depth of penetration of apolipoprotein helical segments into the lipoprotein surface.

Use of fatty acid spin labels to study lipid-bound protein conformations

Protein-lipid interactions in model membranes have been studied in detail using spin-labeled fatty acids (211). Fatty acid spin labels quench via a short-range collisional mechanism. Thus, they have to be present in or near the sphere of action of the fluorophore in order to quench effectively, with an optimal interaction distance of 4-6 Å (212). We have estimated the transverse disposition and depth of penetration of apoLp-III helices in model disc complexes and lipoprotein particles, respectively, based on the parallax fluorescent quenching method originally proposed by Chattopadhyay and London (213). This method recommends the use of spin-labeled phospholipids instead of spin-labeled fatty acids due to the vertical fluctuations and relatively faster lateral mobility of the latter (214). However, our attempts to make discs containing spin-labeled phospholipids were unsuccessful as judged by electron microscopic characterization of the product particles. The choice to use spin-labeled fatty acids in our experiments was

to our advantage since they can be added directly to the lipoprotein or disc system with bound apoLp-III. Quenching by spin-labeled fatty acids has been successfully used in several cases to measure the location of protein-bound fluorophores in membranes by comparison of the quenching efficiency of probes placed at various depths in the membrane (215-217). In 5-DSA, the doxyl moiety is located approximately 6 Å from the membrane/water interface, while in 12-DSA it is located about 15 Å from the interface, deep in the membrane interior (209).

Fluorescence quenching of apoLp-III-phospholipid disc particles

Wild-type apoLp-III contains a single tyrosine residue which is an intrinsic fluorophore. Previous studies have shown that helix 5, in isolation, cannot form complexes with phospholipid *in vitro* (118). However, quenching of its fluorescence by spin-labeled fatty acids when present in the intact helix bundle indicates that, despite its terminal location in the protein sequence, helix 5 contacts the lipid surface in a stable, oriented manner. Pyrene-labeling of two cysteine mutant apoLp-IIIs allowed further quenching studies, yielding information on the disposition of helices 2 and 3, as well. In the lipid-free protein, NMR structural studies revealed that helix 5 interacts with helices 1 and 2, while there are no contacts between helices 1 and 2 themselves (6). In studies of the conformation of apoLp-III in phospholipid disc particles, cross-linking experiments indicate that up to 6 molecules of apoLp-III align around the circumference of the disc complexes (167). On the basis of Fourier transform infrared spectroscopy studies it is concluded that the helices adopt a unique orientation, with their axes oriented perpendicular to the fatty acyl chains of the phospholipid bilayer (172). If conformational opening occurs as proposed, both ends of the molecule should contact the lipid surface. The quenching studies with pyrene-N40C- and pyrene-L90C-apoLp-III support this view. Furthermore, since 5-DSA displayed a more pronounced quenching efficiency than 12-DSA in the disc complexes, the helices containing Tyr145 (helix 5),

pyrene-N40C (helix 2) and pyrene-L90C (helix 3) likely align closer to the water/lipid interface. These data suggest that helix alignment in these complexes is not random, but rather the protein adopts a preferred orientation with respect to the bilayer. Further studies will be required to delineate the precise location of the different helices with respect to each other and the phospholipid bilayer.

Shallow penetration of apoLp-III on lipoprotein surfaces

All exchangeable apolipoproteins identified to date share a common amphipathic α-helix structural motif (164). These helices have well-defined polar and non-polar faces which can interact with the aqueous and hydrophobic milieu, respectively, on a lipoprotein surface. This feature imparts to exchangeable apolipoproteins the structural adaptability to reversibly associate with circulating lipoproteins. We have examined the association of apoLp-III with lipoprotein surfaces by first allowing the pyrene-labeled protein to bind to the surface of LDL particles modified by treatment with phospholipase C, a situation that mimics the physiological setting wherein apoLp-III binds to lipophorin particles in response to DAG enrichment (82). We have estimated the location of the fluorophore within the lipoprotein surface monolayer by comparing the quenching obtained with spin labels at two different depths. With pyrene-N40C-apoLp-III or pyrene-L90C-apoLp-III, the fluorophore was quenched 6 to 10-fold more with 5-DSA than with 12-DSA. Thus, it is estimated that the helices are located near the water/lipid interface with their axes perpendicular to the phospholipid monolayer. Based on the hinged loop opening, it may be envisaged that the hydrophobic interior of the protein is loosely embedded with its helical axes parallel to the lipoprotein surface in contact with the DAG-containing phospholipid monolayer (129). Because we are monitoring fluorescence at both ends of the protein (in its open conformation), this weak binding is representative of the entire protein, implying a "loose binding" of apoLp-III with the lipoprotein surface. This mode of binding of apoLp-III to the lipoprotein surface is functionally relevant given the

reversible nature of exchangeable apolipoprotein interactions. This would facilitate dissociation from lipid surfaces with a small energetic cost and is consistent with displacement studies performed by Liu *et al.* (124) in which apoLp-III was readily displaced from the surface of low density lipophorin by human apoA-I. A similar mode of interaction has been proposed for the binding of class A amphipathic helices of apolipoproteins with the phospholipid monolayer, though a deeper penetration of the nonpolar face has been implied (218). However, in the case of apoLp-III, the binding interaction appears to be correlated with exposed DAG, which probably acts as a trigger for initiating association with the lipoprotein surface.

In summary, using fluorescently-labeled single sites on helices 2, 3 and 5, we have focused on the topography of a full length apolipoprotein whose structure in the lipid-free state is known (6). Using a combination of protein engineering and fluorescence spectroscopy techniques, we have learned the following:

i) the microenvironment of the cysteine residue on each helix changes when lipid-free apoLp-III is bound to discoidal complexes or spherical lipoprotein particles, indicative a conformational change.

ii) helices 2, 3 and 5 align close to the lipid/water interface of discoidal complexes;

iii) the apoLp-III molecule associates weakly with lipoprotein surfaces, consistent with its reversible nature of binding.

CHAPTER 5

Pyrene Excimer Fluorescence: A Spatially Sensitive Probe to Monitor Lipid-induced Repositioning of Helices 2 and 3 in Apolipophorin III*

*Parts of this chapter have already been published.

Sahoo, D., Narayanaswami, V., Kay, C. M. and Ryan, R. O. (2000) Pyrene excimer fluorescence: a spatially sensitive probe to monitor lipid-induced helical rearrangement of apolipophorin III. *Biochemistry* **39**, 6594-6601.

5.1 INTRODUCTION

In the present study, we explore the unique fluorescence properties of N-(1-pyrene)maleimide, an intensely fluorescent extrinsic cysteine-reactive probe, to address proximity issues of helices 2 and 3 in the lipid-free and lipid-bound states. Pyrene displays unique spectral characteristics such as the ability to form excited-state dimers (excimers) when spatially proximal to another pyrene molecule. Cysteine residues were introduced strategically into apoLp-III to create a double-cysteine mutant (N40C/L90C-apoLp-III) that was subsequently labeled with pyrene. Using the pyrene-labeled N40C/L90C-apoLp-III mutant in addition to the two pyrene-labeled single-cysteine mutants used in the previous chapter, we exploit pyrene excimer fluorescence to address the lipid binding-induced helix repositioning in apoLp-III and the relative orientation of lipid-bound apoLp-III in model phospholipid disc complexes.

5.2 RESULTS

Characterization of pyrene-labeled apoLp-III

In the reduced state, the sulfhydryl groups in N40C/L90C-apoLp-III are accessible for labeling with pyrene maleimide in the absence of denaturants. When excited with UV light following SDS-PAGE, pyrene-labeled, but not unmodified apoLp-III, was intensely fluorescent. The extent of pyrene incorporation into N40C/L90C-apoLp-III (18,379 ± 3 Da) was evaluated by electro-spray mass spectrometry. A single mass peak corresponding to an increment of 594 Da was observed (**Figure 5-1**).

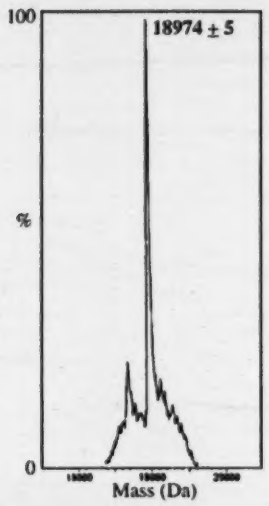

Figure 5-1. Electrospray mass spectrometry profile of pyrene-labeled N40C/L90C-apoLp-III. Pyrene-labeling of double-cysteine apoLp-III yielded a labeled protein with a molecular weight of 18 974 ± 5 Da.

Labeling stoichiometry was calculated using the molar extinction of pyrene as 40 x 10^{-3} $M^{-1}cm^{-1}$ (219). Based on mass spectrometry data, we conclude that pyrene incorporation into the different cysteine mutants was > 95 %, with no evidence of unlabeled protein. Far-UV-CD spectroscopy revealed that the secondary structure content of pyrene-labeled N40C/L90C apoLp-III (67% α-helix) was similar to that of wild-type apoLp-III reported earlier (3). Interestingly, covalent attachment of pyrene to the double mutant increases the protein's mid-point of denaturation by GdnHCl (transition midpoint 0.4 M (3) for wild-type apoLp-III and 1.2 M for pyrene-labeled N40C/L90C-apoLp-III).

Pyrene excimer fluorescence

Pyrene maleimide, when attached to free sulfhydryl groups on target proteins, exhibits spectral properties which are dependent upon its relative proximity to neighboring pyrene molecules. Thus, an excited-state pyrene monomer emits typical emission bands at 375 and 395 nm when excited at 345 nm. In addition, the excited state monomers can interact with a suitably positioned ground-state pyrene to form excited-state dimers or "excimers" (**Figure 5-2**).

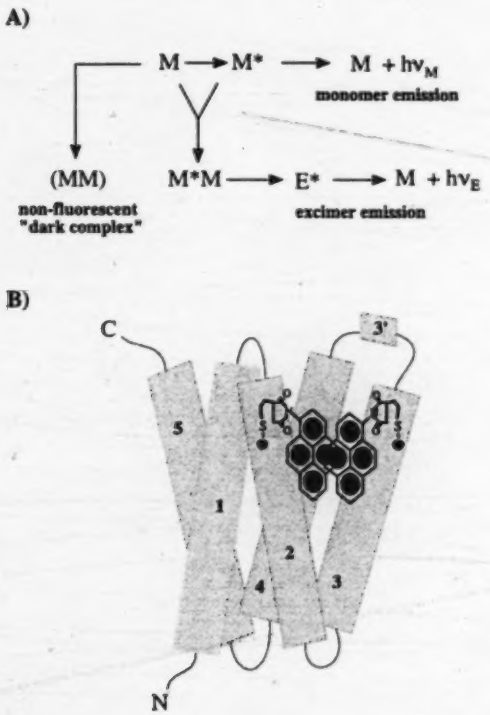

Figure 5-2. A) Schematic representation of pyrene fluorescence properties. Excitation (345 nm) of ground state monomers (M) gives rise to excited state monomers (M*) with typical emission maxima at 375 and 395 nm. When M* interacts with a spatially proximal M in a precise configuration, the resulting M*M dimer results in excimer

emission (E*) at 460 nm. If the dimeric configuration is not favourable for excimer emission, a non-fluorescent "dark complex" will form [modified from (220)]. **B)** An exaggerated schematic of stacking interactions resulting in excimer fluorescence in pyrene-labeled lipid-free N40C/L90C-apoLp-III is shown.

Excimers occupy a lower energy excited state than an excited monomer, and give rise to a characteristic fluorescence emission upon returning to the ground state. Compared to monomer fluorescence, excimer emission is red-shifted and lacks the fine structure which arises from vibrational transitions. Thus, excimer emission results in departure from the mirror image rule of excitation and emission spectra usually observed for non-interacting fluorophores (221). Furthermore, when two pyrene moieties giving rise to excimer fluorescence reposition > 10 Å from one another (e.g., due to conformational change in the labeled protein), excimer fluorescence is decreased or lost entirely. Using the structure of lipid-free apoLp-III as a guide for site-directed mutagenesis (153), we engineered two reactive cysteine residues into the protein at positions which are distal in terms of the linear sequence, yet proximal in terms of the three-dimensional fold of the protein (see Figure 5-2). We hypothesized that covalent attachment of pyrene at these sites will result in manifestation of excimer fluorescence. Upon complexation to lipid, we predict that changes in excimer fluorescence will occur as a result of conformational opening of the helix bundle. At the same time, it is recognized that any change in monomer fluorescence could also influence excimer fluorescence. For example, if monomer fluorescence is independently quenched, the decreased population of excited monomer will result in a decreased excimer population. Thus, interpretation of changes in excimer fluorescence and assignment of such changes to increased distance between pyrene moieties must include appropriate controls.

Fluorescence properties of lipid-free pyrene-labeled apoLp-III

In the lipid-free α-helix bundle state, Asn 40 is located at the N-terminal end of helix 2, while Leu 90 is located at the C-terminal end of helix 3. In the up-and-down amphipathic α-helix bundle these residues reside approximately 9 Å from one another (6). Fluorescence spectra were acquired for pyrene-labeled lipid-free N40C- and L90C-apoLp-III (**Figure 5-3, curves a,b**).

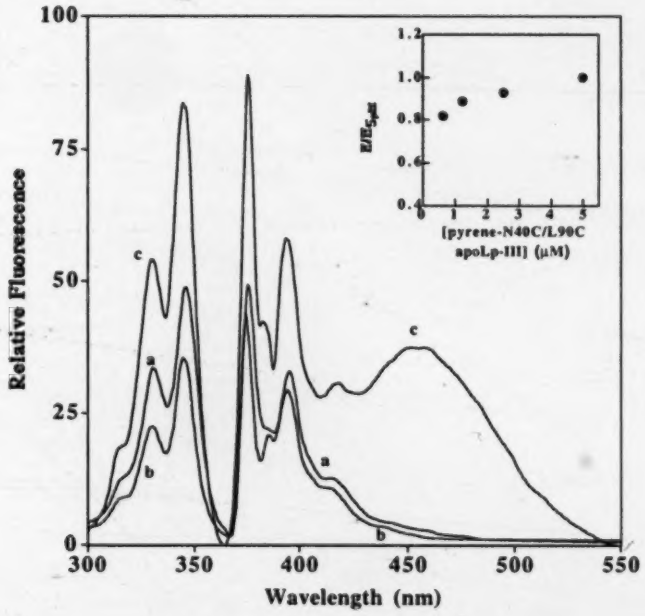

Figure 5-3. Fluorescence excitation and emission spectra of lipid-free pyrene-labeled N40C-, L90C- and N40C/L90C-apoLp-IIIs. Solutions (50 μg/mL) of pyrene-N40C- (curve a), pyrene-L90C- (curve b) or pyrene-N40C/L90C-apoLp-III (curve c) were excited at 345 nm and emission was monitored between 360 nm and 550 nm. Excitation spectra were collected by setting the monomer emission at 375 nm. *Inset*: Effect of dilution on pyrene-labeled apoLp-III excimer fluorescence. $E_{5\,\mu M}$ represents the area under the excimer emission of a 5 μM pyrene-labeled apoLp-III solution and E represents the area under the excimer emission at each concentration. These spectra are representative of three independent experiments.

In both cases, corresponding excitation and emission spectra are mirror images of each other at the concentrations used, with defined major emission maxima at 375 and 395 nm and minor peaks at 385 and 410 nm, characteristic of pyrene monomers. In the case of N40C/L90C-apoLp-III (**Figure 5-3, curve c**), in addition to the emission maxima for monomeric pyrene, a red-shifted, unstructured maximum centered around 460 nm, typical of excimer fluorescence, was observed. Excimer emission was noted at protein concentrations ranging from 0.6 to 5 μM, with little deviation in the ratio of monomer to excimer emission (**Figure 5-3, inset**). The data are consistent with the conclusion that intramolecular, rather than intermolecular pyrene-pyrene interactions are responsible for the observed excimer fluorescence. This interpretation is supported by the lack of excimer fluorescence in apoLp-III molecules bearing a single pyrene moiety and the known existence of lipid-free apoLp-III as a monomer in buffer (6).

Effect of apoLp-III unfolding on pyrene excimer fluorescence

To test the hypothesis that changes in apoLp-III conformation will be manifest by changes in intramolecular pyrene excimer fluorescence, pyrene-labeled N40C/L90C-apoLp-III was exposed to increasing amounts of GdnHCl or heat, two agents that known to cause protein unfolding. Unfolding by GdnHCl was judged by changes in molar ellipticity at 222 nm and correlated with the area under the fluorescence excimer emission peak (**Figure 5- 4**).

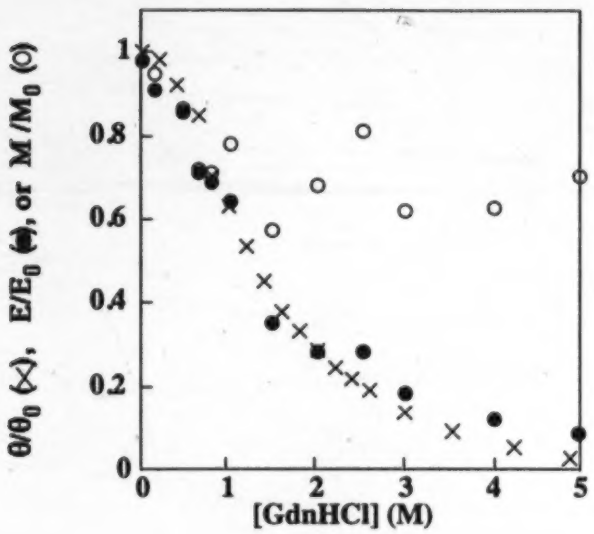

Figure 5-4. Effect of GdnHCl on the secondary structure content and fluorescence of pyrene-N40C/L90C-apoLp-III. Aliquots of 6 M GdnHCl were added to solutions of pyrene-labeled N40C/L90C-apoLp-III (50 μg/mL). CD and fluorescence data, plotted as a function of GdnHCl concentration where molar ellipticity (θ), monomer (M) and excimer (E) emission, are indicated by X, O, and ●, respectively. Values for θ/θ_o, M/M_o and E/E_o were obtained as described in Chapter 2.2.

The GdnHCl transition mid-point, monitored either by molar ellipticity or by excimer fluorescence, was 1.2 M. Although excimer fluorescence steadily decreased with increasing GdnHCl, this was not accompanied by a corresponding increase in monomer fluorescence. To assess whether the observed decrease in monomer fluorescence was due to environmental quenching, the effect of dissolved oxygen, a quencher of almost all known fluorophores, was assessed (221). The results indicate that the apparent quenching was not due to dissolved oxygen, however, since no differences were noted upon extensive degassing of all solutions. Interestingly, quenching of monomer fluorescence occurred when single pyrene-labeled N40C-apoLp-III was denatured with

GdnHCl, suggesting that the decrease in monomer fluorescence is unrelated to the presence of excimer fluorescence (**Figure 5-5**).

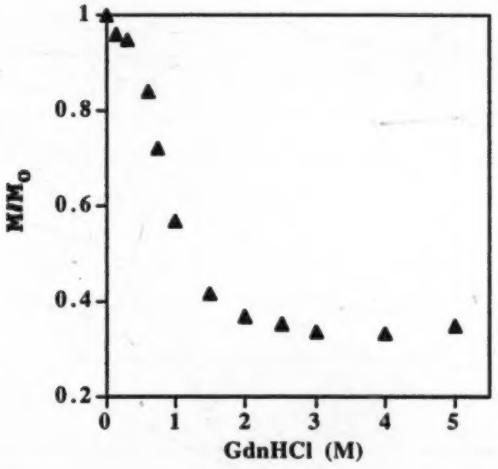

Figure 5-5. Effect of GdnHCl on the monomer fluorescence of pyrene-N40C-apoLp-III. Aliquots of 6 M GdnHCl were added to solutions of pyrene-labeled N40C-apoLp-III (50 μg/mL). Emission was monitored from 360 to 500 nm (excitation 345 nm). Values for M/M_o were obtained as described in Chapter 2.2.

Regardless of the cause of the decrease in monomer fluorescence as a function of GdnHCl, this phenomenon precludes a direct correlation between GdnHCl-induced unfolding of apoLp-III and loss of excimer fluorescence.

To obtain information about the ground state configuration of the pyrenes under different conditions, excitation spectra of monomer (emission 375 nm) and excimer (emission 460 nm) fluorescence were collected for pyrene-labeled N40C/L90C-apoLp-III in 0 M and 5 M GdnHCl (**Figure 5-6**).

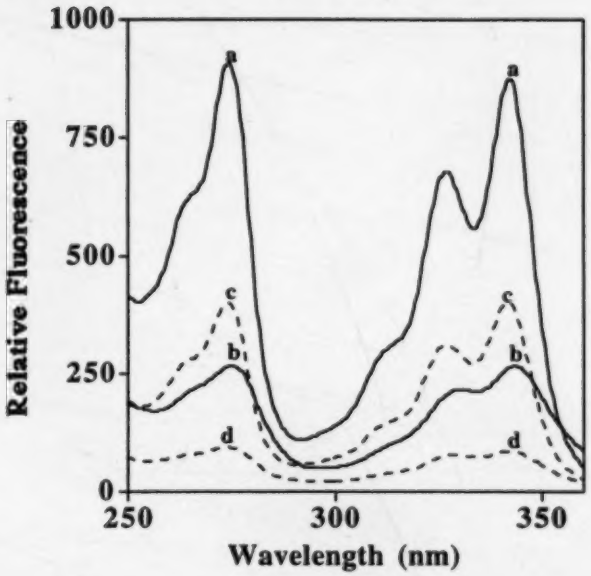

Figure 5-6. Excitation spectra of pyrene-labeled N40C/L90C-apoLp-III in the absence (solid lines) and presence (dashed lines) of GdnHCl. Monomer excitation spectra at 0 M GdnHCl (curve a) and 5 M GdnHCl (curve c) were collected by setting the emission wavelength at 375 nm, while excimer excitation spectra at 0 M GdnHCl (curve b) and 5 M GdnHCl (curve d) were collected by setting the emission wavelength at 460 nm.

In the absence of GdnHCl, there was a broadening and a small red shift of the excimer excitation spectrum (curve b) compared to that of the monomer (curve a). In addition, in the presence of 5 M GdnHCl, the excimer excitation peak (curve d) was further broadened compared not only to that of its corresponding monomer (curve c) but also to the excimer excitation spectrum at 0 M GdnHCl (curve b). These data suggest that, despite denaturation of the protein, the pyrene rings interact in the ground state, and that excimer fluorescence orginates from pyrenes that are in a different environment than pyrenes that produce monomer fluorescence (220, 222). Thus, even at high GdnHCl, wherein there is total loss of ellipticity, pyrenes can still interact.

The same pattern is even more striking in the case of temperature-induced unfolding of pyrene-labeled N40C/L90C-apoLp-III (**Figure 5-7**).

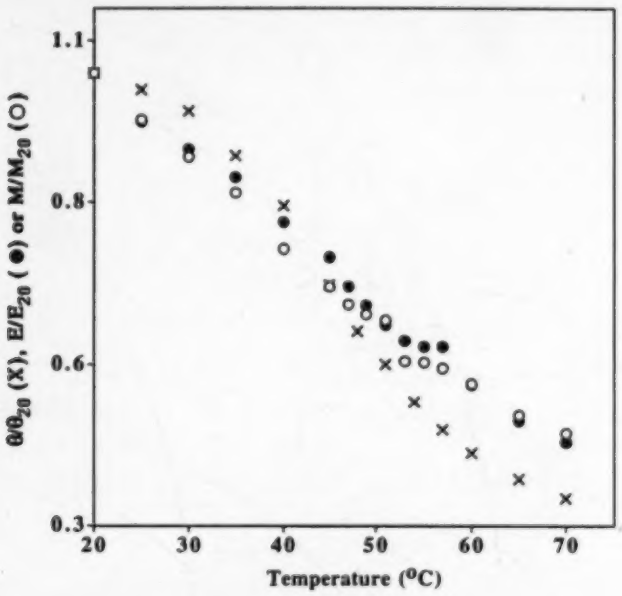

Figure 5-7. Effect of heat on pyrene excimer fluorescence. Molar ellipticity (θ), monomer (M) and excimer (E) fluorescence of pyrene-labeled N40C/L90C-apoLp-III were followed as a function of increasing temperature. θ/θ_{20} (X), M/M_{20} (○) and E/E_{20} (●) were obtained as described in Chapter 2.2.

Although CD reveals that the molar ellipticity of pyrene-labeled N40C/L90C-apoLp-III is lost due to heat-induced unfolding of the protein, loss in excimer fluorescence is coincident with temperature-induced quenching of pyrene monomer fluorescence. Thus, it is not possible to attribute temperature-induced changes in excimer fluorescence directly to unfolding of apoLp-III. In comparison with spectra obtained from GdnHCl experiments, excitation spectra of double pyrene-labeled apoLp-III at 20 °C and 70 °C revealed a similar broadening of the excimer excitation spectra compared to the monomer excitation spectra, suggesting the presence of stacked pyrenes **(Figure 5-8).**

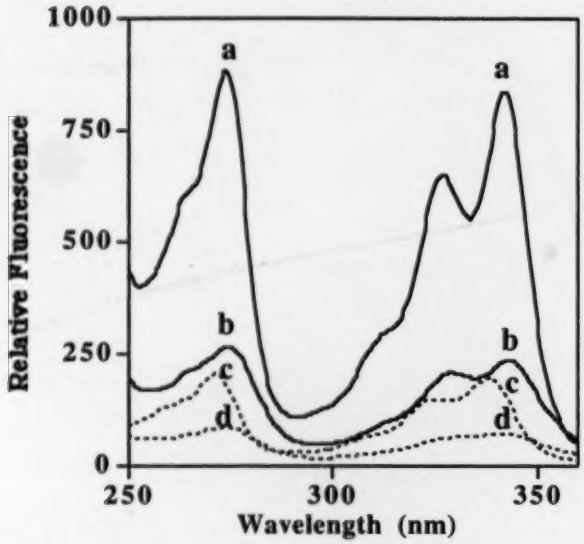

Figure 5-8. Excitation spectra of pyrene-labeled N40C/L90C-apoLp-III at low (solid lines) and high (dashed lines) temperature. Monomer excitation spectra at 20 °C (curve a) and 70 °C (curve b) were collected by setting the emission wavelength at 375 nm, while excimer excitation spectra at 20 °C (curve b) and 70 °C (curve d) were collected by setting the emission wavelength at 460 nm.

Interaction of pyrene-labeled N40C/L90C apoLp-III with trifluoroethanol

Trifluoroethanol has often been used as a helix-stabilizing cosolvent (223-225), that disrupts tertiary structural interactions in proteins while stabilizing secondary structural elements. In the case of helix bundle apolipoproteins, previous studies (189, 206) suggest that TFE induces conformational opening of the helix bundle in a manner analogous to lipid interaction. **Figure 5-9** shows the effect of TFE titration on excimer fluorescence in pyrene-labeled N40C/L90C-apoLp-III.

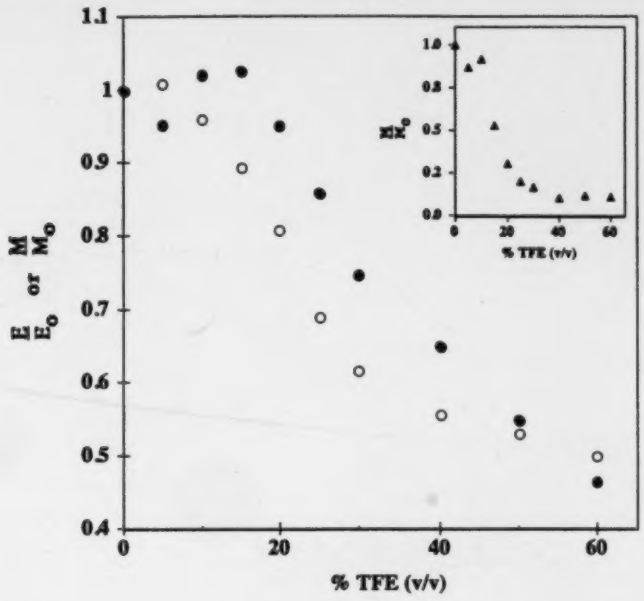

Figure 5-9. Effect of TFE on fluorescence of pyrene-labeled apoLp-III. Aliquots of 100% TFE were added to solutions of pyrene-labeled N40C/L90C-apoLp-III (50 µg/mL). Monomer (M) and excimer (E) fluorescence spectra were collected at increasing TFE concentrations. Values for M/M_o (O) and E/E_o (●) were obtained as described in Chapter 2.2. *Inset*: Effect of TFE on monomer fluorescence of single pyrene-labeled N40C-apoLp-III.

An initial small increase in excimer fluorescence at about 10% TFE is followed by a steady decline with a maximal decrease in excimer fluorescence occurring above 60% TFE (v/v). As in the case of the temperature experiment (Figure 5-7), however, the progressive decrease in area under the excimer curve is accompanied by a corresponding decrease in monomer fluorescence, albeit with a small initial lag. It should be noted that monomer fluorescence of single pyrene-labeled N40C-apoLp-III is also quenched by increasing concentrations of TFE (**Figure 5-9, inset**). Thus, direct correlation of loss of excimer fluorescence with TFE-induced conformational change of the helix bundle is not

possible because of corresponding TFE- and/or solvent-induced quenching of monomer fluorescence.

Helical repositioning of pyrene-labeled apoLp-III on discoidal complexes

Exchangeable apolipoproteins are characterized by their ability to transform phospholipid bilayer vesicles into discoidal structures (167). The discoidal complexes formed generally possess several apolipoprotein molecules, aligned around the perimeter of a disc-shaped phospholipid bilayer (167). The currently-held hypothesis is that the apoLp-III helix bundle opens about hinged loops at one end of the molecule to expose the hydrophobic interior of the protein which interacts with otherwise exposed phospholipid fatty acyl chains around the perimeter of the bilayer disc. Using pyrene-labeled N40C/L90C-apoLp-III, we postulated that a loss in excimer fluorescence would occur as a result of complexation of apoLp-III with DMPC. DMPC-bound pyrene-labeled N40C/L90C-apoLp-III, however, displayed a strong excimer peak, similar to that noted for lipid-free pyrene-apoLp-III (**Figure 5-10, curve a**).

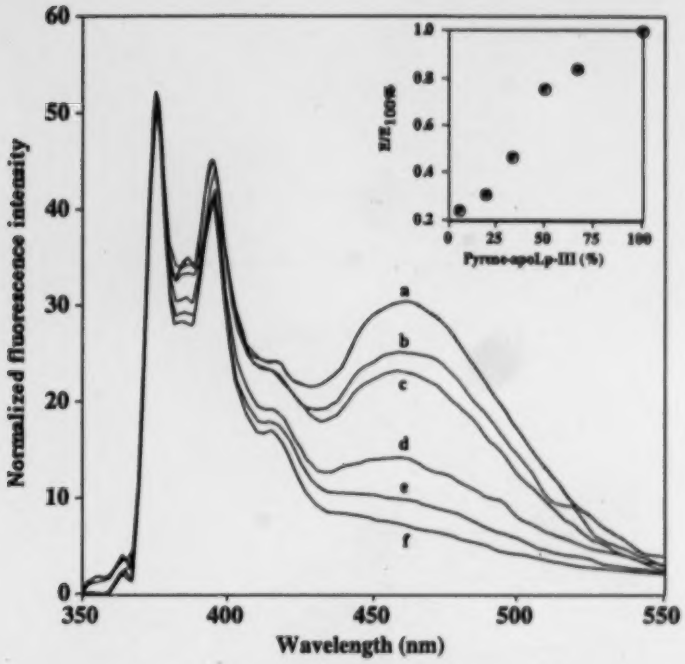

Figure 5-10. Fluorescence emission spectra of pyrene-N40C/L90C-apoLp-III bound to phospholipid bilayer discs. Pyrene fluorescence emission spectra were recorded for discoidal complexes made with only pyrene-N40C/L90C-apoLp-III (curve a; $E_{100\%}$) or a mixture of labeled N40C/L90C-apoLp-III and unlabeled wild-type apoLp-III, where the proportion of labeled apoLp-III was 67% (curve b), 50% (curve c), 33% (curve d), 20% (curve e) and 5% (curve f) . The lipid:protein ratio (w/w) was maintained at 2.5:1. For the various dilutions, the monomer fluorescence was normalized on the basis of the emission peak at 375 nm. *Inset*. Effect of dilution on excimer fluorescence. $E_{100\%}$ represents the area under excimer emission of discs containing only pyrene-labeled apoLp-III, and E represents the area under the excimer emission of discs bearing the indicated percentage of labeled apoLp-III.

Since apoLp-III/DMPC disc complexes possess up to six molecules of apoLp-III per particle (167), we hypothesized that intermolecular pyrene-pyrene interactions may be contributing to excimer fluorescence observed on apoLp-III/DMPC disc complexes. To discern between intramolecular and intermolecular excimer formation, dilution experiments using unlabeled wild-type protein were performed. Thus, during preparation of the disc complexes, pyrene-labeled N40C/L90C-apoLp-III was mixed with increasing

amounts of wild-type apoLp-III. A gradual loss of excimer fluorescence was observed when the percentage of unlabeled protein on the disc was increased (**Figure 5-10, curves b-f**). Importantly, the loss in excimer fluorescence (**Figure 5-10, inset**) was accompanied by a steady increase in the m/e ratio, corrected for dilution (m/e ratio of 1.7 for curve a increasing to 7.2 for curve f). It is therefore rationalized that excimer fluorescence observed on discs bearing only pyrene-labeled N40C/L90C-apoLp-III arises from intermolecular interactions between the pyrene at the end of one molecule with pyrene at the end of a neighboring molecule, in the "open" lipid-bound conformation of the protein. To confirm such intermolecular interactions, crosslinking experiments employing N40C/L90C-apoLp-III were performed using a sulfhydryl-specific crosslinker, *bis*-maleimidohexane (**Figure 5-11**). Crosslinking of up to five molecules of apoLp-III per disc particle was observed, suggesting that the sulfhydryl groups are located at either end of an open molecule of apoLp-III in the lipid-bound configuration.

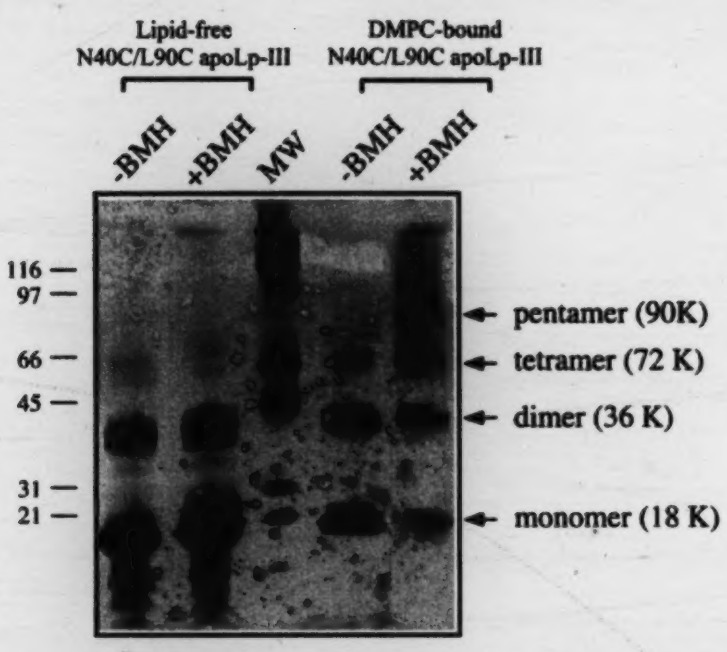

Figure 5-11. Crosslinking of apoLp-III around DMPC discoidal complexes. Sulfhydryl-reactive bis-maleimidohexane (BMH; 1.25 mM final concentration) was used to crosslink N40C/L90C-apoLp-III around discoidal complexes. Samples were electrophoresed on a precast 8-25% SDS gradient gel on the PhastSystem and silver-stained. Lane 1, lipid-free N40C/L90C-apoLp-III in absence of BMH; lane 2, lipid-free N40C/L90C-apoLp-III in presence of BMH; lane 3, molecular weight standards; lane 4, DMPC-bound N40C/L90C-apoLp-III in absence of BMH and; lane 5, DMPC-bound N40C/L90C-apoLp-III in presence of BMH.

Relative orientation of apoLp-III molecules on discoidal complexes

The presence of intermolecular pyrene-pyrene interactions in apoLp-III/phospholipid complexes prompted us to address questions related to the relative orientation apoLp-III adopts in discoidal complexes. In this case, pyrene-labeled N40C- or pyrene-labeled L90C-apoLp-III was complexed to DMPC vesicles to form a uniform population of discoidal bilayer complexes (167). In both cases, upon excitation at 345 nm, there was an absence of excimer fluorescence in the region around 460 nm (**Figure 5-12, curves a and b**).

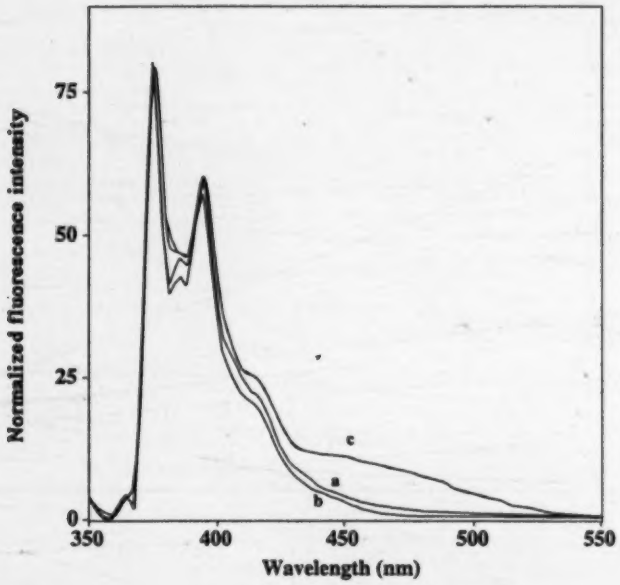

Figure 5-12. Fluorescence emission spectra of single pyrene-labeled apoLp-III/DMPC discs. Emission spectra were collected for DMPC complexes containing: pyrene-N40C-apoLp-III (curve a); pyrene-L90C-apoLp-III (curve b); or equal amounts of pyrene-N40C- and pyrene-L90C-apoLp-III (curve c). The lipid:protein ratio was 2.5:1. Monomer fluorescence was normalized on the basis of the emission peak at 375 nm.

If the end of the apoLp-III molecule harboring the N40C residue is assigned as the "head" and that bearing L90C as the "tail", then a tandem arrangement of apoLp-III molecules may be envisioned. A precise "head-to-tail" orientation of apoLp-III, wherein N40C in one molecule is proximal to L90C from another emerges from these studies. To further examine this ordered arrangement, disc complexes were prepared with equal amounts of pyrene-labeled N40C- and L90C-apoLp-III. In this case, excimer formation was observed, although, not as intense as may be expected (**Figure 5-12, curve c**). It is conceivable that, although equal amounts of both single pyrene-labeled mutants were used to form the discoidal complexes, (i) equal amounts of pyrene-labeled mutants may

not have been recovered in association with the discs or (ii) a random distribution of the labeled proteins on the discs may not have occurred.

5.3 DISCUSSION

Pyrene excimer fluorescence provides a useful tool to study apolipoprotein conformational changes which occur upon lipid interaction and to understand helix organization in the lipid-bound state of exchangeable apolipoproteins. This technique has been successfully used to obtain information about conformational alterations in other proteins including tropomyosin (222, 226, 227), troponin C (228, 229), lactose permease (230, 231) and sarcoplasmic reticulum ATPase (232). In the present study, N-(1-pyrene)maleimide was the extrinsic fluorophore of choice to study lipid binding-induced conformational changes in a model helix bundle apolipoprotein, permitting deduction of its relative orientation in discoidal complexes with DMPC. Pyrene fluorophores serve as unique probes for the following reasons: (i) they possess a high extinction coefficient and the monomer has a long lifetime (up to 90 ns) (233); (ii) the maleimide derivative can be used to selectively label cysteine residues at specified sites on a protein and (iii) excited pyrene monomers can interact with a neighbouring ground-state pyrene, proximal in space, forming dimeric "excimer" complexes. The structure of pyrene crystals indicates that the pyrenes interact as dimers, stacked in a precise manner with a distance of 3.5 Å between the two planes (234). Comparison of the excitation and emission spectra of single-labeled N40C- or L90C-apoLp-III and double-labeled N40C/L90C-apoLp-III clearly shows the exception of excimers to the mirror image rule (221). The emission spectrum of single-labeled apoLp-III is a mirror image of its excitation

spectrum as a result of the same transition being involved in both absorption and emission and the similarities among the vibrational energy levels of the ground and first-excited states. However, the emission spectrum of doubly-labeled apoLp-III is not a mirror image of its excitation spectrum, as the excimer emission is a result of an excited-state reaction which originates from a lower energy excited state than the excited monomer and dissociates upon returning to the ground state. Intrinsic excimer formation in apoLp-III arising from proximal aromatic residues [e.g., Tyr 145 and Phe 148; (235)] in the absence of pyrene labeling can be eliminated since selective excitation at 280 nm does not reveal emission at wavelengths longer than 306 nm for tyrosine residues (121) (*M. sexta* apoLp-III lacks tryptophan residues).

Pyrene-labeled N40C/L90C-apoLp-III displays a higher mid-point of denaturation as compared to that for unlabeled apoLp-III (3). This may arise from stacking of the pyrene rings or, alternatively, pyrene interactions with aromatic residues present in the protein. It is recognized that aromatic interactions contribute to hydrophobic packing in proteins, especially when a network of Tyr, Phe and Trp residues is present (120, 236). While excimer emission arises only from stacked pyrenes, every stacked configuration does not lead to excimer emission. It appears that a range of stacked configurations is present in pyrene-labeled N40C/L90C-apoLp-III, as suggested by a simple numerical addition of the monomer emission spectra of the two pyrene-labeled single mutants (see Figure 5-3). Whereas monomer emission in the double-labeled protein is superimposable on that of the added spectra, it should be less considering that a significant excimer peak appears. Thus, we suggest that different populations of monomer exist in the ground state, with a major portion forming excimers, and a smaller portion forming either

unstacked pyrenes or stacked pyrenes which result in "dark complex" formation wherein the aromatic rings do not attain a precise excimeric configuration.

Pyrene rings proximal in the lipid-free helix bundle state

Pyrene excimer fluorescence occurs only when neighboring pyrenes reside ≤ 10 Å from one another (220). The occurrence of an excimer peak in double-labeled apoLp-III indicates proximity of the pyrene moieties attached to N40C and L90C in the helix bundle state. This interpretation concurs with the earlier observation that these two engineered cysteine residues are able to form a disulfide bond with each other (197) and the NMR-derived global fold of apoLp-III, which reveals that the distance between N40 and L90 is about 9 Å (6). The possibility that intermolecular excimer formation occurs in this system can be eliminated since no change in the ratio of monomer to excimer emission was observed when lipid-free pyrene-labeled N40C/L90C-apoLp-III was diluted 8-fold. Furthermore, neither of the single cysteine mutants displayed excimer fluorescence when labeled with pyrene.

Unfolding of pyrene-labeled apoLp-III

Having demonstrated that the pyrene molecules are proximal in the lipid-free state of apoLp-III, we sought to determine whether changes in apoLp-III conformation could be manifest by changes in excimer quantum yield. Excimer fluorescence can be lost in three ways: (i) the protein undergoes a conformational change which distances the excited-state monomer from the second ground-state pyrene; (ii) the excited-state monomer may become quenched in aqueous solution, thereby preventing its interaction with a ground-

state pyrene to form the excimer configuration; or (iii) the pyrenes are not stacked in the favorable configuration required to produce excimer fluorescence. Denaturation studies were carried out to validate the use of excimer fluorescence to study helix reorientation in apoLp-III. Our rationale was based on the fact that, under denaturing conditions, apoLp-III will unfold, forcing the pyrene-labeled helical segments in question to move away from one another. We hypothesized that such movement would be reflected by a decrease in excimer fluorescence and a corresponding increase in monomer fluorescence. When GdnHCl was used to denature pyrene-labeled N40C/L90C-apoLp-III, however, we noted a concentration-dependent loss in both monomer and excimer fluorescence. The decrease in pyrene monomer fluorescence is accounted for by increased exposure to bulk solvent (or GdnHCl), as seen by loss of monomer fluorescence in single pyrene-labeled N40C-apoLp-III as a function of GdnHCl concentration. Since CD data show complete unfolding of the protein in high GdnHCl, the presence of residual excimer fluorescence is likely due to intermolecular interactions with neighboring unfolded proteins.

When pyrene-labeled N40C/L90C-apoLp-III was subjected to thermal denaturation, excimer fluorescence was lost. However, loss of excimer fluorescence coincided with a loss in monomer fluorescence which is attributed to thermally-activated solvent quenching (237, 238). On the basis of this phenomenon, it is difficult to correlate the loss of excimer fluorescence directly to protein unfolding. In addition to its ability to disrupt tertiary and quarternary structure, previous studies have shown that TFE has a preferential interaction with hydrophobic domains in proteins (239, 240). Analogous to the manner in which helix-helix interactions are replaced by helix-lipid interactions upon lipid-binding of helix-bundle apolipoproteins, we postulated that tertiary contacts in

apoLp-III would be disrupted by TFE with helix-helix interactions in the bundle conformation replaced by helix-TFE interactions. If TFE disrupts helix-helix interactions in double pyrene-labeled apoLp-III, then we expect changes in excimer fluorescence. Increasing amounts of TFE resulted in an initial increase in the area under the excimer peak for pyrene-labeled N40C/L90C-apoLp-III. This may be explained by a tighter packing of the pyrene-labeled α-helical segments, an observation also noted in the case of the N-terminal domain of apolipoprotein E (116), another helix bundle apolipoprotein. Subsequently, increasing TFE concentrations resulted in a steady decrease in the area under the excimer peak. While this may be due to increased flexibility of the helix bundle and movement of helices away from one another, the loss in excimer fluorescence was paralleled by a loss in monomer fluorescence. Indeed, in a separate experiment, when single pyrene-labeled N40C-apoLp-III was titrated with TFE, quenching of monomer fluorescence occurred. Taken together, the data indicate that exposure of pyrene-labeled apoLp-III to GdnHCl, TFE or heat results in a loss of excimer fluorescence. This effect is likely a reflection of both the conformational state of the protein and apparent quenching of monomer fluorescence, due to exposure to the bulk solvent. Interestingly, comparison of excimer excitation spectra under native and denaturing conditions (GdnHCl or heat) revealed that, although excimer fluorescence is lost, pyrene moieties retain stacked interactions.

Lipid-induced tertiary structural reorganization

When pyrene-labeled N40C/L90C-apoLp-III was complexed to discoidal particles, excimer emission was observed. Subsequently, experiments were performed to distinguish whether excimer fluorescence in disc-bound pyrene-labeled N40C/L90C-

apoLp-III was due to intermolecular pyrene-pyrene interactions. We found that, unlike the lipid-free state, where dilution of the sample did not affect the ratio of monomer to excimer emission (suggesting intramolecular excimer formation), an increase in this ratio occurred when the proportion of pyrene-labeled double mutant apoLp-III was diluted with unlabeled wild-type apoLp-III on the surface of the discs (Figure 5-10). Hence, the decrease in the ratio of E/E_{100} emission is likely due to the fact that helices 2 and 3 reposition away from each other in the lipid-bound form. The low excimer fluorescence still present at the highest dilution (5% labeled apoLp-III) may be attributed to residual intermolecular pyrene interactions, although a small contribution from intramolecular pyrene interactions cannot be eliminated. The existence of intermolecular pyrene-pyrene interactions between neighboring apoLp-III molecules in DMPC discoidal complexes was further confirmed by crosslinking up to five apoLp-III molecules around the discoidal complex using a sulfhydryl-specific crosslinker. Most importantly, it should be noted that, while there is a significant change in excimer fluorescence, there is also an increase in the ratio of monomer fluorescence to excimer fluorescence as the amount of pyrene-labeled protein on the disc complexes is decreased. Since the m/e ratio increases from 1.7 to 7.2 at the highest dilution, we attribute loss of excimer fluorescence to a decreased probability of forming intermolecular pyrene-pyrene interactions on the surface of the disc particles.

These results are consistent with previous studies that examined the conformation of apoLp-III in phospholipid disc complexes. Electron microscopic analysis reveals that DMPC/apoLp-III complexes are disc-shaped particles, 22 nm in diameter (167). Crosslinking experiments using dimethyl suberimidate (which crosslinks lysine residues)

indicate that up to six apoLp-III molecules align around the periphery of the disc complexes in an open state. Taken together, geometric calculations suggest that apoLp-III molecules orient with their helical axes perpendicular to the fatty acyl chains (167). This concept has been independently validated by attenuated total reflectance Fourier transform infrared spectroscopy studies (172). In this configuration, adjacent apoLp-III molecules on the same disc would be in close proximity.

Relative orientation of neighboring apoLp-III molecules in disc particles

Pyrene-labeled single mutant apoLp-IIIs provided useful information regarding the orientation of the protein when bound to phospholipid disc particles. When either pyrene-labeled N40C- or L90C-apoLp-III was complexed to the phospholipid bilayer, no excimer fluorescence was observed. This observation suggests that the apoLp-III molecule binds to discoidal complexes in a non-random, ordered orientation. Such an ordered arrangement may arise from the fact that when the five-helix bundle opens, three helical segments in the bundle (helices 1, 2 and 5) move away from helices 3 and 4 as the molecule opens. If this helix arrangement is maintained, alignment of apoLp-III molecules in an ordered manner would create a three-helix/two-helix repeat around the disc perimeter.

In summary, in the presence of lipid, apoLp-III undergoes a conformational opening such that helices 2 and 3 move away from one another. In addition, apoLp-III molecules bind around the periphery of discoidal particles in a non-random orientation. Based on these observations, a model for the conformation of DMPC-bound apoLp-III is presented (**Figure 5-13**).

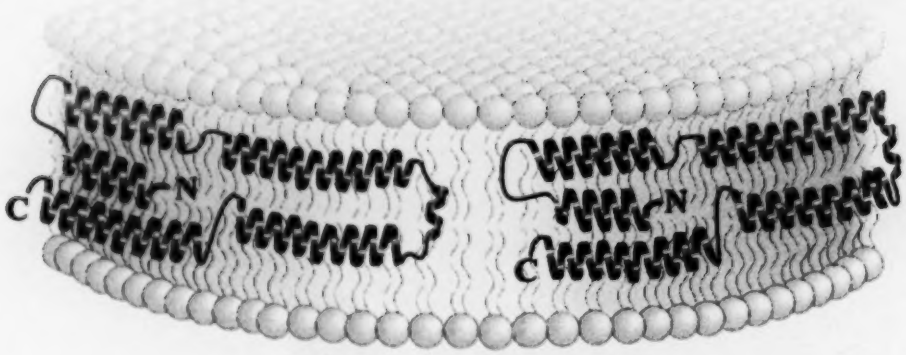

Figure 5-13. Schematic representation of apoLp-III in association with DMPC discoidal complexes. Two molecules of apoLp-III, arranged in a precise orientation, are shown around the periphery of a phospholipid bilayer complex.

Since the probes in the present study are localized to helices 2 and 3, the possible repositioning of helix 1, for example, cannot be excluded without further studies.

CHAPTER 6

Elucidation of the Lipid-associated Conformation of Apolipophorin III Around Discoidal Phospholipid Complexes

6.1 INTRODUCTION

The two previous chapters have described several powerful fluorescence spectroscopic tools which have been used in order to gain structural information about *M. sexta* apoLp-III in the lipid-bound form, particularly with respect to helices 2 and 3. However, very little information is available on the positioning of helices 1, 4 and 5 of apoLp-III in the lipid-bound state. In this chapter, cysteine residues were introduced into either helix 1 and/or helix 5, and labeled with pyrene maleimide. Using methodology outlined in Chapters 4 and 5, the relative repositioning of helices 1 and 5 of apoLp-III in association with model phospholipid disc complexes is evaluated. Their positioning with respect to i) the surrounding environment; ii) the bilayer and iii) to themselves are assessed using aqueous quenchers, spin-labeled fatty acids and pyrene excimer fluorescence, respectively.

6.2 RESULTS

Using the solution structure of apoLp-III as a guide [(6); PDB#1EQ1], Ala8 (close to the N-terminal of helix 1) and/or Ala138 (N-terminal of helix 5) were targeted for site-specific introduction of cysteine residues by site-directed mutagenesis. Extrinsic labeling of the cysteine with pyrene maleimide allows each fluorophore to act as a reporter for their respective helices; additionally, the distance between the cysteine residues in the A8C/A138C-apoLp-III double mutant is ideal for pyrene excimer formation following pyrene labeling in the lipid-free state.

Characterization of single-cysteine apoLp-III mutants

Figure 6-1 shows the bacterial expression of recombinant mutant A8C-apoLp-III and A138C-apoLp-III following induction with IPTG.

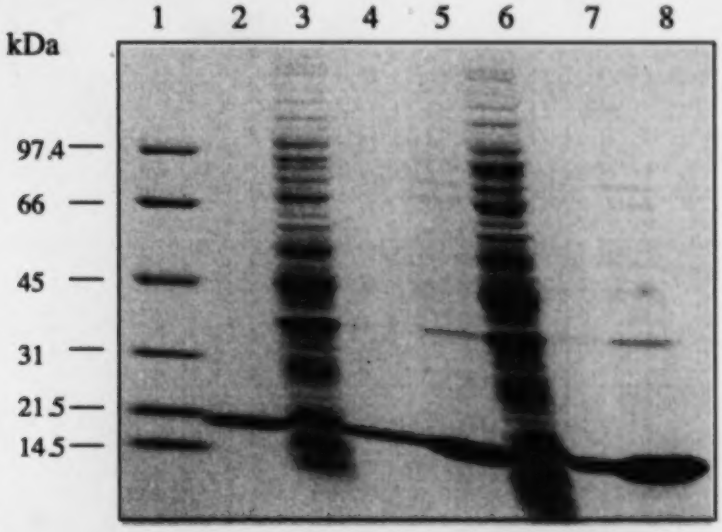

Figure 6-1. Bacterial expression of A8C-apoLp-III and A138C-apoLp-III. Four to five hours following induction with IPTG, bacterial cultures were centrifuged. Samples from pellet, supernatant, or supernatant concentrated by ultrafiltration were electrophoresed on a 12% SDS slab gel and stained with Coomassie blue. Lane 1, low molecular weight standards; lane 2, wild-type apoLp-III; lane 3, A8C-apoLp-III pellet; lane 4, A8C-apoLp-III supernatant; lane 5, A8C-apoLp-III concentrated supernatant; lane 6, A138C-apoLp-III pellet; lane 7, A138C-apoLp-III supernatant; lane 8, A138C-apoLp-III concentrated supernatant.

As with wild-type apoLp-III (119), both A8C- and A138C-apoLp-III (expected molecular weights of 18, 413 Da each) accumulate in the medium. Both proteins were further purified by gel filtration chromatography in order to obtain pure samples for fluorescence studies.

CD spectra reveal that both single-cysteine mutant apoLp-IIIs, similar to wild-type apoLp-III, are highly α-helical. (3). This suggests that mutations introduced into the

apoLp-III primary sequence do not result in any significant changes in the overall structure of the protein.

Modification of A8C- and A138C-apoLp-III by pyrene maleimide resulted in labeling of the single engineered cysteine residue. Fluorescence excitation and emission spectra of pyrene-labeled A8C- and A138C-apoLp-III are shown (**Figure 6-2**).

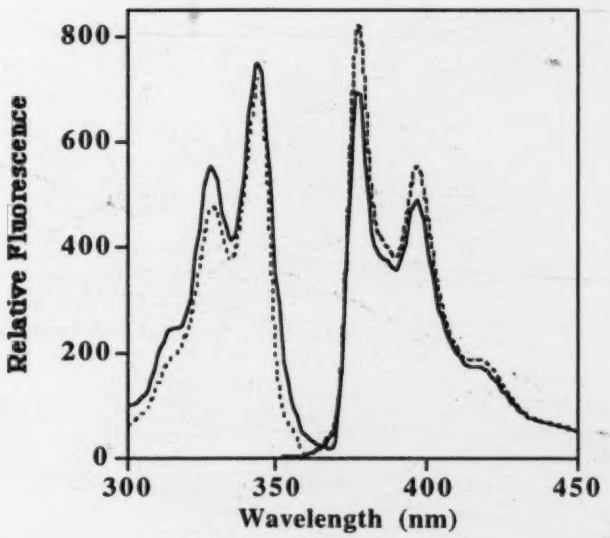

Figure 6-2. Fluorescence excitation and emission spectra of pyrene-labeled A8C- and A138C-apoLp-III. Pyrene-labeled A8C-apoLp-III (solid line) and pyrene-labeled A138C-apoLp-III (dashed line) in the lipid-free state were monitored at an emission wavelength of 375 nm for excitation spectra, and at an excitation wavelength of 345 nm for emission spectra.

Fluorescence quenching studies

Aqueous quenching. KI was used as an aqueous quenching agent in an effort to probe the accessibility and changes in local microenvironment of pyrene-labeled apoLp-IIIs in lipid-free and lipid-bound states. As discussed in Chapter 4, KI is very efficient at

quenching pyrene fluorescence. The effective Stern-Volmer quenching constants (K_{sv}) obtained for pyrene-labeled A8C-apoLp-III and pyrene-labeled A138C-apoLp-III in the lipid-free state are shown in **Table 6-1**.

Table 6-1: Effective Stern-Volmer quenching constants (K_{sv}) for pyrene-labeled A8C- and A138C-apoLp-III using KI

	K_{sv} (M^{-1})[a]	
	Lipid-free	DMPC-bound
A8C-apoLp-III	35.3 ± 2.4	6.1 ± 0.4
A138C-apoLp-III	24.7 ± 3.1	39.8 ± 1.9

[a] K_{SV} values were calculated as described in Chapter 2.2; values shown are the mean ± S.E.M. (n = 3)

The pyrene at the A8C position in lipid-free apoLp-III is highly accessible to KI, as determined by its high K_{sv} value. However, accessibility to the pyrene is dramatically reduced when bound to DMPC discoidal complexes, as evidenced by a 85% decrease in K_{sv}. This reduced quenching efficiency is attributed to either a change in the microenvironment of the pyrene fluorophore upon interaction with lipid, or the burial of the pyrene moiety into the interior of the phospholipid bilayer. The pyrene on A138C-apoLp-III is efficiently quenched in the lipid-free state. In contrast to the pyrene on A8C-apoLp-III, its availability for quenching by KI is increased upon complexation with DMPC (K_{sv} increases by 35%). The high K_{sv} value may reflect the possibility that the pyrene on helix 5 may be located close to the quarternary amines of the choline head groups of the phospholipids.

Lipophilic quenchers. According to the "open conformation model", helices 1, 2 and 5 move away 180° from helices 3 and 4 upon interaction with lipid surfaces such as DMPC disc complexes. In Chapter 4, it was shown that helices 2, 3 and 5 do, in fact, align along the lipid-water interface. The spatial disposition of helices 1 and 5 on a phospholipid bilayer disc complexes was estimated using 5-DSA and 12-DSA spin-labeled fatty acids as quenchers of pyrene fluorescence. **Figure 6-3** depicts the quenching of pyrene fluorescence for A8C-apoLp-III and A138C-apoLp-III, respectively, following association with DMPC complexes.

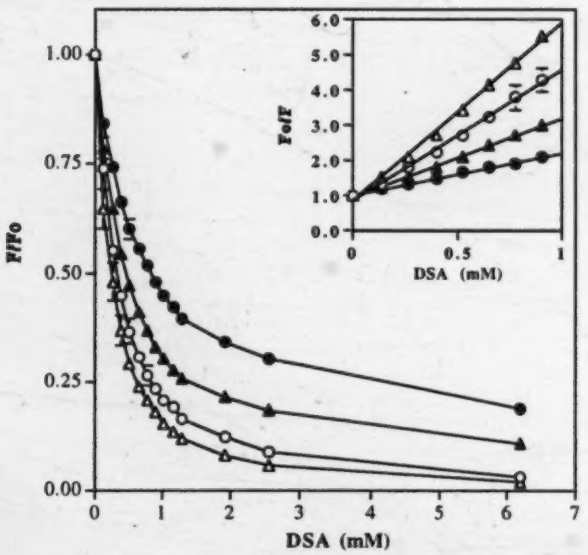

Figure 6-3. Estimation of transverse disposition of helices 1 and 5 in phospholipid disc complexes. Relative fluorescence is plotted as a function of concentration of spin-labeled fatty acid. Pyrene-labeled A8C-apoLp-III (circles) or pyrene-labeled A138C-apoLp-III (triangles) were quenched with 5-DSA (open symbols) or 12-DSA (filled symbols). Samples were excited at 345 nm and emission was measured at 375 nm. *Inset*. Stern-Volmer plot. Initial values were used to calculate K_{app}. Values are the average of three independent measurements ± S.E.M.

The inset of Figure 6-3 represents the Stern-Volmer plot, where the slope of a plot of F_o/F *vs.* quencher concentration yields values for K_{app} as shown in **Table 6-2.**

Table 6-2. Apparent Stern-Volmer constants (K_{app}) for pyrene-labeled A8C- and A138C-apoLp-III using spin-labeled fatty acids.

	K_{app}[a] (x 10^{-3} M^{-1})			
	5-DSA		12-DSA	
	pyrene-A8C apoLp-III	pyrene-A138C apoLp-III	pyrene-A8C apoLp-III	pyrene-A138C apoLp-III
DMPC-bound	3.7 ± 0.4	4.9 ± 0.1	1.2 ± 0.1	2.2 ± 0.2

[a]Apparent K_{app} values were calculated as described in Chapter 2.2; values shown are the mean ± S.E.M. (n = 3).

In the case of both pyrene-labeled apoLp-III mutant/DMPC complexes, 5-DSA seems to quench to a greater extent than 12-DSA. 5-DSA quenches fluorescence 2-3 fold better than 12-DSA for both pyrene-A8C- and pyrene-A138C-apoLp-III. These results confirm previous observations (Chapter 4) indicating that helix 5 aligns closer to the lipid/water interface. Surprisingly, the results also imply that helix 1, too, aligns close to the lipid/water interface of the phospholipid bilayer discs. Contradictory to the model where helix 1 lies in the middle of the bilayer, between helices 2 and 5, this result suggests the possibility that helix 1 may actually extend away from helix 2 in the open conformation of apoLp-III around phospholipid discoidal complexes.

Characterization of double-cysteine mutant apoLp-III

In order to further investigate the helical repositioning of helices 1 and 5 in the presence of lipid, we decided to create a double-cysteine mutant, namely A8C/A138C-apoLp-III.

Figure 6-4 shows the bacterial expression and purity of A8C/A138C-apoLp-III (expected molecular weight of 18,445 Da).

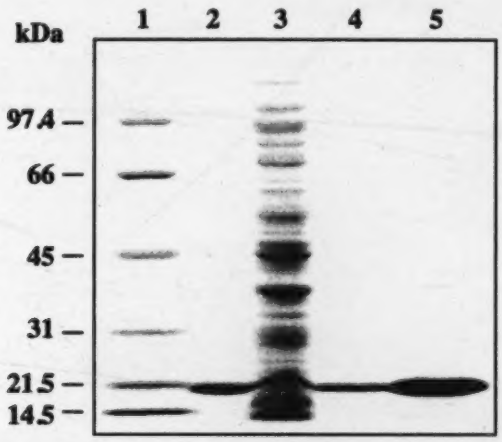

Figure 6-4. Bacterial expression of A8C/A138C-apoLp-III. Following centrifugation, samples from pellet, supernatant, or supernatant concentrated by ultrafiltration were electrophoresed on a 12% SDS slab gel and stained with Coomassie blue. Lane 1, low molecular weight standards; lane 2, wild-type apoLp-III; lane 3, A8C/A138C-apoLp-III pellet; lane 4, A8C/A138C-apoLp-III supernatant; lane 5, A8C/A138C-apoLp-III concentrated supernatant.

According to the NMR solution structure of apoLp-III (6), the distance between Ala8 and Ala138 in lipid-free apoLp-III is approximately 8 Å. After mutagenesis of these residues to cysteine, the next step was to assess if the two cysteines were within disulfide bonding distance from each other. The formation of a disulfide bond was evaluated based on the electrophoretic mobility of oxidized and reduced proteins on 18% SDS-PAGE (**Figure 6-5**).

Figure 6-5. Disulfide bond formation determined by electrophoretic mobility. Reduced (lanes 2 and 3) and oxidized (lanes 5 and 6) wild-type and A8C/A130C-apoLp-III were electrophoresed on a 18% SDS slab gel and stained with Coomassie blue. Lanes 1 and 4, low molecular weight standards; lanes 2 and 5, wild-type apoLp-III; lanes 3 and 6, A8C/A138C-apoLp-III.

Under reducing conditions, both wild-type and A8C/A138C-apoLp-III exhibit similar extend of mobility patterns. However, under oxidizing conditions, A8C/A138C-apoLp-III has an increased mobility when compared to reduced samples. Under the same conditions, wild-type apoLp-III did not elicit changes in mobility patterns as a function of oxidized or reduced states. Faster mobility of oxidized samples is a phenomenon that has been reported in other studies (197, 241-243).

The second approach to assess the proximity of A8C andA138C in the lipid-free state involves the use of *bis*-maleimidohexane, a sulfhydryl-specific crosslinker (**Figure 6-6**).

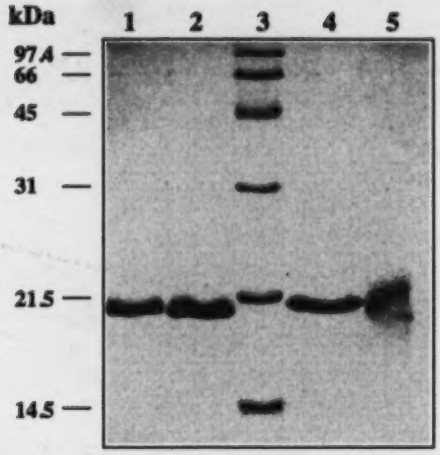

Figure 6-6. Crosslinking of sulfhydryls in A8C/A138C-apoLp-III. *Bis*-maleimidohexane was allowed to react with wild-type or A8C/A138C-apoLp-III as described in Chapter 2.2 Reduced (lanes 1 and 2) and crosslinked (lanes 4 and 5) samples were electrophoresed by 18% SDS-PAGE and visualized by Coomassie blue staining. Lanes 1 and 4, wild-type apoLp-III; lanes 2 and 5, A8C/A138C-apoLp-III; lane 3, low molecular weight standard.

A8C/A138C-apoLp-III appears to crosslink, as observed by a broad band ranging from 16 to 24 Da in size. This "smearing" of a band due to crosslinking has been documented in other studies (167, 187). As expected, wild-type apoLp-III does not form crosslinks when reacted with *bis*-maleimidohexane due to the absence of cysteine residues. Therefore, based on these two approaches, it was concluded that the cysteines in A8C/A138C-apoLp-III are spatially proximal in the lipid-free state, thereby presenting an ideal situation to study the repositioning of helices 1 and 5 upon complexation with lipid.

Pyrene excimer fluorescence

Since the sulfhydryl side chains of A8C/A138C-apoLp-III are proximal, we rationalized that upon labeling with pyrene maleimide, this distance would also be favourable for

formation of pyrene excimers. Indeed, labeling of the cysteine residues in this double mutant apoLp-III did result in strong pyrene excimer fluorescence (**Figure 6-7**).

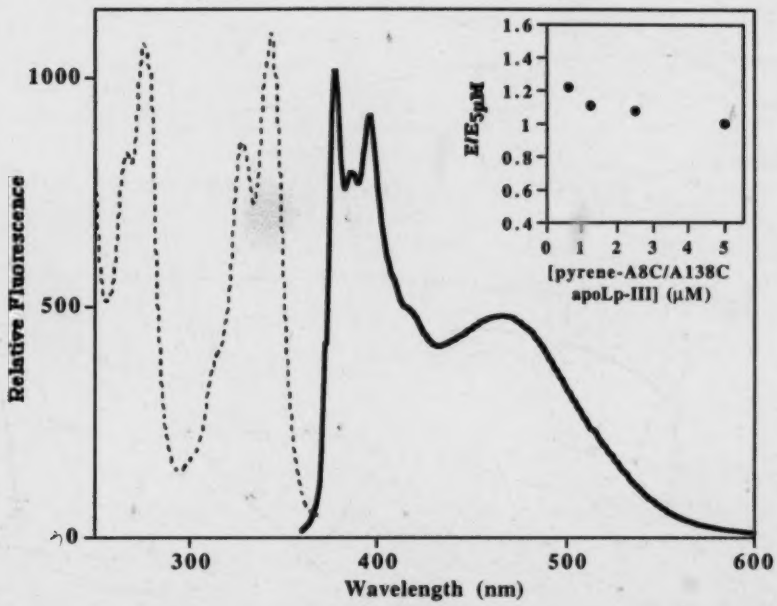

Figure 6-7. Fluorescence excitation and emission spectra of pyrene-labeled A8C/A138C-apoLp-III. Excitation spectrum (dotted line) of lipid-free pyrene-A8C/A138C-apoLp-III was monitored with an emission wavelength of 375 nm, while emission spectrum (solid line) was monitored with an excitation wavelength of 345 nm. *Inset*. Effect of dilution on pyrene-labeled apoLp-III excimer fluorescence. $E_{5\mu M}$ represents the area under the excimer emission of a solution of 5 μM pyrene-A8C/A138C-apoLp-III, and E represents the area under the excimer emission at each concentration.

Since excimer emission was observed at protein concentrations ranging from 0.6 μM to 5 μM, with very little deviation in the m/e ratio (Figure 6-7, inset). Therefore, we can conclude that excimer emission in lipid-free pyrene-labeled A8C/A138C-apoLp-III results from intramolecular, rather than intermolecular, pyrene-pyrene interactions.

Pyrene excimer fluorescence of apoLp-III/DMPC complexes. In theory, excimer fluorescence decreases when two pyrene moieties move away from each other by more than 10 Å. We hypothesized that if apoLp-III undergoes an opening such as that described in the "open conformation model" (Chapter 1.7), then the excimer peak we observe in lipid-free apoLp-III should remain even when apoLp-III is bound to DMPC disc complexes. This is based on the reasoning that helices 1 and 5 are proposed to maintain interaction in the lipid-bound state.

Using similar experimental protocol described in Chapter 5, we prepared DMPC disc complexes using pyrene-labeled A8C/A138C-apoLp-III (**Figure 6-8**).

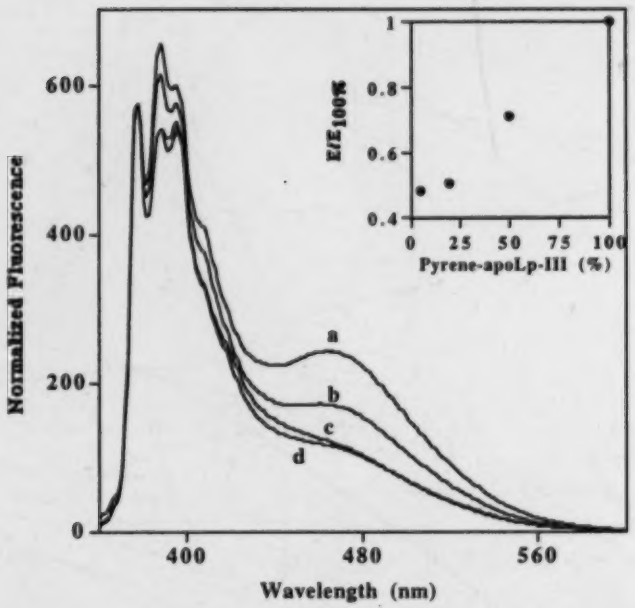

Figure 6-8. Fluorescence emission spectra of pyrene-labeled A8C/A138C-apoLp-III bound to DMPC phospholipid bilayer disc complexes. Pyrene fluorescence emission spectra were recorded for discoidal complexes made with only pyrene-A8C/A138C-apoLp-III (curve a; $E_{100\%}$) or a mixture of labeled A8C/A138C-apoLp-III and unlabeled wild-type apoLp-III, where the proportion of labeled apoLp-III was 50% (curve b), 20% (curve c) and 5% (curve d) . The lipid:protein ratio (w/w) was maintained at 2.5:1. For the various dilutions, the monomer fluorescence was normalized on the basis of the emission peak at 375 nm. *Inset*. Effect of dilution on excimer fluorescence. $E_{100\%}$ represents the area under excimer emission of discs containing only pyrene-labeled apoLp-III, and E represents the area under the excimer emission of discs bearing the indicated percentage of labeled apoLp-III.

Disc complexes were prepared such that pyrene-labeled apoLp-III ranged from 100% pyrene-labeled A8C/A138C-apoLp-III on a single disc to only 5% pyrene-labeled A8C/A138C-apoLp-III on a disc. This latter value is to ensure that only a single pyrene-labeled protein is present on the disc complex. DMPC-bound pyrene-labeled A8C/A138C-apoLp-III displayed a strong excimer peak (Figure 6-8, curve a), very

similar to that observed for lipid-free pyrene-labeled A8C/A138C-apoLp-III. Additional discoidal complexes were prepared where pyrene-labeled A8C/A138C-apoLp-III was mixed with increasing amounts of wild-type apoLp-III. Interestingly, excimer fluorescence decreased as the proportion of wild-type apoLp-III increased (Figure 6-8, curves b-d). This loss in excimer fluorescence was also accompanied by an increase in the monomer to excimer ratio (m/e ratio of 2.1 for curve a increasing to 4.6 for curve d). In general, a loss in excimer fluorescence results from two pyrene moieties moving away from one another. Taken together, it appears that the intense excimer emission noted for discoidal complexes made with 100% pyrene-labeled apoLp-III may result from intermolecular pyrene-pyrene interactions between neighbouring molecules. In addition, the loss of excimer fluorescence and the corresponding increase in the m/e ratio suggests that the pyrene moieties on helices 1 and 5 are moving away from one another. Therefore, the pyrene excimer fluorescence data corroborates the lipophilic quenching results that helices 1 and 5 are localized to a new position with respect to each other upon association with DMPC discoidal particles. It should be noted, though, that excimer fluorescence has not diminished all together. There is still some excimer fluorescence remaining, and this may be attributed to intermolecular pyrene-pyrene interactions resulting from interactions of pyrene from helix 1 of one molecule with pyrene on helix 1 of another molecule (see section 6.3).

6.3 DISCUSSION

Cysteine residues were introduced into apoLp-III at positions Ala8 and/or Ala138 of helices 1 and 5, respectively. All mutant proteins were efficiently overexpressed in bacteria, and following purification, CD analysis revealed that introduction of the mutations did not significantly alter the secondary structural content of the mutant apoLp-IIIs when compared to wild-type protein. Pyrene maleimide was subsequently used to label each cysteine residue, thus serving the role of a reporter for either helix 1 or helix 5 for quenching studies, or functioning as detectors of proximity for pyrene excimer studies.

The ability of KI to access the pyrene moiety on single-cysteine mutant apoLp-IIIs provided a means by which to monitor changes in the local microenvironment as apoLp-III goes from a lipid-free to a lipid-bound state. In the lipid-free helix bundle state, high K_{sv} values for pyrene-labeled A8C- and A138C-apoLp-III single mutants indicate that the pyrene moiety on both single-cysteine mutants is highly accessible to the negatively charged iodide. Examination of the structure of lipid-free apoLp-III reveals that both cysteine residues are located in relatively positively-charged microenvironments (6). Thus, in the case of pyrene-A138C-apoLp-III, KI may quench with ease due to the presence of several lysine residues around A138C, including lysines in the *i*, *i* + 2 and *i*, *i* + 4 positions, all in helix 5. Similarly, in pyrene-A8C-apoLp-III, quenching may be facilitated by the presence of lysine residues in helix 5, as well as at the *i*, *i* + 6 position in helix 1. However, the accessibility to pyrene on A8C-apoLp-III may also be explained by the fact that the A8C residue is actually located just outside the N-terminal boundary

of helix 1 (6). Therefore, this residue is located at the aqueous interface of the helix bundle and is readily available for quenching by KI.

Upon binding to model disc complexes, the K_{sv} for pyrene-labeled A8C-apoLp-III decreases by 85%. In the presence of lipid, it seems that the flexibility of the pyrene outside the helix allows immediate burial of the pyrene into the phospholipid bilayer, thus shielding it from quenching by KI. On the other hand, the Ksv for pryene-A138C-apoLp-III increases following complexation to DMPC disc bilayers. Based on the helical wheel diagram of lipid-free apoLp-III [Wang, 1997 #12; Figure 1-4], the A138C residue is also located very close to the aqueous interface of the helix bundle. But, due to its positioning within the helix, it most likely aligns closer to the quarternary amine of choline head groups of the phospholipids, thus enhancing quenching by KI (210). Similar quenching patterns were observed for the N40C residue on helix 2 (Chapter 4.2). N40C is also located in a similar interfacial location as A138C. The K_{sv} values obtained in the lipid-free and DMPC-bound states were practically identical. Again, this phenomenon was attributed to proximity to the phospholipid choline head groups.

Spatial disposition of helices 1 and 5

Spin-labeled fatty acid were used as "molecular rulers" in order to determine the approximate location of the pyrene fluorophore with respect to the fatty acyl chains of the phospholipid bilayer (209). Since the doxyl moieties on 5-DSA and 12-DSA are located approximately 6 Å and 15 Å away from the membrane/water interface, respectively, we thought they would provide useful information regarding the spatial disposition of helices 1 and 5 on the surface of model disc complexes. In the case of pyrene-A138C-apoLp-III,

K_{sv} values reveal that 5-DSA quenches pyrene fluorescence 2-fold greater than 12-DSA, suggesting that helix 5 aligns closer to the lipid/water interface. This data is supported by similar observations in Chapter 4.2, wherein 5-DSA quenched tyrosine fluorescence with greater efficiency than 12-DSA. Unexpectedly, however, 5-DSA also quenched pyrene fluorescence on DMPC-bound pyrene-A8C-apoLp-III with greater efficiency than 12-DSA. Therefore, contrary to the model whereby helix 1 is embedded between helices 2 and 5 in the open conformation on a discoidal complex as depicted in Figure 5-13, the present data suggests that helix 1 also aligns closer to the lipid/water interface of phospholipid bilayers.

Repositioning of helices 1 and 5 by pyrene excimer fluorescence

The A8C/A138C-apoLp-III double-cysteine mutant was designed specifically for studies regarding the lipid-induced repositioning of helices 1 and 5. Keeping in mind that pyrene excimer fluorescence occurs when two neighbouring pyrene moieties are within a $\lesssim$ 10 Å distance from one another, we engineered cysteines into the lipid-free bundle at the A8 and A138 positions since the distance between the two residues is ~8 Å (6). Indeed, following labeling of the cysteine residues with pyrene maleimide, strong excimer fluorescence was observed in lipid-free apoLp-III. Moreover, it was confirmed that excimer fluorescence resulted from intramolecular pyrene-pyrene interactions, since dilutions of lipid-free pyrene-A8C/A138C-apoLp-III solutions did not significantly alter the m/e ratios (see Figure 6-7, inset).

When pyrene-labeled A8C/A138C-apoLp-III was complexed to DMPC discoidal particles, strong excimer emission was observed. In order to discern between intra- and

intermolecular pyrene-pyrene interactions, discs were prepared such that pyrene-labeled A8C/A138C-apoLp-III was mixed with increasing amounts of unlabeled wild-type apoLp-III. As the proportion of unlabeled apoLp-III increased, it was observed that excimer fluorescence decreased. Furthermore, the loss in excimer fluorescence was accompanied by an increase in the m/e ratio.

A new DMPC-bound conformation of apoLp-III

Initially, the presence of strong excimer emission from discoidal complexes prepared with 100% pyrene-labeled apoLp-III was not surprising. Consistent with the "open conformation" model, where helices 1, 2 and 5 move away from helices 3 and 4, we believed this excimer peak was due to the maintenance of helix1-helix 5 interactions in the lipid-bound state. However, if this were the case, dilution of pyrene-labeled apoLp-III with unlabeled apoLp-III on the discoidal complexes should not result in a change in the m/e ratio. While the intensity of the excimer peak may decrease due to dilution of pyrene-labeled apoLp-III, the presence of intramolecular pyrene-pyrene interactions should not alter the m/e ratio.

Contrary to what we expected based on the "open conformation model", however, the data obtained from these sets of experiments conform to a different model for conformational opening of apoLp-III on discoidal complexes. In this new "partially-extended" model, apoLp-III maintains its opening about hinge regions between helices 2 and 3 and helices 4 and 5, but an additional opening about the hinge between helices 1 and 2 also occurs. This allows helices 1, 2 an 3 to be in an extended conformation around the periphery of the phospholipid disc bilayer (**Figure 6-9**).

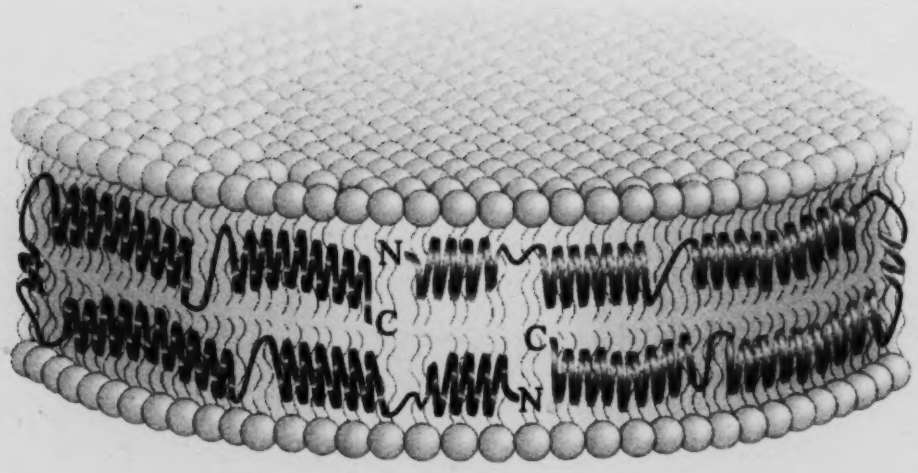

Figure 6-9. Model depicting a "partially-extended" lipid-bound conformation of *M. sexta* apoLp-III. ApoLp-III aligns around the periphery of DMPC discoidal complexes such that the helical axes lie perpendicular to the fatty acyl chains of the phospholipid. Helices 1, 2 and 3 form an "extended" helix, thus allowing intermolecular interactions between two apoLp-III molecules via helix 1.

The data obtained from the pyrene excimer studies are in good agreement with this model. When discs were prepared with 100% pyrene-labeled apoLp-III, the excimer emission that appeared was the result of intermolecular pyrene-pyrene interactions between helix 1 of one apoLp-III molecule with helix 1 of a neighbouring apoLp-III molecule. The excimer fluorescence decreases and them/e ratio increases as a result of the movement of helices 1 and 5 away from one another. The presence of low excimer fluorescence at the highest dilution (5% labeled apoLp-III) is due to the intermolecular pyrene-pyrene interactions between the first helix of each apoLp-III. Examination of the m/e ratios provides further support for this model. Upon dilution of pyrene-labeled A8C/A138C-apoLp-III on discoidal complexes, the m/e ratio increased from 2.1 to 4.6. However, in Chapter 5, dilution of pyrene-labeled N40C/L90C-apoLp-III on the discoidal

complexes resulted in an increase in the m/e ratio from 1.7 to 7.2. In the A8C/A138-apoLp-III study, the m/e ratio may not increase as much as it did with the N40C/L90C-apoLp-III study, since strong pyrene-pyrene interactions remain between the first helix of each apoLp-III molecule.

Further support for this "partially-extended" model was derived from data obtained from the quenching studies using KI and spin-labeled fatty acids. 5-DSA was more effective at quenching pyrene fluorescence on both helices 1 and 5, thus suggesting that both helices align closer to the lipid-water interface.

Determination of this "partially-extended" lipid-bound conformation of apoLp-III is quite exciting considering that recent studies have suggested similar findings for other exchangeable apolipoproteins. Recently, Borhani *et al.* (163) reported the X-ray crystal structure of an N-terminal deletion mutant of human apo Δ(1-43)A-I at 4 Å resolution in the absence of lipid. The structure revealed a continuously curved, horseshoe-shaped surface composed of ten amphipathic α-helices. In addition, four apo Δ(1-43)A-I molecules were arranged as pairs of antiparallel dimers. In fact, it was suggested that this structure represented the conformation of lipid-associated apoA-I, such that apoA-I dimers formed a "belt" around phospholipid disc complexes or around the surface of spherical HDL particles. In another study, Fisher *et al.* (244) used fluorescence resonance energy transfer to determine a semi-extended conformation of the N-terminal domain of apoE around DMPC discoidal complexes. In their model, the four-helix bundle undergoes an opening about the hinge region between helices 2 and 3. However, while helices 1 and 2 maintain contact, helix 4 extends away from helix 3, generating an overall semi-extended conformation around the perimeter of the discoidal complex.

The emergence of new lipid-bound models for other exchangeable apolipoproteins such as apoA-I and the N-terminal domain of apoE have enforced the possibility that, perhaps, the lipid-induced conformational opening of apoLp-III may not be as simple as originally believed. Additional experiments, such as those combining site-directed mutagenesis with fluorescence spectroscopy, are required in order to completely map the relative repositioning of each helix of apoLp-III around the periphery of discoidal complexes.

CHAPTER 7

General Discussion

Exchangeable apolipoproteins play a critical role in plasma lipoprotein metabolism. These proteins function as activators of lipid metabolic enzymes (245), ligands for cell surface receptors (141) or as structural components for stabilization of lipoprotein particles. A hallmark of exchangeable apolipoproteins is the preponderance of amphipathic α-helices, a common structural motif that confers lipid binding properties to these proteins (142, 164). Insect exchangeable apolipoproteins also possess amphipathic α-helices and share the underlying function of lipoprotein binding and particle stabilization. These similarities make the insect system a valuable model for studying the structure-function relationships that mediate protein-lipid interactions (4, 173).

ApoLp-III is a prototypical exchangeable apolipoprotein found in the hemolymph of insects. In adult insects, apoLp-III exists as a lipid-free and a lipid-bound protein. During energy-requiring functions such as flight, apoLp-III plays a role in lipid transport by reversibly binding to lipophorin particles enriched with diacylglycerol (82, 246). In this way, apoLp-III serves to maintain the structural integrity of the lipophorins as they undergo modification of their lipid content en route from the fat body to the flight muscle for energy metabolism. The ability of apoLp-III to reversibly associate with lipophorin particles raises questions regarding the structural features of this protein that allow it to be soluble in the hemolymph, as well as bind to lipophorins. Specifically, what structural rearrangements occur to give apoLp-III such diverse biochemical properties?

X-ray crystallography and three-dimensional heteronuclear NMR studies have revealed that lipid-free apoLp-III exists as a globular bundle consisting of five anti-parallel amphipathic α-helices (5, 6). The hydrophobic residues are buried within the protein interior and stabilized by interhelical contacts (153), while the hydrophilic

residues on the protein exterior allow it to exist as a water-soluble protein. In the presence of a lipid surface, however, the helix bundle undergoes a conformational opening about hinge regions such that its hydrophobic interior is exposed to the lipid, with helix-helix interactions being replaced by helix-lipid interactions.

While evidence has mounted in support of the lipid-induced conformational opening of apoLp-III (2, 3, 167, 179, 187, 195, 197), little information exists with respect to the actual structure of apoLp-III in the lipid-bound form. The use of X-ray crystallography and NMR spectroscopy to determine lipid-bound structures is limited by the large size and heterogeneity of lipid-protein complexes. Several groups have used alternative methods to gain insight into the lipid-bound conformations of apolipoproteins. Epitope mapping (247), Fourier transform infrared spectroscopy (248, 249), computer modeling (168) and synthetic peptide fragment studies (250-252) have been used to investigate this issue. All of the above studies employed protein systems for which the full-length lipid-free structures remain unknown. On the other hand, we have focused on the topography of a full length apolipoprotein whose structure in the lipid-free state is known (6).

Since most exchangeable apolipoproteins exert their biological effects in a lipid-associated state, we sought to elucidate the lipid-bound conformation of *M. sexta* apoLp-III. Using a combination of isotope-labeling for NMR studies, as well as protein engineering and fluorescence spectroscopy techniques, I have determined aspects of the conformational opening, spatial disposition, orientation and lipid-induced helical rearrangement of apoLp-III helical segments on model disc complexes.

7.1 Lipid-induced conformational adaptation of apolipophorin III

High resolution techniques such as NMR spectroscopy and X-ray crystallography are limited by the size of particles examined. However, recent methodology suggests that this limitation can be overcome by employing lipid mimetics such as detergent micelles that are small enough to permit heteronuclear multidimensional NMR analysis (207, 251, 253).

In the experiments outlined in Chapter 3, we used DPC as a model lipid that mimics the phospholipid monolayer of a lipoprotein surface since previous studies have established an association of apoLp-III with DPC micelles (119, 205). Our understanding of the conformational adaptations of apoLp-III has been aided by two factors: i) the availability of a high-level bacterial expression system (119) for ^{15}N-isotopic labeling of specific amino acids of apoLp-III and ii) the recently-determined global fold and secondary structural assignment of *M. sexta* apoLp-III (6) as a reference standard for evaluation of the effect of DPC titration on different regions of the protein.

Initially, uniformly-labeled ^{15}N-apoLp-III was complexed with DPC, yet ^{1}H-^{15}N HSQC spectra revealed significant linebroadening of crosspeaks and major resonance overlap, thus making it difficult to interpret the data. To avoid this problem, we prepared ^{15}N-valine apoLp-III, ^{15}N-leucine apoLp-III, ^{15}N-lysine apoLp-III and ^{15}N-glycine apoLp-III in lieu of uniformly labeled ^{15}N-apoLp-III. We rationalized that the relatively low number of each amino acid in the sequence of apoLp-III would facilitate determination of the lipid-bound conformation, since we would be mapping each residue, one at a time, in the presence of DPC. Additionally, we chose to label these specific amino acids based on their location in the lipid-free helix bundle conformation (6). Valine and leucine are

hydrophobic residues buried in the interior of the apoLp-III helix bundle, lysine is a hydrophilic residue located on the outer hydrophilic surface of the bundle, while glycine is mostly located in the loop regions connecting helical segments.

Resonance assignment in the lipid-bound state was obtained by following changes in each ^{15}N-amino acid chemical shift as a function of DPC concentration. In general, major changes in the chemical shift of these residues were observed, indicative of a significant conformational change. Most dramatic and abrupt changes in crosspeak chemical shift were observed for the hydrophobic residues as DPC concentration reached its CMC. This was also accompanied by broader linewidths for each crosspeak, suggestive of the exchange of helix-helix interactions within the bundle interior for helix-lipid interactions. On the other hand, lysine and glycine residues underwent more gradual changes in chemical shift in response to increasing DPC concentrations. As well, significant linebroadening occurred only after DPC reached its CMC. Taken together, the data obtained provide direct experimental support for conformational opening of apoLp-III upon interaction with a lipid surface, as well as assignment of four kinds of amino acids in the lipid-bound state

To date, the lipid-bound structure of only one full-length human serum apolipoprotein has been determined by NMR spectroscopy. Rozek *et al.* (254) have determined the structure of apoC-I, a 57-residue exchangeable apolipoprotein, in the presence of SDS using uniformly-labeled ^{15}N-apoC-I. However, their data acquisition was simplified due to the length of the full-length protein. To their disadvantage, however, they do not have a solution structure of lipid-free apoC-I to use as reference standard for the evaluation of lipid-induced changes of each specific amino acid.

While the ^{15}N-specific amino acid labeling protocol that we have developed has great potential for elucidating the high resolution NMR structure of lipid-bound apoLp-III, this strategy was not feasible for my purpose of determining the lipid-bound conformation of apoLp-III. Eighteen individual preparations of specific ^{15}N-amino acid labeled protein would have to be prepared (apoLp-III has no cysteine or tryptophan residues) and individual spectra collected at each DPC concentration would have to be compared to the spectra obtained for lipid-free protein. Although the methodology is unique in its applicability to a protein with the size of apoLp-III, it was decided that another, preferably simpler approach should be taken to probe the lipid-bound structure of apoLp-III.

7.2 Rationale for use of pyrene fluorescence spectroscopy

In order to probe the lipid-bound structure of apoLp-III, we decided to use fluorescence spectroscopy, a technique which has been used routinely in the study of protein structure (220, 221, 255). While apoLp-III lacks tryptophan, an intrinsically fluorescent residue, it does contain a single tyrosine residue. However, tyrosine fluorescence is significantly quenched in the lipid-free apoLp-III helix bundle (3, 121). To circumvent this problem, we took advantage of the absence of cysteine residues in the apoLp-III sequence. Using site-directed mutagenesis, a single cysteine residue was introduced into desired locations on different apoLp-III molecules. Subsequently, the sulfhydryl side chain of the cysteine was covalently bound to pyrene maleimide.

Pyrene has several properties which make it amenable for conformational studies of apolipoproteins on a lipid surface. It has a high extinction coefficient (219) and a

relatively long lifetime of monomer fluorescence (233). Furthermore, pyrene fluoresces only when covalently bound to a sulfhydryl group and the excitation wavelength of pyrene does not coincide with excitation wavelengths of tryptophan and tyrosine residues.

7.3 Change in microenvironment upon binding of apoLp-III to lipid surfaces

In order to examine the microenvironment of the pyrene fluorophore on apoLp-III in the lipid-free and lipid-bound state, cysteine residues were introduced into different helices. The table below describes the mutations and notes the helices in which the mutated residues reside (**Table 7-1**). From herein, I will be referring only to the helix that contains the pyrene moiety.

Table 7-1. Cysteine-containing apoLp-III mutants and their helical designations.

Mutation	Helix (H) designation
A8C-apoLp-III	H1
N40C-apoLp-III	H2
L90C-apoLp-III	H3
A138C-apoLp-III	H5

For aqueous quenching studies, KI was chosen to probe the accessibility and change in the local microenvironment of pyrene-labeled apoLp-IIIs in the presence and absence of lipid. Iodide has proved to be an excellent anionic quencher (203) and quenched pyrene fluorescence efficiently.

In the lipid-free helix bundle, K_{sv} values revealed that the pyrene on each of the four helices was quenched with high efficiency. In many cases, the high K_{sv} resulted from the presence of positively-charged lysine residues, in and around the area of the pyrene on each helix. As well, with the exception of the probe on H2, all pyrenes are located close to the aqueous interface of the helix bundle, thus permitting facile quenching by iodide. Pyrene on H2 is located in the hydrophobic interior of the apoLp-III bundle, and its slightly reduced accessibility is reflected by the lower K_{sv} value (see Table 4-1).

When H2 and H3 of apoLp-III were labeled with pyrene and bound to a spherical lipoprotein particle, the pyrene was practically inaccessible to the iodide, as reflected by the 90% decrease in K_{sv} values. This indicated that pyrene was completely sequestered away from the aqueous environment, most probably buried within the hydrophobic lipoprotein monolayer.

When pyrene-labeled apoLp-IIIs were bound to DMPC discoidal complexes, similar observations were noted for H1 and H3. For both helices, the K_{sv} values decreased, thus suggesting that iodide was denied access to the pyrene moieties. This is most likely due to the fact that the hydrophobic pyrene is buried in the interior of the phospholipid bilayer. For the two other helices, K_{sv} values either remained the same (H2) or increased (H5). This observation might be explained by the possibility that both helices may be aligned close to the quarternary amines of the choline head groups of the phospholipid.

Taken together, the differences in K_{sv} values obtained from lipid-free and lipid-bound states of apoLp-III suggest that, be it on a lipoprotein surface, or on a discoidal

particle, a conformational change takes place. While in lipoproteins, we can conclude that the protein adopts a conformation that allows burial of the hydrophobic pyrene moiety, in discoidal complexes, we map the position of each helix based on the data obtained from aqueous and lipophilic quenching studies (summarized below).

7.4 Mode of interaction of apoLp-III with a lipoprotein surface

Spin-labeled fatty acids are valuable tools for measuring the location of protein-bound fluorophores in membranes. Specifically, due to the various locations of the doxyl moiety on different spin-labeled fatty acids, we are able to estimate the depth of penetration of apoLp-III helices on lipoprotein particles. In our experiments, we used 5-DSA and 12-DSA, where the doxyl moiety is located approximately 6 Å and 15 Å away from the membrane/water interface, respectively. Previous studies report that apoLp-III likely binds to a newly-created hydrophobic patch on the surface of lipoprotein particles with its helices between the head groups of phospholipids of the monolayer (127, 129). However, it was not determined whether apoLp-III binds loosely within the monolayer, or whether the protein binds by making direct contact with the particle interior. Using the lipophilic quenchers described above, we showed that on a lipoprotein surface, the pyrene moiety on both H2 and H3 was quenched more effectively by 5-DSA than by 12-DSA. This suggests that the fluorophore is located near the lipid/water interface of lipoprotein particle. In other words, apoLp-III penetrates perhaps 5-7 Å into the monolayer. Based on this data, I suggest a weak interaction of an exchangeable apolipoprotein with a lipoprotein surface. This mode of binding occurs at both ends of the "open" protein, and is hence, representative of the entire apoLp-III molecule (**Figure 7-1**).

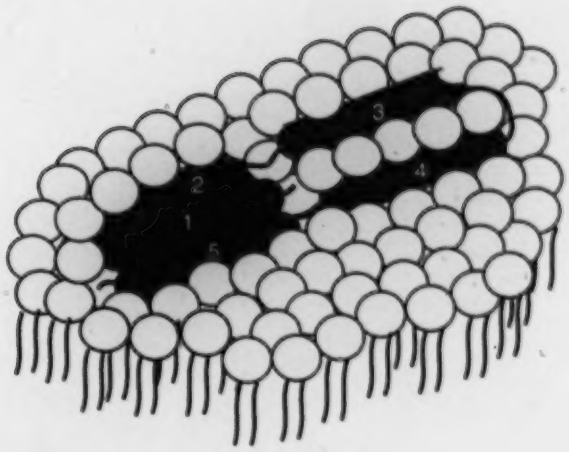

Figure 7-1. Schematic representation of the loose association of apoLp-III to a lipoprotein surface. A section of the lipoprotein surface is shown. ApoLp-III (purple) is depicted to be loosely embedded, interdigitated among phospholipid molecules (eggshell) during interaction with exposed diacylglycerol. The α-helical axes are oriented perpendicular to the fatty acyl chains of the phospholipids.

These results are consistent with the functionality of exchangeable apolipoproteins. The reversible binding to lipoprotein surfaces appears to be the common underlying feature of these proteins and, in general, facilitates their roles in lipoprotein metabolism. Especially with regard to apoLp-III, the weak binding enables the protein to readily associate and dissociate from lipophorin particles following loading of diacylglycerol at the fat body and release of diacylglycerol at the flight muscle, respectively.

7.5 Spatial disposition of apoLp-III helices on DMPC phospholipid bilayers

Lipophilic quenchers were also used to probe the spatial disposition of fluorophores on the periphery of a DMPC phospholipid bilayer. ApoLp-III is known to orient itself around the periphery of DMPC discoidal complexes such that the helical axes lie perpendicular to the fatty acyl chains of the phospholipids (167, 172). Furthermore, according to the currently accepted model, apoLp-III binds to discoidal particles such that helices 1, 2 and 5 move 180° away from helices 3 and 4. This conformation would allow the hydrophobic interior of apoLp-III to bind to the lipid surface (**Figure 7-2**).

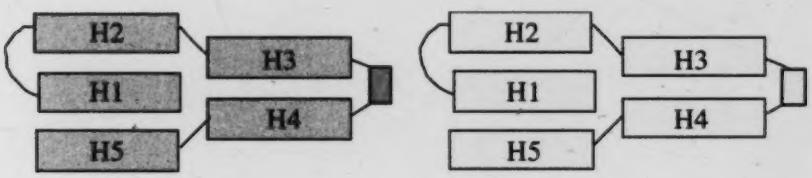

Figure 7-2. Schematic representation of the "open conformation" model of apoLp-III around discoidal complexes. Each molecule of apoLp-III is denoted by a separate colour. The short helix between H3 and H4 represents helix 3'. This conformation is based on the hypothesis first presented by Breiter *et al.* (5).

However, given that the width of an α-helix is approximately 1.5-2.0 nm (132), stacking H1, H2 and H5 may exceed the width of the discoidal complex (4.8 nm) (167).

Data obtained from quenching studies with spin-labeled fatty acids yielded some very interesting results. In all the helices examined, 5-DSA quenched pyrene fluorescence more effectively than 12-DSA. (It should also be noted that 5-DSA also quenched tyrosine fluorescence on H5 in a similar manner, thus complementing the data obtained by pyrene quenching on the same helix). This suggests that H1, H2, H3 and H5

align close to the lipid/water interface of the discoidal complex. Surprisingly, since H1 does not appear to align between H2 and H5 [as proposed earlier (167)], H1 must, therefore, extend away from H2, forming a "partially extended" conformation around the periphery of discoidal complexes. In addition to the altered accessibility to KI quenching discussed earlier, further support for this model was obtained using pyrene excimer fluorescence spectroscopy, as described below.

7.6 Lipid-induced helical repositioning of apoLp-III on DMPC phospholipid bilayers

Pyrene fluorophores have the unique property of forming excimers when two interacting ring systems are within 10 Å of one another. The presence of excimers is reflected by an additional emission peak at ~460 nm following excitation of the pyrene at 345 nm. However, when the pyrene moieties move away from each other, excimer fluorescence is lost, as noted by a decrease in the emission at longer wavelengths. This fluorescence property has been exploited by many researchers for structure studies relating to proximity relationships and protein conformational change (256). To our knowledge, we are the first to apply pyrene excimer fluorescence in the study of lipid-induced conformational changes of exchangeable apolipoproteins.

In an effort to study the helical repositioning that occurs upon binding of apoLp-III to DMPC discoidal complexes, two double-cysteine mutant apoLp-IIIs were designed. Based on the coordinates of the lipid-free helix bundle structure (PDB #1EQ1; (6), N40C/L90C-apoLp-III contained cysteines 9 Å apart between H2 and H3, while A8C/A138C-apoLp-III contained cysteines 8 Å apart between H1 and H5. Both apoLp-

IIIs emitted strong excimer fluorescence in the lipid-free state. We rationalized that, should each helical pair move apart upon binding to a lipid surface, then excimer fluorescence should decrease. Indeed, in both cases, excimer fluorescence decreased when pyrene-labeled apoLp-IIIs were bound to DMPC discoidal complexes. Further, the loss in excimer fluorescence was due to loss of intramolecular pyrene-pyrene interactions, as confirmed by the increase in the m/e ratios. Therefore, the data reveal that, on a discoidal complex, H2 moves away from H3 and H1 moves away from H5.

While the repositioning of H2 away from H3 is consistent with the "open conformation" model, the repositioning of H1 away from H5 is not (refer to Figure 5-13). One way the H1/H5 data can be explained is if H1 moves away from H5 (and H2) and forms a "partially extended" conformation around the periphery of the phospholipid bilayer (see Figure 6-9). In fact, looking back at Figure 5-10, we observed that although pyrene excimer fluorescence decreases, there is still some residual excimer fluorescence remaining. Based on the "partially extended" model, this excimer fluorescence may be the result of intermolecular pyrene-pyrene interactions between H3 of two neighbouring apoLp-III molecules. Moreover, the fact that excimer fluorescence has not completely diminished (see Figure 6-8) must be due to intermolecular pyrene-pyrene interactions between H1 neighbouring apoLp-III molecules, especially since H1 of one apoLp-III molecule appears to establish contacts with H1 of another apoLp-III molecule. Certainly, the pyrene excimer data concur with that obtained from the lipophilic quenching studies, providing further evidence for this new lipid-bound model of apoLp-III. The evidence acquired herein suggests to a lipid-bound conformation of apoLp-III that differs from that previously suggested (5, 141).

7.7 Relative orientation of apoLp-III around phospholipid bilayer complexes

The fact that intermolecular pyrene-pyrene interactions can take place on discoidal complexes allowed us to address questions regarding the orientation of apoLp-III molecules around a bilayer disc complexes. When disc complexes were prepared using a either pyrene-labeled H2 or pyrene-labeled H3 mutants, no excimer formation was observed. However, a mixture of pyrene-labeled H2 and pyrene-labeled H3 apoLp-III resulted in excimer formation. At the time of Chapter 5's publication, we still believed the validity of the "open conformation" model. Therefore, our interpretation of the data at the time was such that apoLp-III orients itself around the periphery of a discoidal complex in a precise, non-random manner since the pyrene at the beginning of H2 was forming excimers with the pyrene at the end of H3 (see Figure 5-13). Although a "partially extended" model is postulated, we are still confident that apoLp-III still orients itself in a precise manner, however, the excimer formation on the discoidal complexes made from a mixture of the two single-cysteine mutant apoLp-III results from intermolecular pyrene-pyrene interactions from H3 of one apoLp-III molecule and H3 of another apoLp-III molecule (see Figure 6-9).

7.8 Applicability of lipid-bound apoLp-III model to other lipid-bound models

The "partially-extended" model proposed in this thesis is not the first to challenge the generally accepted "open conformation" model (5, 141). In recent years, models representing varying lipid-bound conformations of exchangeable apolipoproteins have been proposed, some of which are described below. Each will also be discussed in terms

of its applicability to the lipid-bound conformation of apoLp-III based on the data presented in this thesis.

A) Human apoA-I

The tendency for apoA-I to self-associate complicates structural studies of its lipid-free and lipid-bound conformations. However, there is accumulating evidence suggesting that lipid-free apoA-I may adopt a helix bundle organization (206, 257-259). Very recently, the X-ray crystal structure of a human apolipoprotein A-I (apoA-I) N-terminal deletion mutant at 4 Å resolution revealed an extended α-helical horseshoe-shaped structure (163, 260). The protein appears as an elliptical ring-like structure consisting of four truncated apoA-I molecules arranged as pairs of antiparallel dimers. The four molecules associate via the hydrophobic faces of their amphipathic helices to form a four-helix bundle. It must be noted, however, that while the lipid-free structures of apoLp-III and the N-terminal domain of apoE are intramolecular helix bundles (5, 6, 156), the lipid-free apo Δ(1-43)A-I structure is an intermolecular bundle. It was further proposed that the structure of the apoA-I deletion mutant mimics the lipid-associated conformation of apoA-I, thus forming a "belt" around the circumference of spherical HDL (163). Similarly, it was proposed that truncated apoA-I wraps around the edge of phospholipid bilayer discs with its α-helices perpendicular to the fatty acyl chains of the phospholipid (163, 261). Segrest *et al.* (262) used computer-modeling to propose that two molecules of apoA-I can wrap around discoidal complexes in an anti-parallel manner. In further support for the "belt model", depth-dependent quenching studies on helix 4 (one of the central helices) of apoA-I revealed that at least this helix exists in an

orientation that is compatible with the "belt" conformation, lying perpendicular to the phospholipid acyl chains (263).

We were interested in determining whether apoLp-III could adopt the "belt" model conformation demonstrated by truncated human apoA-I. If so, then apoLp-III would align around the periphery of discoidal complexes as depicted in **Figure 7-3**.

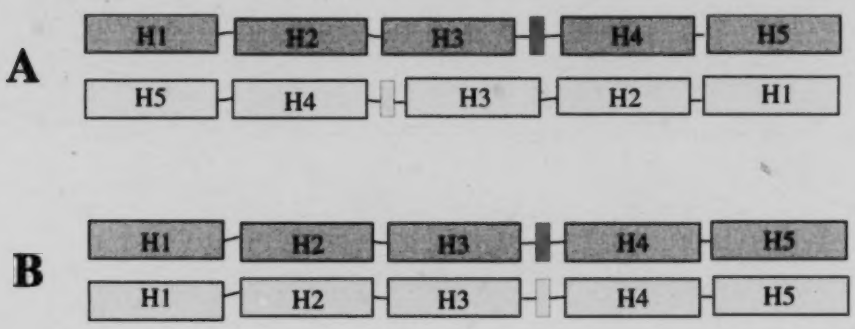

Figure 7-3. Schematic representation of "belt" conformations of apoLp-III around discoidal complexes. ApoLp-III molecules could hypothetically bind around the periphery of phospholipid bilayer discs in an anti-parallel (A) or parallel (B) manner. Each molecule of apoLp-III is denoted by a separate colour. The short helix between H3 and H4 represents helix 3'. Both models are based on the proposed "belt" conformation model of truncated human apoA-I (163).

Based on the geometry of DMPC/apoLp-III complexes (167), the circumference of the particles is 58.1 nm, with a diameter of 18.5 nm and a width of 4.8 nm. Since the width of an α-helix is 1.5-2.0 nm (132), two molecules of apoLp-III can comfortably fit along the width of the disc complex (4 molecules in total around the circumference, with each existing as a dimer). Therefore, if a helix is labeled with pyrene and both of the same helices of adjacent molecules are directly juxtaposed to one another as shown by H3 in Figure 7-3, then the probes would be within 4 Å of one another, a distance which is ideal

for pyrene excimer formation. However, when discoidal complexes were prepared with pyrene-labeled H2 or pyrene-labeled H3 alone, excimer formation was absent (Figure 5-12). Furthermore, when sulfhydryl-specific crosslinker was used to crosslink cysteines on a discoidal complex, we were able to see multimeric complexes of apoLp-III (Figure 5-11). If apoLp-III were to open as depicted in Figure 7-3, then only dimer bands would be visible on a gel (due to crosslinking of H3 in Figure 7-3A or crosslinking of H2 or H3 in Figure 7-3B). Therefore, the evidence obtained in Chapter 5 reinforces that neither models in Figure 7-3 are applicable to apoLp-III. It should be noted that it is possible for two molecules of apoLp-III to exist on discoidal complexes as a dimer as shown in Figure 7-3, yet offset by one (or more) helices. Further experiments are required to test these possibilities.

B) N-terminal domain of human apoE

The N-terminal domain of apoE [apoE(NT)], which houses the LDL receptor binding region, has been studied extensively. Isolated apoE(NT) is unable to bind to the LDL receptor in the absence of lipid. However, when it is complexed with phospholipid to form disc complexes, apoE(NT) binds efficiently to the LDL receptor (158). Therefore, it is postulated that apoE undergoes a lipid-binding induced conformational change in order for it to function as a ligand for the LDL receptor.

The lipid-free structure of apoE(NT) has been determined by X-ray crystallography (156). Although a four-helix bundle, its structure bears remarkable similarity to lipid-free structure of apoLp-III [(5, 6); Wang, Sykes and Ryan, unpublished results (PDB#1EQ1)]. Given the similarity in molecular architecture between apoLp-III

and apoE(NT) in the lipid-free state, it would not be surprising if both proteins underwent similar conformational adaptations in response to lipid.

A "picket fence" model has been proposed wherein the helical segments need to be "broken" to form 17-residue anti-parallel helical segments oriented parallel to the acyl chains of the phospholipid disc complex (193). Similar to apoLp-III, however, an "open conformation" model has been proposed whereby helices 1 and 2 of apoE(NT) move 180° away from helices 3 and 4 about a hinge region between helices 2 and 3 (141). Data obtained from surface area measurements at the air-water interface (264) and disulfide bond engineering studies (265) are in favour of this model. Furthermore, infrared spectroscopy experiments suggest that the α-helices of apoE(NT) align perpendicular to the acyl chains of the phospholipids in discoidal complexes (266).

Interestingly, the "partially-extended" model for apoLp-III on discoidal particles that is postulated in this thesis closely resembles a recently-proposed lipid-bound conformation for apoE(NT) (116, 244) which is a variation of the "open conformation" model (141). Evidence obtained by fluorescence resonance energy transfer suggests a "semi-extended" model whereby apoE(NT) (residues 1-183) binds to DMPC discoidal particles such that the protein opens about the hinge region between helices 2 and 3. In addition, however, helix 4 extends away from helix 3. Therefore, helices 1 and 2 maintain contact while helices 3 and 4 move away from one another, generating an overall semi-extended conformation.

Looking at the structure of apoLp-III, two partially-extended models can be envisioned (**Figure 7-4**).

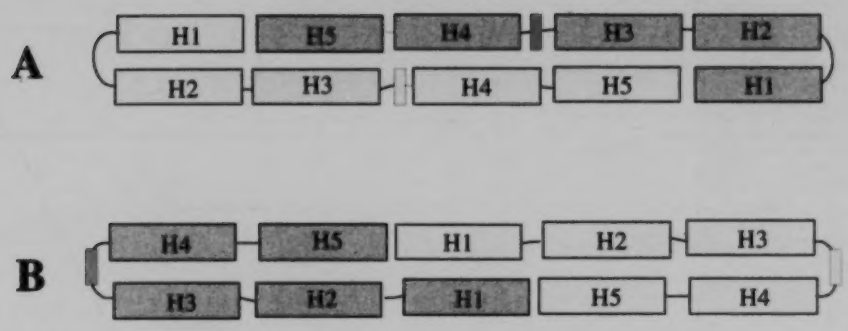

Figure 7-4. Schematic representation of "partially-extended" conformations of apoLp-III around discoidal complexes. ApoLp-III molecules could possibly bind around the periphery of phospholipid bilayer discs as shown (A) or (B). Each molecule of apoLp-III is denoted by a separate colour. The short helix between H3 and H4 represents helix 3'. Model (B) is supported by data presented in this thesis.

It came to our attention that, in the mutant apoLp-IIIs, the pyrene on H3 and the pyrene on H5 would be located directly adjacent to one another (in two locations) if the model shown in Figure 7-4A is correct. This distance is ideal for pyrene excimer formation. To test this model, discoidal complexes were prepared with equal amounts of pyrene-H3 and pyrene-H5 apoLp-IIIs. The sample was excited at 345 nm and the emission spectrum was collected. As shown in **Figure 7-5**, there was no indication of excimer formation since the longer emission peak at ~460 nm was absent.

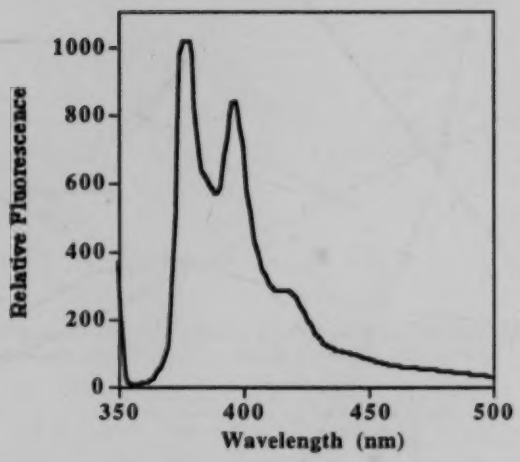

Figure 7-5. Emission spectrum of DMPC discoidal complexes associated with two different pyrene-labeled apoLp-IIIs. DMPC discoidal complexes were prepared with a mixture of pyrene-labeled L90C-apoLp-III and pyrene-labeled A138C-apoLp-III. The sample was excited at 345 nm.

Therefore, on the basis of this data, model A of Figure 7-4 was eliminated.

The model depicted in Figure 7-4B (also Figure 6-9) is supported by evidence summarized in sections 7.3 to 7.6. Moreover, in this particular conformational opening, it seems easier for apoLp-III to undergo opening about 3 hinge domains as we describe, as opposed to 4 or more openings as depicted in models in Figures 7-3 and 7-4A. This is in light of the fact that apoLp-III must readily associate and dissociate from lipophorin particles in response to diacylglycerol content.

C) Apolipophorin III

The proposal of this lipid-bound conformation of *M. sexta* apoLp-III brings up the issue of the lipid-bound conformations of other apoLp-IIIs such as *L. migratoria* apoLp-

III. Recently, using *L. migratoria* apoLp-III, Soulages *et al.* (267, 268) propose a DMPC-bound model that is significantly different from any that have been mentioned above. In the first study, tryptophans were introduced into each helix of apoLp-III and intrinsic fluorescence of each helix was monitored for conformation flexibility and the hydration of the protein in the lipid-free state (267). Their observations suggest that in lipid-free apoLp-III, H2, H3 and H4 constitute a well-packed domain, whereas H1 and H5 constitute a more relaxed protein domain. Due to their great conformational flexibility and weak interhelical interactions, the authors propose that, in the presence of lipid, H1 and H5 form a "gate" to allow exposure of the hydrophobic core of the apoLp-III molecule. In a subsequent study, based on spectroscopic data obtained from the single-tryptophan mutant apoLp-IIIs bound to DMPC discoidal complexes, a new lipid-bound model for apoLp-III on disc complexes was proposed (268). In this model, H1, H4 and H5 interact with the acyl chains of the phospholipid, while H2 and H3 remain together and interact with a more polar region of the complex such as the polar headgroups of the phospholipid or the polar/hydrocarbon interface. While this hypothesis is interesting, it certainly does not gain support from the data obtained from my own work presented in this thesis. This is especially in reference to the data obtained from pyrene excimer studies where clearly, H2 and H3 were shown to move away from one another (Chapter 5). Furthermore, the conformation proposed by Soulages and coworkers can not be reconciled in terms of the area occupied by apoLp-III at the air-water interface (2) and the size of the DMPC discoidal complexes (187).

7.9 Future studies on the "partially-extended" lipid-bound model of apoLp-III

The data discussed in this thesis provides evidence for a lipid-induced conformational opening of apoLp-III that differs from the "open conformation" model. While it is fairly certain that H1 moves away from H5 and aligns near to the lipid/water interface of DMPC discoidal particles, several more experiments are needed to support a "partially-extended" conformation.

A) Disulfide bond engineering

In Chapter 6, it was shown that the H1/H5 double-cysteine mutant apoLp-III was able to form an intramolecular disulfide bond. Using this to our advantage, experiments could be performed that test the binding ability of oxidized vs. reduced apoLp-III to DMPC discoidal particles. If apoLp-III must remain oxidized in order to transform DMPC vesicles into discoidal complexes, then we cannot rule out the open conformation model as shown in **Figure 7-6**.

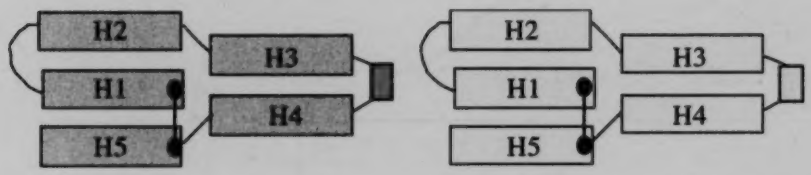

Figure 7-6. Schematic representation depicting the location of disulfide bonds in the "open conformation" model of apoLp-III around discoidal complexes. Each molecule of apoLp-III is denoted by a separate colour. Cysteine residues (filled circles) form a disulfide bond (line between cysteines) under oxidizing conditions.

Other double-cysteine mutants that promote disulfide bond formation can be designed. In particular, a disulfide bond between H1 and H2 should not be able to transform DMPC vesicles into discoidal particles.

B) Pyrene excimer fluorescence spectroscopy.

The same double-cysteine mutant apoLp-IIIs can be useful for pyrene excimer fluorescence studies upon labeling with pyrene maleimide. If the helices remain proximal, excimer fluorescence will be emitted; however, if the helices move apart, then excimer fluorescence will decrease. On a similar note, intermolecular pyrene-pyrene interactions between different single pyrene-labeled mutant apoLp-IIIs on the same discoidal particle can reveal information about proximity of helices. For example, a pyrene fluorophore bound to the beginning of H1 would form strong excimer fluorescence with a pyrene moiety at the end of H2 in the lipid-free state. In the "partially-extended" conformation of apoLp-III on discoidal complexes, excimer fluorescence would decrease since H1 moves away from H2. At this point, it should be noted that apoLp-III containing a mutation in H4 has not yet been designed. Therefore, a H4 mutant apoLp-III in combination with other mutant apoLp-IIIs using several different techniques can provide very useful information.

C) Crosslinking studies

Single-cysteine apoLp-III mutants can provide useful information regarding the lipid-bound structure of apoLp-III on phospholipid bilayers. Two H1 single-cysteine

mutant apoLp-IIIs on a disc in the "partially-extended" conformation should be crosslinked with a sulfhydryl-specific crosslinker.

D) Fluorescence resonance energy transfer spectroscopy (FRET)

FRET relies upon an energy donor (such as tryptophan) to transfer energy to an acceptor [such as pyrene maleimide or N-iodoacetyl-N'-(5-sulfo-1-naphthyl)ethylenediamine (IAEDANS) bound to the sulfhydryl of a cysteine residue]. The efficiency of transfer depends on the proximity of the two fluorophores such that the closer the two fluorophores are, the greater the energy transfer will be. Furthermore, FRET has the advantage of providing quantitative data, therefore, the actual distance between fluorophores upon helical realignment can be measured. In the case of apoLp-III, complete mapping of the repositioning of helix is possible if single-tryptophan/IAEDANS-labeled single-cysteine mutants are produced for each helical pair in apoLp-III. In our laboratory, we have designed a double-mutant apoLp-III wherein a tryptophan residue is located in H3 and a cysteine residue (labeled with IAEDANS) is located in H2. Preliminary data has shown that there is strong energy transfer from the Trp in H3 to IAEDANS on H2; however, in the presence of lysophosphatidylcholine, energy transfer is decreased, suggestive of movement of helices 2 and 3 away from one another in the presence of lipid (unpublished results, Sahoo and Ryan). Thus, FRET has great potential in providing information about the lipid-bound conformation of apoLp-III.

7.10 Binding of apoLp-III to discoidal vs. spherical particles

While most of the data obtained from my research is based on the conformation of apoLp-III on discoidal particles, it is important to note that the same lipid-bound conformation may not apply for apoLp-III bound to spherical lipoprotein surfaces. On a discoidal particle, apoLp-III must bind within a spatially constrained area around the periphery of the complexes. However on the surface of a spherical lipoprotein particle, it is possible that apoLp-III may have more freedom to adopt an alternative, energetically favourable conformation such as that originally proposed by Breiter *et al.* (5) where apoLp-III adopts a lipid-bound conformation via one single movement about hinge domains.

Several studies have demonstrated a fundamental difference in the mode of interaction of exchangeable apolipoproteins with discoidal vs. spherical particles. Two different conformations of apoE on discoidal particles and HDL were obtained when the microenvironments of reductively methylated lysine residues were studied using ^{13}C-NMR (269). Using similar techniques, it was shown that the microenvironments of lysine residues of human apoA-I in discoidal particles differ from that of spherical complexes (270). In terms of apoLp-III, Narayanaswami *et al.* (197) demonstrated that oxidized *M. sexta* apoLp-III (bond between H2 and H3) was unable to bind to lipoproteins particles, whereas the same oxidized protein was capable of binding to discoidal complexes. Weers *et al.* (180) showed that *L. migratoria* apoLp-III containing mutations in the "hydrophobic sensor" region were unable to bind to lipoprotein particles; however, the same mutant apoLp-IIIs were able to transform DMPC or DMPG vesicles into discoidal complexes. From my own research, aqueous quenching data reveal clear

differences in the microenvironment of the pyrene probe upon association with discoidal complexes vs. lipoprotein particles. Therefore, there appear to be distinct differences between the mode of interaction of apoLp-III on the surface of discoidal particles and lipoproteins. Certainly, the same methodology presented in my research, including that suggested for future studies, can be applied towards the study of the lipid-bound conformation of apoLp-III on spherical LDL particles. Furthermore, the apolipoprotein/lipoprotein complexes we created using phospholipase C-modified LDL are a structurally relevant lipid-bound system from which we can gain useful information regarding the lipid-bound conformation of apoLp-III – information that can be applied towards exchangeable apolipoproteins in general.

7.11 Concluding remarks

Using isotopically-labeled recombinant protein, in addition to site-directed mutagenesis to facilitate incorporation of reactive site-specific probes, we have used spectroscopic techniques to examine apoLp-III in terms of its conformational changes, spatial disposition, helical repositioning and orientation upon association with a lipid surface. More importantly, this thesis provides evidence for the possibility of a "partially-extended" conformation of apoLp-III around the periphery of DMPC discoidal particles as shown in Figure 6-9. To this point, we have obtained data to exclude the "open conformation" of apoLp-III on discoidal complexes, specifically relating to the observations that H1 does not exist between H2 and H3 as proposed (5), but rather moves away from H5. Also noteworthy is the fact that our data also exclude the DMPC-bound conformation apoLp-III described by Wientzek *et al.* (167) where H5 is located between

H1 and H2. However, until the lipid-bound structure of apoLp-III is solved in its entirety, further experiments must be performed to distinguish between the many models of lipid-bound exchangeable apolipoproteins that exist.

The ability to form a stable interaction with lipid surfaces represents a common function shared by all exchangeable apolipoproteins and is essential for the expression of their various functions in lipoprotein metabolism. Several contributions towards understanding of structure-function relationships of exchangeable apolipoproteins have been made from studies on apoLp-III. It is the common structural motif shared among insect and mammalian exchangeable apolipoproteins that provides strong support for the concept that apoLp-III represents a model of exchangeable apolipoproteins in higher organisms and that elucidation of the mechanism of interaction of apoLp-III with lipids could be directly applicable to mammalian apolipoproteins.

CHAPTER 8

Bibliography

1. Cole, K. D., Fernando-Warnakulasuriya, G. P., Boguski, M. S., Freeman, M., Gordon, J. I., Clark, W. A., Law, J. H., and Wells, M. A. (1987) Primary structure and comparative sequence analysis of an insect apolipoprotein. Apolipophorin-III from *Manduca sexta*. *J. Biol. Chem.* **262**, 11794-11800.

2. Kawooya, J. K., Meredith, S. C., Wells, M. A., Kézdy, F. J., and Law, J. H. (1986) Physical and surface properties of insect apolipophorin III. *J. Biol. Chem.* **261**, 13588-13591.

3. Ryan, R. O., Oikawa, K., and Kay, C. M. (1993) Conformational, thermodynamic, and stability properties of *Manduca sexta* apolipophorin III. *J. Biol. Chem.* **268**, 1525-1530.

4. Smith, A. F., Owen, L. M., Strobel, L. M., Chen, H., Kanost, M. R., Hanneman, E., and Wells, M. A. (1994) Exchangeable apolipoproteins of insects share a common structural motif. *J. Lipid Res.* **35**, 1976-1984.

5. Breiter, D. R., Kanost, M. R., Benning, M. M., Wesenberg, G., Law, J. H., Wells, M. A., Rayment, I., and Holden, H. M. (1991) Molecular structure of an apolipoprotein determined at 2.5-Å resolution. *Biochemistry* **30**, 603-608.

6. Wang, J., Gagné, S. M., Sykes, B. D., and Ryan, R. O. (1997) Insight into lipid surface recognition and reversible conformational adaptations of an exchangeable apolipoprotein by multidimensional heteronuclear NMR techniques. *J. Biol. Chem.* **272**, 17912-17920.

7. Brown, M. S., and Goldstein, J. L. (1986) A receptor-mediated pathway for cholesterol homeostasis. *Science* **232**, 34-47.

8. Fielding, C. J., and Fielding, P. E. (1995) Molecular physiology of reverse cholesterol transport. *J. Lipid Res.* **36**, 211-228.

9. Chino, H., Downer, R. G. H., Wyatt, G. R., and Gilbert, L. I. (1981) Lipophorins, a major class of lipoproteins of insect haemolymph. *Insect Biochem.* **11**, 491-498.

10. Haunerland, N. H., and Bowers, W. S. (1989) Comparative studies on arthropod lipoproteins. *Comp. Biochem. Physiol.* **92B**, 137-141.

11. Pattnaik, N. M., Mundall, E. C., Trambusti, B. G., Law, J. H., and Kézdy, F. J. (1979) Isolation and characterization of a larval lipoprotein from the hemolymph of *Manduca sexta*. *Comp. Biochem. Physiol.* **63B**, 469-476.

12. Prasad, S. V., Ryan, R. O., Law, J. H., and Wells, M. A. (1986) Changes in lipoprotein composition during larval-pupal metamorphosis of an insect, *Manduca sexta*. *J. Biol. Chem.* **261**, 558-562.

13. Ryan, R. O., Prasad, S. V., Henriksen, E. J., Wells, M. A., and Law, J. H. (1986) Lipoprotein interconversions in an insect, *Manduca sexta*. Evidence for a lipid transfer factor in the hemolymph. *J. Biol. Chem.* **261**, 563-568.

14. Kawooya, J. K., Osir, E. O., and Law, J. H. (1988) Uptake of the major hemolymph lipoprotein and its transformation in the insect egg. *J. Biol. Chem.* **263**, 8740-8747.

15. Prasad, S. V., Fernando-Warnakulasuriya, G. J., Sumida, M., Law, J. H., and Wells, M. A. (1986) Lipoprotein biosynthesis in the larvae of the tobacco hornworm, *Manduca sexta*. *J. Biol. Chem.* **261**, 17174-17176.

16. Haunerland, N. H., and Bowers, W. S. (1986) A larval specific lipoprotein: purification and characterization of a blue chromoprotein from *Heliothis zea*. *Biochem. Biophys. Res. Comm.* **134**, 580-586.

17. Shipman, B. A., Ryan, R. O., Schmidt, J. O., and Law, J. H. (1987) Purification and properties of a very high density lipoprotein from the hemolymph of the honeybee *Apis mellifera*. *Biochemistry* **26**, 1885-1889.

18. Law, J. H., and Wells, M. A. (1989) Insects as biochemical models. *J. Biol. Chem.* **264**, 16335-16338.

19. Ryan, R. O. (1990) Dynamics of insect lipophorin metabolism. *J. Lipid Res.* **31**, 1725-1739.

20. Gondim, K. C., Oliveira, P. L., Coelho, H. S. L., and Masuda, H. (1989) Lipophorin from *Rhodinius prolixus*: purificaion and partial characterization. *Insect Biochem.* **19**, 153-161.

21. Chapman, M. J. (1986) Comparative analysis of mammalian plasma lipoproteins. *Methods Enzymol.* **128**, 70-143.

22. Blomquist, G. J., Nelson, D. R., and de Renobales, M. (1987) Chemistry, biochemistry, and physiology of insect cuticular lipids. *Arch. Insect Biochem. Physiol.* **6**, 227-265.

23. Katagiri, C., Kimura, J., and Murase, N. (1985) Structural studies of lipophorin in insect blood by differential scanning calorimetry and ^{13}C nuclear magnetic relaxation measurements. Location of hydrocarbons. *J. Biol. Chem.* **260**, 13490-13495.

24. Steel, C. G. H., and Davey, K. G. (1985) in *Comprehensive Insect Physiology, Biochemistry and Pharmacology* (Kerkut, G. A., and Gilbert, L. I., Eds.) pp 1-35, Pergamon Press, Oxford.

25. Ryan, R. O., Schmidt, J. O., and Law, J. H. (1984) Chemical and immunological properties of lipophorins from seven insect orders. *Arch. Insect Biochem. Physiol.* **1**, 375-383.

26. Shapiro, J. P., Keim, P. S., and Law, J. H. (1984) Structural studies on lipophorin, an insect lipoprotein. *J. Biol. Chem.* **259**, 3680-3685.

27. Kashiwazaki, Y., and Ikai, A. (1985) Structure of apoproteins in insect lipophorins. *Arch. Biochem. Biophys.* **237**, 160-169.

28. Mundall, E. C., Pattnaik, N. M., Trambusti, B. F., Hromnak, G., Kézdy, F. J., and Law, J. H. (1980) Structural studies on an insect high density lipoprotein. *Ann. N. Y. Acad. Sci.* **348**, 431-432.

29. Weers, P. M. M., Van Marrewijk, W. J. A., Beenakkers, A. M. T., and Van der Horst, D. J. (1993) Biosynthesis of locust lipophorin: Apolipophorins I and II originate from a common precursor. *J. Biol. Chem.* **268**, 4300-4303.

30. Kawooya, J. K., Keim, P. S., Ryan, R. O., Shapiro, J. P., Samaraweera, P., and Law, J. H. (1984) Insect apolipophorin III. Purification and properties. *J. Biol. Chem.* **259**, 10733-10737.

31. Van der Horst, D. J., Van Doorn, J. M., and Beenakkers, A. M. T. (1984) Hormone induced rearrangement of locust haemolymph lipoproteins: The involvement of glycoprotein C_2. *Insect Biochem.* **14**, 495-504.

32. Shen, B. W., Scanu, A. M., and Kézdy, F. J. (1977) Structure of human serum lipoproteins inferred from compositional analysis. *Proc. Natl. Acad. Sci. U. S. A.* **74**, 837-841.

33. Edelstein, C., Kézdy, F. J., Scanu, A. M., and Shen, B. W. (1979) Apolipoproteins and the structural organization of plasma lipoproteins: human plasma high density lipoprotein-3. *J. Lipid Res.* **20**, 143-153.

34. Chino, H., Downer, R. G. H., and Takahashi, K. (1986) Effect of adipokinetic hormone on the structure and properties of lipophorin in locusts. *J. Lipid Res.* **27**, 21-29.

35. Chino, H., Hirayama, Y., Kiyomoto, Y., Downer, R. G. H., and Takahashi, K. (1987) Spontaneous aggregation of locust lipophorin during hemolymph colletion. *Insect Biochem.* **17**, 89-97.

36. Katagiri, C. (1985) Structure of lipophorin in insect blood: location of phospholipid. *Biochim. Biophys. Acta* **834**, 139-143.

37. Katagiri, C., Kimura, J., and Murase, N. (1985) Structural studies of lipophorin in insect blood by differential scanning calorimetry and ^{13}C-nuclear magnetic relaxation measurements: Location of hydrocarbons. *J. Biol. Chem.* **260**, 13490-13495.

38. Kawooya, J. K., Van der Horst, D. J., Van Heusden, M. C., Brigot, B. L. J., Van Antwerpen, R., and Law, J. H. (1991) Lipophorin structure analyzed by *in vitro* treatment with lipases. *J. Lipid Res.* **32**, 1781-1788.

39. Soulages, J. L., Rimoldi, O. J., and Brenner, R. R. (1988) Lipid thermotropic transitions in *Triatoma infestans* lipophorin. *J. Lipid Res.* **29**, 172-182.

40. Shapiro, J. P., Law, J. H., and Wells, M. A. (1988) Lipid transport in insects. *Ann. Rev. Entomol.* **33**, 297-318.

41. Van der Horst, D. J. (1990) Lipid transport function of lipoproteins in flying insects. *Biochim. Biophys. Acta* **1047**, 195-211.

42. Katagiri, C., Sato, M., and Tanaka, N. (1987) Small-angle X-ray scattering study of insect lipophorin. *J. Biol. Chem.* **262**, 15857-15861.

43. Van der Horst, D. J., Van Heusden, M. C., Schulz, T. K. F., and Beenakkers, A. M. T. (1987) in *Molecular Entomology* (Law, J. H., Ed.) pp 247-256, Alan R. Liss, New York.

44. Schulz, T. K. F., Van der Horst, D. J., Amesz, H., Voorma, H. O., and Beenakkers, A. M. T. (1987) Monoclonal antibodies specific for apoproteins of lipophorins from the migratory locust. *Arch. Insect Biochem. Physiol.* **6**, 97-107.

45. Weers, P. M. M., Van der Horst, D. J., Van Marrewijk, W. J. A., Van den Eijnden, M., Van Doorn, J. M., and Beenakkers, A. M. T. (1992) Biosynthesis and secretion of insect lipoprotein. *J. Lipid Res.* **33**, 485-491.

46. Capurro, M. d. L., and de Bianchi, A. G. (1990) Larval *Musca domestica* lipophorin biosynthesis. *Comp. Biochem. Physiol.* **97B**, 649-653.

47. Venkatesh, K., Lenz, C. J., Bergman, K., and Chippendale, G. M. (1987) Synthesis and release of lipophorin in larvae of the southwestern corn borer *Diatraea grandiosella*: an *in vitro* study. *Insect Biochem.* **17**, 1173-1180.

48. Bergman, D. K., and Chippendale, G. M. (1989) *In vitro* release of lipophorin from the fat body of nondiapause and diapause larvae of the southwestern corn borer, *Diatraea grandiosella*. *Insect Biochem.* **19**, 361-365.

49. Prasad, S. V., Tsuchida, K., Cole, K. D., and Wells, M. A. (1987) in *Molecular Entomology* (Law, J. H., Ed.) pp 267-273, Alan R. Liss, New York.

50. Tsuchida, K., and Wells, M. A. (1988) Digestion, absorption, transport and storage of fat during the last larval stadium of *Manduca sexta*. Changes in the role of lipophorin in the delivery of dietary lipid to the fat body. *Insect Biochem.* **18**, 263-268.

51. Wells, M. A., Ryan, R. O., Kawooya, J. K., and Law, J. H. (1987) The role of apolipophorin III in *in vivo* lipoprotein interconversions in adult *Manduca sexta*. *J. Biol. Chem.* **262**, 4172-4176.

52. Holm, C., Langin, D., Manganiello, V., Belfrage, P., and Degerman, E. (1997) Regulation of hormone-sensitive lipase activity in adipose tissue. *Methods Enzymol.* **286**, 45-67.

53. Arrese, E. L., and Wells, M. A. (1994) Purification and properties of a phosphorylatable triacylglycerol lipase from the fat body of an insect, *Manduca sexta*. *J. Lipid Res.* **35**, 1652-1660.

54. Orchard, I. (1987) Adipokinetic hormones-an update. *J. Insect Physiol.* **33**, 451-463.

55. Beenakkers, A. M. T., Bloemen, R. E. B., de Vlieger, T. A., Van der Horst, D. J., and Van Marrewijk, W. J. A. (1985) Insect adipokinetic hormones. *Peptides* **6**, 437-444.

56. Ziegler, R., Eckart, K., Schwarz, H., and Keller, R. (1985) Amino acid sequence of *Manduca sexta* adipokinetic hormone elucidated by combined fast atom bombardment (FAB)/tandem mass spectrometry. *Biochem. Biophys. Res. Comm.* **133**, 337-342.

57. Diederen, J. H. B., Maas, H. A., Pel, H. J., Schooneveld, H., Jansen, W. F., and Vullings, H. G. B. (1987) Co-localization of the adipokinetic hormones I and II in the same glangular cells and in the same secretory granules of the corpus cardiacum of *Locusta migritoria* and *Schistocerca gregaria*. *Cell Tissue Res.* **249**, 379-389.

58. Oudejans, R. C. H. M., Kooiman, F. P., Heerma, W., Versluis, C., Slotboom, A. J., and Beenakkers, A. M. T. (1991) Isolation and structure elucidation of a novel adipokinetic hormone (Lom-AKH-III) from the glandular lobes of the corpus cardiacum of the migratory locust, *Locusta migratoria*. *Eur. J. Biochem.* **195**, 351-359.

59. Beenakkers, A. M. T., Van der Horst, D. J., and Van Marrewijk, W. J. A. (1985) Insect lipids and lipoproteins, and their role in physiological processes. *Prog. Lipid Res.* **24**, 19-67.

60. Lum, P. Y., and Chino, H. (1990) Primary role of adipokinetic hormone in the formation of low density lipophorin in locusts. *J. Lipid Res.* **31**, 2039-2044.

61. Wang, Z., Hayakawa, Y., and Downer, R. G. H. (1990) Factors influencing cyclic AMP and diacylglycerol levels in fat body of *Locusta migratoria*. *Insect Biochem.* **20**, 325-330.

62. Arrese, E. L., Flowers, M. T., Gazard, J. L., and Wells, M. A. (1999) Calcium and cAMP are second messengers in the adipokinetic hormone-induced lipolysis of triacylglycerols in *Manduca sexta* fat body. *J. Lipid Res.* **40**, 556-564.

63. Ogoyi, D. O., Osir, E. O., and Olembo, N. K. (1998) Fat body triacylglycerol lipase in solitary and gregarious phases of *Schistocerca gregaria* (Forskal) (Orthoptera: Acrididae). *Comp. Biochem. Physiol.* **B119**, 163-169.

64. Lok, C. M., and Van der Horst, D. J. (1980) Chiral 1,2-diacylglycerols in the haemolymph of the locust, *Locusta migratoria*. *Biochim. Biophys. Acta* **618**, 80-87.

65. Tietz, A., and Weintraub, H. (1980) The stereospecific nature of haemolymph and fat-body 1,2 -diacylglycerol from *Locusta migratoria*. *Insect Biochem.* **10**, 61-63.

66. Arrese, E. L., and Wells, M. A. (1997) Adipokinetic hormone-induced lipolysis in the fat body of an insect, *Manduca sexta*: synthesis of sn-1,2-diacylglycerols. *J. Lipid Res.* **38**, 68-76.

67. Arrese, E. L., Rojas-Rivas, B. I., and Wells, M. A. (1996) Synthesis of sn-1,2-diacylglycerols by monoacylglycerol acyltransferase from *Manduca sexta* fat body. *Arch. Insect Biochem. Physiol.* **31**, 325-335.

68. Van Heusden, M. C., and Law, J. H. (1989) An insect lipid transfer particle promotes lipid loading from fat body to lipoprotein. *J. Biol. Chem.* **264**, 17287-17292.

69. Ryan, R. O., Wells, M. A., and Law, J. H. (1986) Lipid transfer protein from *Manduca sexta* hemolymph. *Biochem. Biophys. Res. Comm.* **136**, 260-265.

70. Ryan, R. O., Senthilathipan, K. R., Wells, M. A., and Law, J. H. (1988) Facilitated diacylglycerol exchange between insect hemolymph lipophorins. Properties of *Manduca sexta* lipid transfer particle. *J. Biol. Chem.* **263**, 14140-14145.

71. Ryan, R. O., Van Antwerpen, R., Van der Horst, D. J., Beenakkers, A. M. T., and Law, J. H. (1990) *Manduca sexta* lipid transfer particle acts upon a lipoprotein to catalyze lipid and apoprotein disproportionation. *J. Biol. Chem.* **265**, 546-552.

72. Chino, H., and Yazawa, M. (1986) Apolipophorin III in locusts: purification and characterization. *J. Lipid Res.* **27**, 377-385.

73. Van der Horst, D. J., Ryan, R. O., Van Heusden, M. C., Schulz, T. K., Van Doorn, J. M., Law, J. H., and Beenakkers, A. M. T. (1988) An insect lipoprotein hybrid helps to define the role of apolipophorin III. *J. Biol. Chem.* **263**, 2027-2033.

74. Van Heusden, M. C., Van der Horst, D. J., Van Doorn, J. M., Wes, J., and Beenakkers, A. M. T. (1986) Lipoprotein lipase activity in the flight muscle of *Locusta migratoria* and its specificity for hemolymph lipoproteins. *Insect Biochem.* **16**, 517-523.

75. Wheeler, C. H., Van der Horst, D. J., and Beenakkers, A. M. T. (1984) Lipolytic activity in the flight muscles of *Locusta migratoria* measured with haemolymph lipoproteins as substrates. *Insect Biochem.* **14**, 261-266.

76. Wheeler, C. H., and Goldsworthy, G. J. (1985) Specificity and localisation of lipoprotein lipase in the flight muscles of *Locusta migratoria*. *Biol. Chem. Hoppe-Seyler* **366**, 1071-1077.

77. Van Heusden, M. C. (1993) Characterization and identification of a lipoprotein lipase from *Manduca sexta* flight muscle. *Insect Biochem. Mol. Biol.* **23**, 785-792.

78. Haunerland, N. H., and Chisholm, J. M. (1990) Fatty acid binding protein in flight muscle of the locust, *Schistocerca gregaria*. *Biochim. Biophys. Acta* **1047**, 233-238.

79. Smith, A. F., Tsuchida, K., Hanneman, E., Suzuki, T. C., and Wells, M. A. (1992) Isolation, characterization, and cDNA sequence of two fatty acid-binding proteins from the midgut of *Manduca sexta* larvae. *J. Biol. Chem.* **267**, 380-384.

80. Downer, R. G. H., and Chino, H. (1985) Turnover of protein and diacylglycerol components of lipophorin in insect hemolymph. *Insect Biochem.* **15**, 627-630.

81. Chino, H., and Kitazawa, K. (1981) Diacylglycerol-carrying lipoprotein of hemolymph of the locust and some insects. *J. Lipid Res.* **22**, 1042-1052.

82. Blacklock, B. J., and Ryan, R. O. (1994) Hemolymph lipid transport. *Insect Biochem. Mol. Biol.* **24**, 855-873.

83. Van Heusden, M. C., Van der Horst, D. J., Voshol, J., and Beenakkers, A. M. T. (1987) The recycling of protein components of the flight-specific lipophorin in *Locusta migratoria*. *Insect Biochem.* **17**, 771-776.

84. Van Antwerpen, R., Linnemans, W. A. M., Van der Horst, D. J., and Beenakkers, A. M. T. (1988) Immunocytochemical localization of lipophorins in the flight muscles of the migratory locust (*Locusta migratoria*) at rest and during flight. *Cell Tissue Res.* **252**, 661-668.

85. Van Heusden, M. C., Van der Horst, D. J., Kawooya, J. K., and Law, J. H. (1991) *In vivo* and *in vitro* loading of lipid by artificially lipid-depleted lipophorins: evidence for the role of lipophorin as a reusable lipid shuttle. *J. Lipid Res.* **32**, 1789-1794.

86. Fielding, P. E., and Fielding, C. J. (1996) in *Biochemistry of Lipids, Lipoproteins and Membranes* (Vance, D. E., and Vance, J. E., Eds.) pp 495-541, Elsevier Science B. V., Amsterdam.

87. Stein, O., Stein, Y., Lefevre, M., and Roheim, P. S. (1986) The role of apolipoprotein A-IV in reverse cholesterol transport studied with cultured cells and liposomes derived from an ether analog of phosphatidylcholine. *Biochim. Biophys. Acta* **878**, 7-13.

88. Steinmetz, A., Barbaras, R., Ghalim, N., Clavey, V., Fruchart, J. C., and Ailhaud, G. (1990) Human apolipoprotein A-IV binds to apolipoprotein A-I/A-II receptor sites and promotes cholesterol efflux from adipose cells. *J. Biol. Chem.* **265**, 7859-7863.

89. Steinmetz, A., and Utermann, G. (1985) Activation of lecithin:cholesterol acyltransferase by human apolipoprotein A-IV. *J. Biol. Chem.* **260**, 2258-2264.

90. Ryan, R. O. (1996) Structural studies of lipoproteins and their apolipoprotein components. *Biochem. Cell Biol.* **74**, 155-164.

91. Cole, K. D., and Wells, M. A. (1990) A comparison of adult and larval *Manduca sexta* apolipophorin-III. *Insect Biochem.* **20**, 373-380.

92. Shapiro, J. P., and Law, J. H. (1983) Locust adipokinetic hormone stimulates lipid mobilization in *Manduca sexta*. *Biochem. Biophys. Res. Comm.* **115**, 924-931.

93. Wells, M. A., Ryan, R. O., Prasad, S. V., and Law, J. H. (1985) A novel procedure for the purification of apolipophorin III. *Insect Biochem.* **15**, 565-571.

94. Haunerland, N. H., Ryan, R. O., Law, J. H., and Bowers, W. S. (1986) Lipophorin from the grasshopper, *Gastrimargus africanus*: isolation and properties of apolipohorin III. *Insect Biochem.* **16**, 797-802.

95. Ryan, R. O., Ziegler, R., Van der Horst, D. J., and Law, J. H. (1990) Characterization of apolipophorin III from *Barytettix psolus* and *Melanoplus differentialis*. *Insect Biochem.* **20**, 127-133.

96. Burks, C. S., Shelby, K. S., and Chippendale, G. M. (1992) Characteristics of apolipophorin-III of the southwestern corn borer, *Diatraea grandiosella*. *Insect Biochem.* **22**, 905-915.

97. Yamauchi, Y., Hoeffer, C., Yamamoto, A., Takeda, H., Ishihara, R., Maekawa, H., Sato, R., Su-Il, S., Sumida, M., Wells, M. A., and Tsuchida, K. (2000) cDNA and deduced amino acid sequences of apolipophorin IIIs from *Bombyx mori* and *Bombyx mandarina*. *Arch. Insect. Biochem. Physiol.* **43**, 16-21.

98. Weise, C., Franke, P., Kopacek, P., and Weisner, A. (1998) Primary structure of apolipophorin III from the greater wax moth, *Galleria mellonella*. *J. Protein Chem.* **17**, 633633-633641.

99. Cole, K. D., Smith, A. F., and Wells, M. A. (1990) The structure of the apolipophorin-III gene from *Manduca sexta*. *Insect Biochem.* **20**, 381-388.

100. Steiner, D. F., Quinn, P. S., Chan, S. J., Marsh, J., and Tager, H. S. (1980) Processing mechanisms in the biosynthesis of proteins. *Ann. N. Y. Acad. Sci.* **343**, 1-16.

101. Gordon, J. I., Budelier, K. A., Sims, H. F., Edelstein, C., Scanu, A. M., and Strauss, A. W. (1983) Biosynthesis of human preproapolipoprotein A-II. *J. Biol. Chem.* **258**, 14054-14059.

102. Nagashima, N., Morris, G., Howlett, G., Fidge, N., and Schreiber, G. (1986) Amino acid sequence of rat apolipoprotein A-II deduced from the nucleotide sequence of cloned cDNA. *J. Lipid Res.* **27**, 706-712.

103. Boguski, M. S., Freeman, M., Elshourbagy, N., Taylor, J. M., and Gordon, J. I. (1986) On computer-assisted analysis of biological sequences: proline punctuation, consensus sequences, and apolipoprotein repeats. *J. Lipid Res.* **27**, 1011-1034.

104. Stone, W. L., and Reynolds, J. A. (1975) The self-association of the apo-Gln-I and apo-Gln-II polypeptides of human high density serum lipoproteins. *J. Biol. Chem.* **250**, 8045-8048.

105. Gwynne, J., Palumbo, G., Osborne, J. C. J., Brewer, H. B. J., and Edelhoch, H. (1975) The self-association of apoA-II, an apoprotein of the human high density lipoprotein complex. *Arch. Biochem. Biophys.* **170**, 204-212.

106. Yokoyama, S., Kawai, Y., Tajima, S., and Yamamoto, A. (1985) Behaviour of human apolipoprotein E in aqueous solutions and at interfaces. *J. Biol. Chem.* **260**, 16375-16382.

107. Van Holde, K. E. (1971) *Physical Biochemistry*, Prentice-Hall, Englewood Cliffs, New Jersey.

108. Provencher, S. W., and Glöckner, J. (1981) Estimation of globular protein secondary structure from circular dichroism. *Biochemistry* **20**, 33-37.

109. Gwynne, J., Brewer, H. B. J., and Edelhoch, H. (1975) The molecular behavior of apoA-I in human high density lipoproteins. *J. Biol. Chem.* **250**, 2269-2274.

110. Tall, A. R., Shipley, G. G., and Small, D. M. (1976) Conformational and thermodynamic properties of apoA-I of human plasma high density lipoproteins. *J. Biol. Chem.* **251**, 3749-3755.

111. Weinberg, R. B., and Spector, M. S. (1985) Structural properties and lipid binding of human apolipoprotein A-IV. *J. Biol. Chem.* **260**, 4914-4921.

112. Reynolds, J. A. (1976) Conformational stability of the polypeptide components of human high density serum lipoprotein. *J. Biol. Chem.* **251**, 6013-6015.

113. Edelstein, C., and Scanu, A. M. (1980) Effect of guanidine hydrochloride on the hydrodynamic and thermodynamic properties of human apolipoprotein A-I in solution. *J. Biol. Chem.* **255**, 5747-5754.

114. Reijngoud, D. J., and Phillips, M. C. (1982) Mechanism of dissociation of human apolipoprotein A-I from complexes with dimyristoylphosphatidylcholine as studied by guanidine hydrochloride denaturation. *Biochemistry* **21**, 2969-2976.

115. Wetterau, J. R., Aggerbeck, L. P., Rall, S. C., Jr., and Weisgraber, K. H. (1988) Human apolipoprotein E3 in aqueous solution. I. Evidence for two structural domains. *J. Biol. Chem.* **263**, 6240-6248.

116. Fisher, C. A., and Ryan, R. O. (1999) Lipid binding-induced conformational changes in the N-terminal domain of human apolipoprotein E. *J. Lipid Res.* **40**, 93-99.

117. Mantulin, W. W., Rohde, M. F., Gotto, A. M., Jr., and Pownall, H. J. (1980) The conformational properties of human plasma apolipoprotein C-II. A spectroscopic study. *J. Biol. Chem.* **255**, 8185-8191.

118. Narayanaswami, V., Kay, C. M., Oikawa, K., and Ryan, R. O. (1994) Structural and binding characteristics of the carboxyl terminal fragment of apolipophorin III from *Manduca sexta*. *Biochemistry* **33**, 13312-13320.

119. Ryan, R. O., Schieve, D., Wientzek, M., Narayanaswami, V., Oikawa, K., Kay, C. M., and Agellon, L. B. (1995) Bacterial expression and site-directed mutagenesis of a functional recombinant apolipoprotein. *J. Lipid Res.* **36**, 1066-1072.

120. Burley, S. K., and Petsko, G. A. (1985) Aromatic-aromatic interaction: a mechanism of protein structure stabilization. *Science* **229**, 23-28.

121. Narayanaswami, V., Frolov, A., Schroeder, F., Oikawa, K., Kay, C. M., and Ryan, R. O. (1996) Fluorescence studies of lipid association-induced conformational adaptations of an exchangeable amphipathic apolipoprotein. *Arch. Biochem. Biophys.* **334**, 143-150.

122. Rosseneu, M., Soetewey, F., Peeters, H., Bausserman, L. L., and Herbert, P. N. (1976) Interaction of the apoproteins of very low density and high density lipoproteins with synthetic phospholipids. *Eur. J. Biochem.* **70**, 285-289.

123. Weinberg, R. B., and Spector, M. S. (1985) Human apolipoprotein A-IV: displacement from the surface of triglyceride-rich particles by HDL2-associated C-apoproteins. *J. Lipid Res.* **26**, 26-37.

124. Liu, H., Malhotra, V., and Ryan, R. O. (1991) Displacement of apolipophorin III from the surface of low density lipophorin by human apolipoprotein A-I. *Biochem. Biophys. Res. Comm.* **179**, 734-740.

125. Fisher, C. A., Kiss, R. S., Francis, G. A., Gao, P., and Ryan, R. O. (1999) Human apolipoprotein E N-terminal domain displacement of apolipophorin III from insect low density lipophorin creates a receptor-competent hybrid lipoprotein. *Comp. Biochem. Physiol. Part B.* **122**, 447-451.

126. Lund-Katz, S., and Phillips, M. C. (1986) Packing of cholesterol molecules in human low-density lipoprotein. *Biochemistry* **25**, 1562-1568.

127. Wang, J., Liu, H., Sykes, B. D., and Ryan, R. O. (1992) ^{31}P-NMR study of the phospholipid moiety of lipophorin subspecies. *Biochemistry* **31**, 8706-8712.

128. Soulages, J. L., and Brenner, R. R. (1991) Study on the composition-structure relationship of lipophorins. *J. Lipid Res.* **32**, 407-415.

129. Wang, J., Liu, H., Sykes, B. D., and Ryan, R. O. (1995) Identification and localization of two distinct microenvironments for the diacylglycerol component of lipophorin particles by ^{13}C NMR. *Biochemistry* **34**, 6755-6761.

130. Ryan, R. O., Wessler, A. N., Price, H. M., Ando, S., and Yokoyama, S. (1990) Insect lipid transfer particle catalyzes bidirectional vectorial transfer of diacylglycerol from lipophorin to human low density lipoprotein. *J. Biol. Chem.* **265**, 10551-10555.

131. Singh, T. K., Scraba, D. G., and Ryan, R. O. (1992) Conversion of human low density lipoprotein into a very low density lipoprotein-like particle *in vitro*. *J. Biol. Chem.* **267**, 9275-9280.

132. Stryer, L. (1995) *Biochemistry*, W. H. Freeman and Company, New York.

133. Suits, A. G., Chait, A., Aviram, M., and Heinecke, J. W. (1989) Phagocytosis of aggregated lipoproteins by macrophages: low density lipoprotein receptor-dependent foam cell formation. *Proc. Natl. Acad. Sci. U. S. A.* **86**, 2713-2717.

134. Xu, X.-X., and Tabas, I. (1991) Sphingomyelinase enhances low density lipoprotein uptake and ability to induce cholesterol ester accumulation in macrophages. *J. Biol. Chem.* **266**, 24849-24858.

135. Liu, H., Scraba, D. G., and Ryan, R. O. (1993) Prevention of phospholipase-C induced aggregation of low density lipoprotein by amphipathic apolipoproteins. *FEBS Lett.* **316**, 27-33.

136. Singh, T. K., Liu, H., Bradley, R., Scraba, D. G., and Ryan, R. O. (1994) Effect of phospholipase C and apolipophorin III on the structure and stability of lipophorin subspecies. *J. Lipid Res.* **35**, 1561-1569.

137. Sun, D., Ziegler, R., Milligin, C. E., Fahrbach, S., and Schwartz, L. M. (1995) Apolipophorin III is dramatically up-regulated during the programmed cell death of insect skeletal muscle and neurons. *J. Neurobiol.* **26**, 119-129.

138. Truman, J. W., and Schwartz, L. M. (1984) Steroid regulation of neuronal death in the moth nervous system. *J. Neurosci.* **4**, 274-280.

139. Schwartz, L. M., and Truman, J. W. (1983) Hormonal control of rates of metamorphic development in the tobacco hornworm *Manduca sexta*. *Dev. Biol.* **99**, 103-114.

140. Niere, M., Meiblitzer, C., Dettloff, M., Weise, C., Ziegler, M., and Wiesner, A. (1999) Insect immune activation by recombinant *Galleria mellonella* apolipophorin III. *Biochim. Biophys. Acta* **1433**, 16-26.

141. Weisgraber, K. H. (1994) Apolipoprotein E: structure-function relationships. *Adv. Prot. Chem.* **45**, 249-302.

142. Segrest, J. P., Jackson, R. L., Morrisett, J. D., and Gotto, M., Jr. (1974) A molecular theory of lipid-protein interactions in the plasma lipoproteins. *FEBS Lett.* **38**, 247-253.

143. Eisenberg, D., Wesson, M., and Wilcox, W. (1989) *Predictions of Protein Structure and the Principles of Protein Conformation*, Plenum Publishing Corp., New York.

144. Karathanasis, S. K., Zannis, V. I., and Breslow, J. L. (1983) Isolation and characterization of the human apolipoprotein A-I gene. *Proc. Natl. Acad. Sci. U. S. A.* **80**, 6147-6151.

145. Das, H. K., McPherson, J., Bruns, G. A. P., Karathansis, S. K., and Breslow, J. L. (1985) Isolation, characterization, and mapping to chromosome 19 of the human apolipoprotein E gene. *J. Biol. Chem.* **260**, 6240-6247.

146. Paik, Y.-K., Chang, D. J., Reardon, C. A., Davies, G. E., Mahley, R. W., and Taylor, J. M. (1985) Nucleotide sequence and structure of the human apolipoprotein E gene. *Proc. Natl. Acad. Sci. U. S. A.* **82**, 3445-3449.

147. Karathanasis, S. K., Yunis, I., and Zannis, V. I. (1986) Structure, evolution and tissue-specific synthesis of human apolipoprotein A-IV. *Biochemistry* **25**, 3962-3970.

148. Mathews, F. S., Levine, M., and Argos, P. (1972) Three-dimensional Fourier synthesis of calf liver cytochrome b5 at 2-8 Å resolution. *J. Mol. Biol.* **64**, 449-464.

149. Weber, P. C., Bartsch, R. G., Cusanovich, M. A., Hamilton, R. C., Howard, A., Jordan, S. R., Kamen, M. D., Meyer, T. E., Weatherford, D. W., Xuong, N. H., and Salemme, R. (1980) Structure of cytochrome c': a dimeric, high-spin haem protein. *Nature (London)* **286**, 302-304.

150. Richardson, J. S. (1981) The anatomy and taxonomy of protein structure. *Adv. Prot. Chem.* **34**, 167-339.

151. Marqusee, S., and Baldwin, R. L. (1987) Helix stabilization by Glu-...Lys+ salt bridges in short peptides of *de novo* design. *Proc. Natl. Acad. Sci. U. S. A.* **84**, 8898-8902.

152. Narayanaswami, V., Weers, P. M., Bogerd, J., Kooiman, F. P., Kay, C. M., Scraba, D. G., Van der Horst, D. J., and Ryan, R. O. (1995) Spectroscopic and lipid binding studies on the amino and carboxyl terminal fragments of *Locusta migratoria* apolipophorin III. *Biochemistry* **34**, 11822-11830.

153. Wang, J., Narayanaswami, V., Sykes, B. D., and Ryan, R. O. (1998) Interhelical contacts are required for the helix bundle fold of apolipophorin III and its ability to interact with lipoproteins. *Prot. Sci.* **7**, 336-341.

154. Kanost, M. R., Boguski, M. S., Freeman, M., Gordon, J. I., Wyatt, G. R., and Wells, M. A. (1988) Primary structure of apolipophorin-III from the migratory locust, *Locusta migratoria*. Potential amphipathic structures and molecular evolution of an insect apolipoprotein. *J. Biol. Chem.* **263**, 10568-10573.

155. Holden, H. M., Kanost, M. R., Law, J. H., Rayment, I., and Wells, M. A. (1988) Crystallization and preliminary analysis of crystals of apolipophorin III isolated from *Locusta migratoria*. *J. Biol. Chem.* **263**, 3960-3962.

156. Wilson, C., Wardell, M. R., Weisgraber, K. H., Mahley, R. W., and Agard, D. A. (1991) Three-dimensional structure of the LDL receptor-binding domain of human apolipoprotein E. *Science* **252**, 1817-1822.

157. Mahley, R. W. (1988) Apolipoprotein E: cholesterol transport protein with expanding role in cell biology. *Science* **240**, 622-630.

158. Innerarity, T. L., Friedlander, E. J., Rall, S. C., Jr., Weisgraber, K. H., and Mahley, R. W. (1983) The receptor-binding domain of human apolipoprotein E. Binding of apolipoprotein E fragments. *J. Biol. Chem.* **258**, 12341-12347.

159. Luo, C.-C., Li, W.-H., Moore, N., and Chan, L. (1986) Structure and evolution of the apolipoprotein multigene family. *J. Mol. Biol.* **187**, 325-340.

160. Pownall, H. J., Pao, Q., Hickson, D., Sparrow, J. T., and Gotto, A. M., Jr. (1982) Thermodynamics of lipid-protein association in human plasma lipoproteins. *Biophys. J.* **37**, 175-177.

161. Aggerbeck, L. P., Wetterau, J. R., Weisgraber, K. H., Mahley, R. W., and Agard, D. A. (1988) Crystallization and preliminary X-ray diffraction studies on the amino-terminal (receptor-binding) domain of human apolipoprotein E3 from serum very low density lipoproteins. *J. Mol. Biol.* **202**, 179-181.

162. Aggerbeck, L. P., Wetterau, J. R., Weisgraber, K. H., Wu, C. S., and Lindgren, F. T. (1988) Human apolipoprotein E3 in aqueous solution. II. Properties of the amino- and carboxyl-terminal domains. *J. Biol. Chem.* **263**, 6249-6258.

163. Borhani, D. W., Rogers, D. P., Engler, J. A., and Brouillette, C. G. (1997) Crystal structure of truncated human apolipoprotein A-I suggests a lipid-bound conformation. *Proc. Natl. Acad. Sci. U. S. A.* **94**, 12291-12296.

164. Segrest, J. P., Garber, D. W., Brouillette, C. G., Harvey, S. C., and Anantharamaiah, G. M. (1994) The amphipathic α helix: a multifunctional structural motif in plasma apolipoproteins. *Adv. Prot. Chem.* **45**, 303-369.

165. Wlodawer, A., Segrest, J. P., Chung, B. H., Chiovetti, R., Jr., and Weinstein, J. N. (1979) High-density lipoprotein recombinants: evidence for a bicycle tire micelle structure obtained by neutron scattering and electron microscopy. *FEBS Lett.* **104**, 231-235.

166. Atkinson, D., Small, D. M., and Shipley, G. G. (1980) X-ray and neutron scattering studies of plasma lipoproteins. *Ann. N. Y. Acad. Sci.* **348**, 284-298.

167. Wientzek, M., Kay, C. M., Oikawa, K., and Ryan, R. O. (1994) Binding of insect apolipophorin III to dimyristoylphosphatidylcholine vesicles. Evidence for a conformational change. *J. Biol. Chem.* **269**, 4605-4612.

168. Brasseur, R., De Meutter, J., Vanloo, B., Goormaghtigh, E., Ruysschaert, J.-M., and Rosseneu, M. (1990) Mode of assembly of amphipathic helical segments in model high-density lipoproteins. *Biochim. Biophys. Acta* **1043**, 245-252.

169. Wald, J. H., Goormaghtigh, E., De Meutter, J., Ruysschaert, J. M., and Jonas, A. (1990) Investigation of the lipid domains and apolipoprotein orientation in reconstituted high density lipoproteins by fluorescence and IR methods. *J. Biol. Chem.* **265**, 20044-20050.

170. Segrest, J. P. (1977) Amphipathic helixes and plasma lipoproteins: thermodynamic and geometric considerations. *Chem. Phys. Lipids* **18**, 7-22.

171. Brouillette, C. G., Jones, J. L., Ng, T. C., Kercret, H., Chung, B. H., and Segrest, J. P. (1984) Structural studies of apolipoprotein A-I/phosphatidylcholine recombinants by high-field proton NMR, nondenaturing gradient gel electrophoresis, and electron microscopy. *Biochemistry* **23**, 359-367.

172. Raussens, V., Narayanaswami, V., Goormaghtigh, E., Ryan, R. O., and Ruysschaert, J. M. (1995) Alignment of the apolipophorin-III α-helices in complex with dimyristoylphosphatidylcholine. A unique spatial orientation. *J. Biol. Chem.* **270**, 12542-12547.

173. Segrest, J. P., Jones, M. K., De Loof, H., Brouillette, C. G., Venkatachalapathi, Y. V., and Anantharamaiah, G. M. (1992) The amphipathic helix in the exchangeable apolipoproteins: a review of secondary structure and function. *J. Lipid Res.* **33**, 141-166.

174. Gazzara, J. A., Phillips, M. C., Lund-Katz, S., Palgunachari, M. N., Segrest, J. P., Anantharamaiah, G. M., and Snow, J. W. (1997) Interaction of class A amphipathic helical peptides with phospholipid unilamellar vesicles. *J. Lipid Res.* **38**, 2134-2146.

175. Zhang, Y., Lewis, R. N., McElhaney, R. N., and Ryan, R. O. (1993) Calorimetric and spectroscopic studies of the interaction of *Manduca sexta* apolipophorin III with zwitterionic, anionic, and nonionic lipids. *Biochemistry* **32**, 3942-3952.

176. Soulages, J. L., and Wells, M. A. (1994) Lipophorin: the structure of an insect lipoprotein and its role in lipid transport in insects. *Adv. Prot. Chem.* **45**, 371-415.

177. Upadhyaya, M., Oikawa, K., Kay, C. M., Scraba, D. G., Bradley, R., and Ryan, R. O. (1995) Role of charged amino acid side chains in the stability and lipid binding of *Manduca sexta* apolipophorin III. *Arch. Insect. Biochem. Phys.* **30**, 211-223.

178. Soulages, J. L., and Wells, M. A. (1994) Effect of diacylglycerol content on some physicochemical properties of the insect lipoprotein, lipophorin. Correlation with the binding of apolipophorin-III. *Biochemistry* **33**, 2356-2362.

179. Soulages, J. L., Salamon, Z., Wells, M. A., and Tollin, G. (1995) Low concentrations of diacylglycerol promote the binding of apolipophorin III to a phospholipid bilayer: a surface plasmon resonance spectroscopy study. *Proc. Natl. Acad. Sci. U. S. A.* **92**, 5650-5654.

180. Weers, P. M. M., Narayanaswami, V., Kay, C. M., and Ryan, R. O. (1999) Interaction of an exchangeable apolipoprotein with phospholipid vesicles and lipoprotein particles. Role of leucines 32, 34, and 95 in *Locusta migratoria* apolipophorin III. *J. Biol. Chem.* **274**, 21804-21810.

181. Narayanaswami, V., Wang, J., Schieve, D., Kay, C. M., and Ryan, R. O. (1999) A molecular trigger of lipid binding-induced opening of a helix bundle exchangeable apolipoprotein. *Proc. Natl. Acad. Sci. U. S. A.* **96**, 4366-4371.

182. Kahalley, J., Stroud, P., Cannon, G., and McCormick, C. L. (1999) Examination of the structure/function relationship in the exchangeable apolipoprotein, apolipophorin III. *Biopolymers* **50**, 486-495.

183. Soulages, J. L., and Bendavid, O. J. (1998) The lipid binding activity of the exchangeable apolipoprotein apolipophorin III correlates with the formation of a partially folded conformation. *Biochemistry* **37**, 10203-10210.

184. Gursky, O., and Atkinson, D. (1996) Thermal unfolding of human high-density apolipoprotein A-I: implications for a lipid-free molten globular state. *Proc. Natl. Acad. Sci. U. S. A.* **93**, 2991-2995.

185. Weinberg, R. B., and Jordan, M. K. (1990) Effects of phospholipid on the structure of human apolipoprotein A-IV. *J. Biol. Chem.* **265**, 8081-8086.

186. Tajima, S., Yokoyama, S., Kawai, Y., and Yamamoto, A. (1982) Behavior of apolipoprotein C-II in an aqueous solution. *J. Biochem. (Tokyo)* **91**, 1273-1279.

187. Weers, P. M. M., Kay, C. M., Oikawa, K., Wientzek, M., Van der Horst, D. J., and Ryan, R. O. (1994) Factors affecting the stability and conformation of *Locusta migratoria* apolipophorin III. *Biochemistry* **33**, 3617-3624.

188. Lux, S. E., Hirz, R., Shrager, I., and Gotto, A. M. (1972) The influence of lipid on the conformation of human plasma high density apolipoproteins. *J. Biol. Chem.* **247**, 2598-2606.

189. Narayanaswami, V., and Ryan, R. O. (1997) Protein-lipid interactions of apolipophorin-III, a model exchangeable amphipathic apolipoprotein. *Biochem Soc Trans* **25**, 1113-1118.

190. Narayanaswami, V., Yamauchi, Y., Weers, P. M. M., Maekawa, H., Sato, R., Tsuchida, K., Oikawa, K., Kay, C. M., and Ryan, R. O. (2000) Spectroscopic characterization of the conformational adaptability of *Bombyx mori* apolipophorin III. *Eur. J. Biochem.* **267**, 728-736.

191. Jonas, A., Privat, J. P., Wahl, P., and Osborne, J. C., Jr. (1982) Nanosecond rotational motions of apolipoprotein C-I in solution and in complexes with dimyristoylphosphatidylcholine. *Biochemistry* **21**, 6205-6211.

192. Davidson, W. S., Arnvig-McGuire, K., Kennedy, A., Kosman, J., Hazlett, T. L., and Jonas, a. (1999) Structural organization of the N-terminal domain of apolipoprotein A-I: studies of tryptophan mutants. *Biochemistry* **43**, 14387-14395.

193. De Pauw, M., Vanloo, B., Weisgraber, K., and Rosseneu, M. (1995) Comparison of lipid-binding and lecithin:cholesterol acyltransferase activation of the amino- and carboxyl-terminal domains of human apolipoprotein E3. *Biochemistry* **34**, 10953-10966.

194. Weers, P. M. M., Prenner, E. J., Kay, C. M., and Ryan, R. O. (2000) Lipid binding of the exchangeable apolipoprotein apolipophorin III induces major changes in fluorescence properties of tryptophans 115 and 130. *Biochemistry* **39**, 6874-6880.

195. Raussens, V., Narayanaswami, V., Goormaghtigh, E., Ryan, R. O., and Ruysschaert, J. M. (1996) Hydrogen/deuterium exchange kinetics of apolipophorin-III in lipid-free and phospholipid-bound states. An analysis by Fourier transform infrared spectroscopy. *J. Biol. Chem.* **271**, 23089-23095.

196. Lumry, R. (1995) in *Protein-Solvent Interactions* (Gregory, R. B., Ed.) pp 1-141, Dekker Inc., New York.

197. Narayanaswami, V., Wang, J., Kay, C. M., Scraba, D. G., and Ryan, R. O. (1996) Disulfide bond engineering to monitor conformational opening of apolipophorin III during lipid binding. *J. Biol. Chem.* **271**, 26855-26862.

198. Laemmli, U. K. (1970) Cleavage of structural proteins during the assembly of the head of bacteriophate T4. *Nature* **227**, 680-685.

199. Sanger, F., Nicklen, S., and Coulson, A. R. (1977) DNA sequencing with chain-terminating inhibitors. *Proc. Natl. Acad. Sci. U. S. A.* **74**, 5463-5467.

200. Sambrook, J., Fritsch, E. F., and Maniatis, T. (1989) *Molecular Cloning*, Vol. **3**, Cold Spring Harbor Laboratory Press.

201. Zhang, O., Kay, L. E., Olivier, J. P., and Forman-Kay, J. D. (1994) Backbone ^{1}H and ^{15}N resonance assignments of the N-terminal SH3 domain of drk in folded and unfolded states using enhanced-sensitivity pulsed field gradient NMR techniques. *J. Biomol. NMR* **4**, 845-858.

202. Eftink, M. R., and Ghiron, C. A. (1976) Exposure of tryptophanyl residues in proteins. Quantitative determination by fluorescence quenching studies. *Biochemistry* **15**, 672-680.

203. Lehrer, S. S. (1971) Solute perturbation of protein fluorescence. The quenching of the tryptophyl fluorescence of model compounds and of lysozyme by iodide ion. *Biochemistry* **10**, 3254-3263.

204. Abrams, F. S., and London, E. (1992) Calibration of the parallax fluorescence quenching method for determination of membrane penetration depth: refinement and comparison of quenching by spin-labeled and brominated lipids. *Biochemistry* **31**, 5312-5322.

205. Wang, J., Sahoo, D., Schieve, D., Gagné, S. M., Sykes, B. D., and Ryan, R. O. (1997) in *Techniques in Protein Chemistry*, Academic Press, New York.

206. Kiss, R. S., Kay, C. M., and Ryan, R. O. (1999) Amphipathic a-helix bundle organization of lipid-free chicken apolipoprotein A-I. *Biochemistry* **38**, 4327-4334.

207. Kallick, D. A., Tessmer, M. R., Watts, C. R., and Li, C.-Y. (1995) The use of dodecylphosphocholine micelles in solution NMR. *J. Magn. Reson.* **109**, 60-65.

208. Henry, G. D., and Sykes, B. D. (1994) Methods to study membrane protein structure in solution. *Methods Enzymoll.* **239**, 515-535.

209. Voges, K.-P., Jung, G., and Sawyer, W. H. (1987) Depth-dependent fluorescent quenching of a tryptophan residue located at defined positions on a rigid 21-peptide helix in liposomes. *Biochim. Biophys. Acta* **896**, 64-76.

210. Grieser, F., and Tausch-Treml, R. (1980) Quenching of pyrene fluorescence by single and multivalent metal ions in micellar solutions. *J. Am. Chem. Soc.* **102**, 7258-7264.

211. Blatt, E., and Sawyer, W. H. (1985) Depth-dependent fluorescent quenching in micelles and membranes. *Biochim. Biophys. Acta* **822**, 43-62.

212. Green, J. A., Singer, L. A., and Parks, F. H. (1973) Fluorescence quenching by the stable free radical di-*t*-butylnitroxide. *J. Chem. Phys.* **58**, 2690-2695.

213. Chattopadhyay, A., and London, E. (1987) Parallax method for direct measurement of membrane penetration depth utilizing fluorescence quenching by spin-labeled phospholipids. *Biochemistry* **26**, 39-45.

214. Dalton, L. A., McIntyre, J. O., and Fleischer, S. (1987) Distance estimate of the active center of D-β-hydroxybutyrate dehydrogenase from the membrane surface. *Biochemistry* **26**, 2117-2130.

215. Chatelier, R. C., and Sawyer, W. H. (1985) The transverse organisation of ubiquinones in mitochondrial membranes as determined by fluorescence quenching. Evidence for a two-site model. *Eur. Biophys. J.* **11**, 179-185.

216. Mitra, B., and Hammes, G. G. (1990) Membrane-protein structural mapping of chloroplast coupling factor in asolectin vesicles. *Biochemistry* **29**, 9879-9884.

217. Narayanaswami, V., Kim, J., and McNamee, M. G. (1993) Protein-lipid interactions and *Torpedo californica* nicotinic acetylcholine receptor function. 1. Spatial disposition of cysteine residues in the γ subunit analyzed by fluorescence-quenching and energy-transfer measurements. *Biochemistry* **32**, 12413-12419.

218. Segrest, J. P., De Loof, H., Dohlman, J. G., Brouillette, C. G., and Anantharamaiah, G. M. (1990) Amphipathic helix motif: classes and properties. *Prot. Struct. Funct. Genet.* **8**, 103-117.

219. Wu, C. W., and Yarbrough, L. R. (1976) N-(1-pyrene)maleimide: a fluorescent cross-linking reagent. *Biochemistry* **15**, 2863-2868.

220. Lehrer, S. S. (1995) *Subcellular Biochemistry*, Vol. **24**.

221. Lakowicz, J. R. (1999) *Principles of Fluorescence Spectroscopy*, Second Edition ed., Kluwer Academic/Plenum Publishers, New York.

222. Betcher-Lange, S. L., and Lehrer, S. S. (1978) Pyrene excimer fluorescence in rabbit skeletal ααtropomyosin labeled with N-(1-pyrene)maleimide. A probe of sulfhydryl proximity and local chain separation. *J. Biol. Chem.* **253**, 3757-3760.

223. Nelson, J. W., and Kallenbach, N. R. (1986) Stabilization of the ribonuclease S-peptide α-helix by trifluoroethanol. *Proteins: Struct. Funct. Genet.* **1**, 211-217.

224. Sönnichsen, F. D., Van Eyk, J. E., Hodges, R. S., and Sykes, B. D. (1992) Effect of trifluoroethanol on protein secondary structure: an NMR and CD study using a synthetic actin peptide. *Biochemistry* **31**, 8790-8798.

225. MacPhee, C. E., Perugini, M. A., Sawyer, W. H., and Howlett, G. J. (1997) Trifluoroethanol induces the self-association of specific amphipathic peptides. *FEBS Lett.* **416**, 265-268.

226. Lin, T.-I. (1982) Excimer fluorescence of pyrene-tropomyosin adducts. *Biophys. Chem.* **15**, 277-288.

227. Burtnick, L. D., Sanders, C., and Smillie, L. B. (1988) Fluorescence from pyrene-labeled native and reconstituted chicken gizzard tropomyosins. *Arch. Biochem. Biophys.* **266**, 622-627.

228. Verin, A. D., and Gusev, N. B. (1988) Ca2+-induced conformational changes in cardiac troponin C as measured by N-(1-pyrene)maleimide fluorescence. *Biochim. Biophys. Acta* **956**, 197-208.

229. Liou, Y.-M., and Fuchs, F. (1992) Pyrene-labeled cardiac troponin C. Effect of Ca2+ on monomer and excimer fluorescence in solution and in myofibrils. *Biophys. J.* **61**, 892-901.

230. Jung, K., Jung, H., Wu, J., Privé, G. G., and Kaback, H. R. (1993) Use of site-directed fluorescence labeling to study proximity relationships in the lactose permease of *Escherichia coli*. *Biochemistry* **32**, 12273-12278.

231. Jung, K., Jung, H., and Kaback, H. R. (1994) Dynamics of lactose permease of *Escherichia coli* determined by site-directed fluorescence labeling. *Biochemistry* **33**, 3980-3985.

232. Ludi, H., and Hasselbach, W. (1983) Excimer formation of ATPase from sarcoplasmic reticulum labeled with N-(3-pyrene)maleinimide. *Eur. J. Biochem.* **130**, 5-8.

233. Weltman, J. K., Szaro, R. P., Frackelton, A. R. J., Dowben, R. M., Bunting, J. R., and Cathou, B. E. (1973) N-(3-pyrene)maleimide: a long lifetime fluorescent sulfhydryl reagent. *J. Biol. Chem.* **248**, 3173-3177.

234. Birks, J. B. (1967) Excimers and exciplexes. *Nature* **214**, 1187-1190.

235. Lehrer, S. S., and Fasman, G. D. (1965) Excimer fluorescence in liquid phenol, p-ethylphenol, and anisole. *J. Am. Chem. Soc.* **87**, 4687-4691.

236. Gellman, S. H., Haque, T. S., and Newcomb, L. F. (1996) New evidence that the hydrophobic effect and dispersion are not major driving forces for nucleotide base stacking. *Biophys. J.* **71**, 3523-3526.

237. Birks, J. B. (1970) in *Photophysics of Aromatic Molecules* (Birks, J. B., Ed.) pp 301-370, Wiley-Interscience, New York.

238. Chandross, E. A., and Dempster, C. J. (1970) Intramolecular excimer formation and fluorescence quenching in dinaphthylalkanes. *J. Am. Chem. Soc.* **92**, 3586-3593.

239. Lau, S. Y. M., Taneja, A. K., and Hodges, R. S. (1984) Effects of high performance liquid chromatography solvents and hydrophobic matrices on the secondary and quaternary structure of a model protein. *J. Chromatogr.* **317**, 129-140.

240. Rothemund, S., Weibhoff, H., Beyermann, M., Krause, E., Bienert, M., Mugge, C., Sykes, B. D., and Sonnichsen, F. D. (1996) Temperature coefficients of amide proton NMR resonance frequencies in trifluoroethanol: a monitor of intramolecular hydrogen bonds in helical peptides. *J. Biomol. NMR* **8**, 93-97.

241. Scheele, G., and Jacoby, R. (1982) Conformational changes associated with proteolytic processing of presecretory proteins allow glutathione-catalyzed formation of native disulfide bonds. *J. Biol. Chem.* **257**, 12277-12282.

242. Mitchinson, C., and Wells, J. A. (1989) Protein engineering of disulfide bonds in subtilisin BPN'. *Biochemistry* **28**, 4807-4815.

243. Matsumura, M., Signor, G., and Matthews, B. W. (1989) Substantial increase of protein stability by multiple disulphide bonds. *Nature* **342**, 291-293.

244. Fisher, C. A., Narayanaswami, V., and Ryan, R. O. (2000) The lipid-associated conformation of the LDL receptor binding domain of human apolipoprotein E. *J. Biol. Chem.* **In Press**, .

245. Dolphin, P. J. (1992) in *Structure and Function of Apolipoproteins* (Rosseneu, M., Ed.) pp 295-362, CRC Press, Inc., Boca Raton, FL.

246. Ryan, R. O., and Van der Horst, D. J. (2000) Lipid transport biochemistry and its role in energy production. *Annu. Rev. Entomol.* **45**, 233-260.

247. Calabresi, L., Meng, Q. H., Castro, G. R., and Marcel, Y. L. (1993) Apolipoprotein A-I conformation in discoidal particles: evidence for alternate structures. *Biochemistry* **32**, 6477-6484.

248. Lins, L., Brasseur, R., Rosseneu, M., Vanloo, B., and Ruysschaert, J. M. (1993) Structure of the apolipoprotein A-IV/lipid discoidal complexes: an attenuated total reflection polarized Fourier transform infrared spectroscopy study. *Biochim. Biophys. Acta* **1149**, 267-277.

249. Shaw, R. A., Buchko, G. W., Wang, G., Rozek, A., Treleaven, W. D., Mantsch, H. H., and Cushley, R. J. (1997) Infrared spectroscopy of human apolipoprotein fragments in SDS/D_2O: relative lipid-binding affinities and a novel amide I assignment. *Biochemistry* **36**, 14531-14538.

250. Benetollo, C., Lambert, G., Talussot, C., Vanloo, E., Cauteren, T. V., Rouy, D., Dubois, H., Baert, J., Kalopissis, A., Denefle, P., Chambaz, J., Brasseur, R., and Rosseneu, M. (1996) Lipid-binding properties of synthetic peptide fragments of human apolipoprotein A-II. *Eur. J. Biochem.* **242**, 657-664.

251. Rozek, A., Buchko, G. W., and Cushley, R. J. (1995) Conformation of two peptides corresponding to human apolipoprotein C-I residues 7-24 and 35-53 in the presence of sodium dodecyl sulfate by CD and NMR spectroscopy. *Biochemistry* **34**, 7401-7408.

252. Buchko, G. W., Rozek, A., Hoyt, D. W., Cushley, R. J., and Kennedy, M. A. (1998) The use of sodium dodecyl sulfate to model the apolipoprotein environment. Evidence for peptide-SDS complexes using pulsed-field gradient NMR spectroscopy. *Biochim. Biophys. Acta* **1392**, 101-108.

253. Clayton, D., Brereton, I. M., Kroon, P. A., and Smith, R. (1999) NMR studies of the low-density lipoprotein receptor-binding peptide of apolipoprotein E bound to dodecylphosphocholine micelles. *Prot. Sci.* **8**, 1797-1805.

254. Rozek, A., Sparrow, J. T., Weisgraber, K. H., and Cushley, R. J. (1999) Conformation of human apolipoprotein C-I in a lipid-mimetic environment determined by CD and NMR spectroscopy. *Biochemistry* **38**, .

255. Eftink, M. R., and Ghiron, C. A. (1981) Fluorescence quenching studies with proteins. *Anal. Biochem.* **114**, 199-227.

256. Lehrer, S. S. (1997) in *Methods in Enzymology* (Brand, L., and Johnson, M. L., Eds.) pp 286-295, Academic Press, New York.

257. Nolte, R. T., and Atkinson, D. (1992) Conformational analysis of apolipoprotein A-I and E-3 based on primary sequence and circular dichroism. *Biophys. J.* **63**, 1221-1239.

258. Roberts, L. M., Ray, M. J., Shih, T.-W., Hayden, E., Reader, M. M., and Brouillette, C. G. (1997) Structural analysis of apolipoprotein A-I: limited proteolysis of methionine-reduced and -oxidized lipid-free and lipid-bound human apoA-I. *Biochemistry* **36**, 7615-7624.

259. von Eckardstein, A., and Assmann, G. (1998) High density lipoproteins and reverse cholesterol transport: lessons from mutations. *Atherosclerosis* **137**, S7-11.

260. Borhani, D. W., Engler, J. A., and Brouillette, C. G. (1999) Crystallization of truncated human apolipoprotein A-I in a novel conformation. *Acta Cryst.* **D55**, 1578-1583.

261. Koppaka, V., Silvestro, L., Engler, J. A., Brouillette, C. G., and Axelsen, P. H. (1999) The structure of human lipoprotein A-I. Evidence for the "belt model". *J. Biol. Chem.* **274**, 14541-14544.

262. Segrest, J. P., Jones, M. K., Klon, A. E., Sheldahl, C. J., Hellinger, M., De Loof, H., and Harvey, S. C. (1999) A detailed molecular belt model for apolipoprotein A-I in discoidal high density lipoprotein. *J. Biol. Chem.* **274**, 31755-31758.

263. Maiorano, J. N., and Davidson, W. S. (2000) The orientation of helix 4 in apolipoprotein A-I-containing reconstituted high density lipoproteins. *J. Biol. Chem.* **275**, 17374-17380.

264. Weisgraber, K. H., Lund-Katz, S., and Phillips, M. C. (1992) in *High Density Lipoproteins and Atherosclerosis* (Miller, N. E., and Tall, A. R., Eds.) pp 175-181, Elsevier, Amsterdam.

265. Lu, B., Morrow, J. A., and Weisgraber, K. H. (2000) Conformational reorganization of the four-helix bundle of human apolipoprotein E in binding to phospholipid. *J. Biol. Chem.* **275**, 20775-20781.

266. Raussens, V., Fisher, C. A., Goormaghtigh, E., Ryan, R. O., and Ruysschaert, J. M. (1998) The low density lipoprotein receptor active conformation of apolipoprotein E. Helix organization in N-terminal domain-phospholipid disc particles. *J. Biol. Chem.* **273**, 25825-25830.

267. Soulages, J. L., and Arrese, E. L. (2000) Dynamics and Hydration of the α-helices of apolipophorin III. *J. Biol. Chem.* **In Press**, .

268. Soulages, J. L., and Arrese, E. L. (2000) Fluorescence spectroscopy of single tryptophan mutants of apolipophorin III in discoidal lipoproteins of dimyristoylphosphatidylcholine. *Biochemistry* **In Press**, .

269. Lund-Katz, S., Weisgraber, K. H., Mahley, R. W., and Phillips, M. C. (1993) Conformation of apolipoprotein E in lipoproteins. *J. Biol. Chem.* **268**, 23008-23015.

270. Sparks, D. L., Phillips, M. C., and Lund-Katz, S. (1992) The conformation of apolipoprotein A-I in discoidal and spherical recombinant high density lipoprotein particles. *J. Biol. Chem.* **267**, 25830-25838.